Investigating the organizing principles of the mouse claustrum

Andrew McDowall Shelton

Christ Church College

University of Oxford

A thesis submitted for the degree of

Doctor of Philosophy

Trinity 2022

For my grandmothers, Janet and Erma.

Acknowledgements

"And this gray spirit yearning in desire

To follow knowledge like a sinking star,

Beyond the utmost bound of human thought."

- From Ulysses by Alfred, Lord Tennyson

I have met very few people like Adam Packer and it is he who is brought to my mind when I read the quote above from my great-great grandfather's 1910 edition of Tennyson. Never have I experienced the yearning and exuberance for knowledge in such abundance as I have experienced in him. Adam, you are a nuclear reactor in human form – an unending fount of energy, dynamism, and enthusiasm that sets you apart from those around you. Your passion for science inspired every interaction we had, whether it was peering through the green-pink tint of a dichroic mirror, breaking out your secret stash of both metric and imperial Allen keys, or in the triumphant roar of "UP TOP" before a two-handed high-five over some sweet, sweet new data. You are a scientist's scientist and have left an enduring impression. I now can only envision a future where I, too, tenaciously stare at data or vigorously plan experiments, as you have taught me.

To m'Lord Professor Simon Butt, the cell-typing sage: you have my gratitude for checking the hubris that tends to arise when I forget that, for researchers of the cortex, the claustrum still stands as a "minor nucleus of the forebrain." We claustrum folk tend to get very excited about our little strip of gray matter and it was a pleasure to have you in the wings, injecting a dose of reality every now and again to keep us in our place and on track. After all, if we solve consciousness what will be left for everyone else? Your patience, your kindness, your jolliness, and your insightfulness provided irreplaceable guidance that matched and complemented Adam's perfectly. I feel very fortunate to have had you both as mentors and role models in science.

Success in any endeavor is as much a statement of will as it is a reflection of those who support and surround you – and I have strove with gods. It would have been

impossible for me to complete this work without the titanic help of my friends and the raw talent of my colleagues. First and foremost, here's a pint of sausages to Drs Jimmy Rowland and Rob (Lees) Fodder of the OG Packer crew. Though you have now moved on and may never see this note, you framed my entire DPhil experience. You were my mates, my late-nighters in the lab, my drive to keep pushing. You are Python charmers and organizational Olympians of the highest caliber. Filippo Ghezzi, my favorite Buttite, this project truly wouldn't have succeeded without you. Your impossible patching skill and humble patience with my ceaseless questioning took me from being a bumbling researcher to a much better scientist than I could have thought possible. David Oliver, Canadian prince, edit-master extraordinaire, my brother-in-arms for team claustrum. You gave me the knowledge and hope that I wasn't soloing my way through my degree and were endlessly helpful in figure-making and prose-eliminating. To Ivan Priela Lazarte, godspeed. No one in the lab has made me more proud as a mentor or reminded me so consistently of the importance of gratitude through their actions. You are a top-notch friend and will be an even better scientist than I have ever known because of your immeasurable grace and kindness. You, along with Hamish Forrest, Gabi Ocana-Santero, and Tristan Markert, widened my perspective and rescued me from pessimism through your good will (and a few pints).

To the handful of students I've seen through, not least of which are Caitlin Ashcroft, Jake Swann, and Ishaan Kapoor, thank you for tolerating my occasional cantankerousness and unsolicited pontificating, not to mention the indispensable work you did for free. You are bound to be better students and scientists than I, and I can only hope you learned as much from me as I did from you.

A note of thanks and acknowledgement to my scientific inspirations, Christof Koch and Doug Ollerenshaw. Whenever I have felt any doubt in the importance of my work or in the strength of my abilities, I have looked back to our conversations and found a deep seam of confidence and wisdom that runs down to the core of who I want to be as a scientist and as a person.

To Grandma McPhee, for whom my education was always the highest priority, and to Grandma Shelton, whose life inspired this adventure and from whom I have gratefully inherited my great-great grandfather's book of poems, I dedicate this thesis to you. To my parents, from whom springs all of my passion, quirkiness, drive, introvertedness, extrovertedness, eyes, smile, and laughter, you made my whole world possible. If I can reach higher, it is because I am standing on your shoulders. Finally, to Carlie. There are no words to describe the height of my affection or the depth of my gratitude for you seeing me through this nonsense that has been living in ol' Blighty. Here's to a life of love and learning, together.

"To strive, to seek, to find, and not to yield."

Abstract

The claustrum is highly interconnected with many structures in the brain, but the organizing principles governing its vast connectivity have yet to be fully explored. In this thesis, I investigate the architecture of circuits between the claustrum and neocortex and within the claustrum itself. Immunohistochemistry, neuronal tract tracing, *in vitro* whole-cell patch-clamp electrophysiology, dual-color optogenetic circuit mapping, and *in vivo* calcium imaging of neural activity were used to assess whether claustrum neurons combine inputs from multiple cortical areas and what impact claustrum neurons have on the cortex. I determined that individual claustrum neurons frequently integrate inputs from more than one cortical site, most commonly between regions of the frontal cortex. Additionally, I found that neurons in the claustrum receive inputs from an array of sensory and associative cortical areas, albeit to a lesser extent. Neuronal tract tracing and electrophysiology further indicated that input integration from frontal cortical regions depends on the cell type and output target of claustrum neurons. Optogenetic mapping revealed that intraclaustral connectivity was far more frequent than previously reported, particularly among neurons that did not share the same output target. Finally, activity in claustrum axons recorded with *in vivo* calcium imaging showed responses to combinations of sensory stimuli that were then transmitted to downstream cortical targets. My findings shed light on the organizing principles of claustrum connectivity, demonstrating that individual claustrum neurons integrate afferent inputs and redistribute this information back to cortex after performing output target- and cell type-dependent local computations.

Summary of contributions

I declare that this thesis is my own and that attribution has been given where information was derived from other sources. Aside from the exceptions outlined below, I conceptualized the project, designed and assembled the equipment, performed the experiments, analyzed the data and constructed all figures. While all writing contained herein is my own, the project as a whole has relied on key contributions from others. Throughout, the text uses the pronoun 'we' indicating myself and the team below.

David Oliver: Two-photon calcium imaging data acquisition. **Caitlin Ashcroft**, **Jake Swann**, **Simon Williams**: collectively ∼75% of morphological reconstruction and processing of single-cell images (under supervision from myself). **Ishaan Kapoor**, **Ivan Priela Lazarte**: ∼7.5% of all electrophysiological recordings (under supervision from myself). **Ivan Priela Lazarte**, **David Oliver**: collectively ∼10% of surgeries. **Adam Packer**, **Simon Butt**: Conceptualization and supervision throughout.

Contents

List of Figures

List of Tables

1

Introduction

Contents

Essential to understanding the function of a neural system in the context of animal behavior and cognition is a firm grounding in its structure. How electrical activity is transformed and shuttled around the brain and how this information is related to the characteristics of the neurons in different parts of it remains a pervasive challenge in modern neuroscience[1,2]. Recent, large-scale efforts to map and completely delineate the anatomical[3,4], functional[5–8], and genetic[9–11] boundaries within the nervous

systems of mice have shed an important new light on how the brain, especially the cortex, is structured and organized. However, many regions have yet to be explored in such detail. It is vital that all areas of the brain receive this level of scrutiny as the diversity among clinical presentations[12,13] in neurological dysfunction and their underlying causes[14–16] often imply the involvement of widely distributed and specialized structures.

The claustrum (CLA) is such a structure. The CLA is a small, bilateral sheet of gray matter located beneath the insular cortex, adjacent to the striatum on the lateral side of the external capsule. Thin and elongated, it is difficult to study and easy to miss. Despite this, its reciprocal connectivity with many regions of the brain[17–19] has inspired several ideas of its function[20–25] that center the CLA as an important hub in many cortical and subcortical networks. Clinical lesion studies of the CLA in humans have implicated it in a number of dysfunctional brain states, including epilepsy[26], sleep disturbances[27], and general loss of consciousness[28]. Complementary hypotheses posit that the CLA supports a range of associational, attentional, perceptual, and sleep-related processes[29,30] that would underpin the dysfunctions seen after its destruction or disruption. Anatomical[18,19,31–34] and behavioral[35–39] experiments in mice generally support these findings, though many questions remain about how the CLA mechanistically participates in these cognitive processes at a synaptic and cellular level. Analysis of these features was essential to revealing important mechanisms underlying visual processing[40–43]; a holistic understanding of CLA function will necessarily require a similar scrutiny of CLA circuit architecture.

To address this problem, my colleagues and I optimized a previously reported[31,34,44,45] retrograde neuronal tract tracing method for labeling and targeting CLA neurons that project to the retrosplenial cortex (RSP). Reports using anterograde neuronal tract tracing[18,46] have demonstrated little connectivity to RSP by structures adjacent to CLA — RSP therefore represents an ideal candidate for specific labeling of CLA via retrograde tracing methods. We compared this method to existing markers of

the CLA and developed an anatomical and electrophysiological framework in which we next investigated CLA circuit structure. We used retrograde adeno-associated viruses[47,48] (AAVs) to express light-sensitive opsin proteins in RSP-projecting CLA (CLA_{RSP}) neurons so that we could determine the frequency of excitatory connections within the CLA. We could then study the effect these projections have on downstream cortical targets both *in vitro* and *in vivo*. Anterograde AAV expression of opsins sensitive to different wavelengths of light in different cortical axons allowed for the reverse experiment: to reveal the extent to which individual CLA neurons integrate information from more than one cortical area at a time.

Here, we show that the use of retrograde techniques to target a specific population of CLA neurons in rodents offers a useful tool for identifying the CLA *in vitro* and for introducing optogenetic methods for perturbing neurons with light. Doing so revealed several key aspects of CLA synaptic structure and physiology that are fundamentally important to consider in its broader function. First, the CLA is composed of a variety of excitatory and inhibitory cell types that are defined by their intrinsic electrophysiological properties and the likelihood that they project to midline cortices like the RSP. Second, CLA_{RSP} neurons are regularly interconnected with other excitatory projection neurons and interneurons of the CLA via chemical synapses, but are rarely connected to each other. Third, afferent axons from across the cortex are organized into modules along the dorsoventral axis of the CLA that center on the CLA_{RSP} region. Fourth, CLA_{RSP} neurons act as the primary substrate for integrating information from frontal cortices but are less strongly connected to sensorimotor cortices than other CLA neural populations. Finally, CLA axons can carry sensory-related information and differentially innervate the cortex depending on region and layer.

To perform these experiments and to make these findings, I expanded on an anatomical preparation in mice[34,46] which allowed us to specifically target a population of CLA neurons without contamination from other nearby brain areas. This technique was deployed in a number of experimental settings to probe the

physiology and structure of CLA circuits both to and from the cortex and within the CLA itself. With the aid of my colleagues, I used surgical interventions to prepare animals for later use in *in vitro* and *in vivo* procedures. I built the hardware and optimized experimental conditions for acquiring single-cell neural recordings while delivering automated optogenetic stimulation of neural circuits, digitally reconstructed morphologies of recorded neurons, prepared and imaged tissue containing immunohistochemically, virally, or retrogradely labeled neurons. Using these data, I developed and automated analysis pipelines from which I draw conclusions about the principles of CLA circuit organization.

In this thesis, I briefly summarize the findings of CLA research to date, outline methods for accessing and perturbing CLA neurons, describe how these methods are used to understand CLA circuit architecture, and how the data obtained in our experiments were interpreted statistically. Finally, I compare these findings to those in existing literature to identify commonalities and discrepancies that may be informative for further explorations of CLA structure and function.

1.1 The claustrum

The CLA has been recognized as a distinguishable nucleus of the telencephalon for at least two centuries, known to Cajal and Brodmann[21,49,50]. It is an evolutionarily ancient structure as well; correlates of the CLA can be found in birds[51], reptiles[52,53], and most extant mammals thus far examined[54–56]. Buried beneath the insular cortex in both hemispheres, the CLA is a small strip of gray matter wedged between the external and extreme capsules in mammals. Among mammals lacking an extreme capsule, the CLA is otherwise located lateral to the external capsule in the region of the insula[22,25]. From a historical perspective, however, large strides have been made only recently in assessing the cognitive and behavioral impacts of CLA activity and how this might intersect with its gross anatomy[22,25,30]. Here, I will outline past and present research on the CLA with respect to its cells, synapses, structure, and

hypothesized function. Later, I will describe the remaining gaps in our collective knowledge, some of which this thesis seeks to fill.

Arguably the most relevant feature of the CLA is its dense reciprocal connectivity with cortex – the highest per regional volume in the human brain, based on DTI tractography and fMRI studies[57,58]. Anatomical studies in the mid-twentieth century described how the CLA appeared to connect to all areas of cortex in rabbits, cats, and macaques[59–62], with subsequent functional studies designating topographically organized zones of innervation from primary sensory, motor, and association areas[63–67]. Later comparative anatomical studies[51,52,54,68] expanded the range of species thought to have a CLA or CLA-like structure to birds, reptiles, and all therian[25] and some monotreme[56,69] mammals. Together, these early findings provided an important first step forward in presenting the CLA as an ancient structure worthy of attention — few cerebral nuclei other than the those comprising the thalamus had demonstrated a similar density or pattern of innervation[70,71].

During this period, some of the most important insights were made in immunohistochemically labeling the CLA of rodents, insights that would shape conventional opinions of its borders in most subsequent literature for the remainder of the century and well into the next. Parvalbumin (PV), a calcium-binding protein that primarily labels GABAergic interneurons throughout the brain, was instrumental in delineating structural boundaries in the brainstem, thalamus, and layers of the cerebral cortex[72–77]. PV and other calcium-binding proteins[78] were among the first to provide some structural marker for the CLA[31,32,79] as well. PV-rich axon fibers reliably form a dense plexus of neuropil in the "core"[32,34,80] of the CLA and are visibly distinguishable from the overlying layers of cortex and from the ventrally-situated dorsal endopiriform nucleus (dEN) in immunohistochemcial preparations. This critical discovery aided later physiological and anatomical experiments where a reliable marker for the CLA was necessary.

As these findings were being made, clinical cases of damage to the CLA reported deficits in mental functioning congruent with those one might expect in cases of

disruption to such a well-connected area. Patients suffering from CLA damage (incurred as a result of trauma, encephalitis, or another cause) often reported highly variable symptoms including, but not limited to: electrical disturbances and epilepsy[17,26,81,82], delusions[14], disturbances in memory[83–85], decreased perceptual sensitivity[86], loss of vision and hearing[26], sleep disturbances[27], and generalized loss of consciousness[28,87,88]. A recent comprehensive summary of these clinical lesion cases notes the consistent inconsistency in the symptoms reported between studies, an observation parsimoniously explained by a multi-functional or global role for the CLA in brain activity[30].

The accumulating experimental and clinical conclusions about CLA anatomy, physiology, and pathology in the twentieth century sparked a twenty-first century renaissance of CLA research in animals. This revival was fueled by hypotheses that posited the CLA may act as a central node[89] in the neural mechanisms of sensorimotor integration underlying conscious perception[22,23,90]. Studies in monkeys[91–94], recapitulating those that had been done in cats, found largely segregated zones of primary sensory input into the CLA, typically organized into a rough topography, while frontal cortical input innervated most CLA regions. Genetic[95–97] and electrophysiological[98,99] studies, more frequently performed in rodents as transgenic tools became more readily available[9,100–102], deepened the knowledge of CLA intrinsic properties. It became apparent that the CLA housed mostly spiny[33,62,103] and glutamatergic[80,104] projection neurons that seemed to be rarely interconnected[99]. The CLA appeared fairly cortical with respect to the ratio of its projection and inhibitory neurons[32,105]. It was discovered that CLA interneurons are connected at gap-junctions[99] and that the CLA is genetically distinct from comparable structures such as the cortical subplate and dEN[52,106,107]. Moreover, like the cat and monkey CLA, rodents appeared to have a functionally organized CLA as well, albeit with some structural differences[18,108,109]. These observations collectively inspired new ideas of CLA activity that came to include attentional allocation[39,97], salience detection[25], synchronization of cortical oscillations[23,24], task-engagement[110], and mediating behavioral or cognitive state transitions[37,53,96,111], such as those that

occur from sleeping to waking or during activation of the stress-induced anxiety response.

1.2 The problem of the claustrum

Uncertainty still surrounds the CLA despite an increased research focus in recent decades. Comprehensive functional descriptions of the CLA remain relatively intractable and most of the ambiguity can be encapsulated in two categories of research — anatomical definitions and physiology — both of which inform each other as well as perspectives on CLA activity overall. Here, I will begin by considering how difficulties in defining the CLA along these axes have contributed to continued puzzlement among CLA researchers about its function. I will end by describing how our gaps in knowledge represent opportunities for continued research before going on to outline the methods my colleagues and I used to probe the CLA experimentally.

Anatomy

The problem of defining the CLA anatomically has been significantly influenced by the preponderance of nomenclature used to describe it[50] — a direct result of the CLA having few hard borders in animals lacking an extreme capsule, such as rodents. This problem was succinctly diagnosed by Wang et al (2022) in which the authors described four possible arrangements of CLA anatomy based on previous findings: 1) the CLA is composed of dorsal and ventral compartments, 2) the CLA is a homogeneous and singular structure with no subdivisions that sits immediately below L6 of insular cortex and abuts directly onto the external capsule, 3) a "core" and "shell" arrangement defined by output connectivity and interneuron neuropil where the CLA core is insulated from direct contact with the capsule and cortex, and 4) that the CLA is embedded in L6 of insular cortex on all sides but is otherwise not subdivided[19]. Although compelling evidence has been shown for each definition, a convergent view of CLA anatomy is obscured by the different CLA markers or methodologies used in each case.

In the first anatomical definition, dorsal and ventral aspects arise from the apparent continuity of the CLA with the dEN, which some have referred to as the "ventral claustrum"[25,31,59]. The similarity between and individuality of these structures is underscored by the following observations. Firstly, that the CLA and dEN both express several of the same genetic markers — including Gng2[95], Gnb4[19], and Nurr1[112,113] — implying a common ontogenetic heritage. Secondly, that PV-rich fibers preferentially localize in the dorsal (CLA) compartment, implying a functional discontinuity. Confusingly, the terms "dorsal" and "ventral" CLA have changed in what they refer to over time as the dEN became viewed less and less as a part of the CLA and more as a related, but independent nucleus[112,114]. Recent definitions in rodents have divided what was once the dorsal CLA into the dorsal and ventral CLA[115,116], nomenclature that has since stabilized among CLA researchers.

In the second instance, the CLA is undivided and directly opposed to the external capsule medially, the dEN ventrally, the cortical subplate and cortical layer L6 dorsally and laterally. Apparent structural uniformity in both cellular morphology[103] and PV labeling[78] has led some to view the CLA as distinct and apart from the cortex but structurally homogeneous throughout its rostrocaudal length[25,117]. This view is additionally supported by an interruption in cellular expression of some genetic markers for the subplate in the region of the CLA, such as Cplx3[118]. As in the previous case, differences between cortical and claustral expression of genetic markers supports a developmental as well as structural definition of CLA that is apart from that of cortex.

The third arrangement argues for the existence of central and periphery regions in and around the CLA, all of which constitute the CLA but each having unique properties. The term "core" as nomenclature for a central component of the CLA appears to have originated in an immunohistochemical study of calcium-binding proteins by Real et al (2003) but has roots in a study of cadherin proteins published two years before[119]. Cadherin staining showed three CLA components, rather than two as discussed earlier, which were organized as dorsal, central, and ventral

compartments of the CLA. The authors of the study noted the differential expression of n- and r-cadherin in three discrete zones of the CLA which spanned the CLA dorsoventral axis deep to the agranular insular cortex and were distinguishable from superficial cortical laminae. The results were then expanded on in subsequent immunohistochemical studies which showed a similar arrangement not only for calcium-binding proteins but also for VGLUT2, a vesicular transporter of glutamate and a marker for excitatory neurons[32,80,104]. Modern experiments using retrograde neuronal tract tracing and single-cell RNA sequencing recapitulated these findings from the standpoint of CLA efferents[34,107] — the core, defined as the PV+ region containing CLA neurons that projected to the RSP, and the dorsal and ventral shells were composed of neurons of disparate efferent identity. The authors of this study additionally demonstrated differences in neuropeptide Y and somatostatin labeling that also conformed to a core/shell arrangement. Finally, an anterograde tracing study[109] indicated this same arrangement was present for cortical afferents to the CLA as well. These combined data have led proponents of a CLA organized into a core and shell to posit that these compartments represent integrated but discrete functional units, each with its own interneuron subnetwork providing inhibitory tone to designated input and output pathways.

The final possibility for CLA anatomical organization that Wang et al outlined (which the authors of the study support) defines the CLA as the an anatomically homogeneous nucleus that lies embedded in L6b of insular cortex. This view pools evidence from convergent methodologies including gene expression patterns in transgenic animals, axonal tract tracing, and cytoarchitectonics[18,19,114,120]. Indirect support from physiological and behavioral experiments in the CLA and insula show different functional properties between these regions[110,121]; the CLA "shell", from a connectivity, functional, and genetic standpoint, should be considered insular L6b. This perspective on CLA structure, in consideration with the other perspectives, has continued to drive conversations in the field about the implications of CLA anatomy for other properties of the CLA and its ultimate evolutionary or functional purpose in vertebrate brains.

Physiology

As discussed above, the CLA is structurally complex and deeply buried within the brain. These features have made physiological and behavioral characterization practically and conceptually challenging, but not impossible. Early *in vivo* experiments[63,66,67,91] in awake or anesthetized cats and monkeys were foundational in establishing the topographic and reciprocal nature of CLA inputs and outputs, providing key insights into its global connectivity. A notable *in vivo* investigation[98] of CLA intrinsic electrophysiology in rodents, in which the first recordings from single CLA neurons were made, demonstrated the similarities between CLA projection neurons and those of the cortex[122,123]. Confounding these findings, however, was any clear marker for the CLA and a small sample size, which made interpreting the apparent homogeneity in CLA projection neurons and their similarity to cortex difficult. This type of characterization represented an essential first step in assembling the CLA circuit but cried out for more work.

Direct inquiries into CLA physiology remained relatively sparse during the first decade of the twenty-first century, although several important anatomical[32,80,124,125] and genetic[95] discoveries were made during this time. The last several years, however, have seen a rapid increase in the number physiological studies that either directly support or challenge the hypothesis that CLA underlies the "binding" of sensorimotor and cognitive information set out previously[22]. Studies challenging this view did so based on a number of lines of evidence[25,92,93,99]. These include past anatomical reports[63,66] of mostly segregated input zones in the CLA combined with modern *in vivo* and *in vitro* electrophysiological, optogenetic, and behavioral experiments which found excitatory connectivity between CLA neurons to be rare and bounded by pervasive feed-forward inhibition promoted by local PV+ interneurons[35,99]. Additionally, conforming to anatomical findings, CLA neurons appeared to be unimodal in their inputs during *in vivo* recordings in monkeys[92].

The implications of the data presented in the above studies precludes the possibly that information relayed to the CLA from cortex can be transformed in a mean-

ingful way either by the CLA as a structure or within CLA neurons themselves. Recurrent excitatory connectivity, a hallmark of corticocortical and thalmocortical circuits[126,127], is apparently absent in the CLA and positions it functionally closer to coincidence and/or salience detection processes, both of which are among the current hypotheses of CLA function[25,92,99]. However, no experiments have yet been done to test connections from more than one cortex at a time onto a single CLA neuron *in vitro*, and, therefore, it remains unknown how cortical information from across the brain is pooled, transformed, and redistributed by individual CLA neurons.

Contrary to evidence showing a lack of intraclaustral excitatory-excitatory connectivity, other studies conducted during this same time found just that, both anatomically and physiologically[45,128,129]. How could these disparate findings come about and how could they be explained? As recent reports[19,34,130] have demonstrated, the CLA comprises a heterogeneous mix of cells and output pathways that localize into efferent-defined modules[108]. It is entirely possible that connectivity within genetically- or retrogradely-defined populations of CLA neurons is indeed sparse and that cortical inputs to these cells does not instantiate much excitatory recurrent activity. Excitatory CLA neurons of different identities, however, may be more likely to communicate with each other and carry out the mechanisms posited in some hypotheses. Taking the gross anatomy of the CLA into mind, it is also possible that intraclaustral connections are specified along some geometrical axis, such as the rostrocaudal axis, and would appear absent when this element is unaccounted for. These particular facets of CLA physiology have yet to be tested experimentally.

The final physiological perspective taken into consideration here is the effect CLA projection neurons have on the cortex. This aspect is perhaps most fraught with the potential for confounds or ambiguity and is, therefore, the most in need of rigorous anatomical definition with appropriate cross-referencing to other labeling methods prior to experimentation. As seen in a number of studies this far, CLA output neurons spatially segregate along a dorsoventral and anteroposterior gradient[19,34,45],

which can have functional implications in behavioral task performance depending on how these populations are targeted[110].

In vivo experiments in which CLA function could be accurately and reliably perturbed were often prohibitively difficult or impossible prior to the advent of recent genetic and viral technologies. The use of transgenic tools has been specifically beneficial in identifying and probing CLA neurons with high penetrance and fidelity. Physiological studies using such technology have reported indispensable knowledge about CLA circuitry through either transgenic expression of some indicator or neural actuator in the CLA or in combination with a Cre-dependent virus. For instance, *in vivo* studies using transgenic approaches have revealed CLA involvement in ignoring distracting auditory stimuli via disynaptic inhibition of auditory cortex[97,131], mediating the generation of slow waves and sleep/wake transitions via recruitment of cortical interneurons[96], flexibly controlling stimulus-reward associations during attentional set-shifting via connectivity to prefrontal cortex[39], and bidirectionally inducing anxiety responses during stress via input from basolateral amygdala[111]. *In vitro* assessments of CLA activity in cortex largely bear these findings out, indicating that the CLA preferentially drives action potentials in cortical interneurons[132], although the ratio of CLA-mediated inhibition to excitation varies by cortex and cortical layer[133].

While certainly helpful in determining the broad-stroke functionality of CLA circuits, transgenic strategies in this context are typically accompanied by one major confound: the lack of precise, CLA-specific expression of markers, and, thus, difficulty in making CLA-specific conclusions. This is particularly true in chemogenetic experiments using DREADDs (Designer Receptors Exclusively Activated by Designer Drugs)[96,97,134–139] where the systemic application of a chemical ligand to transgenically-expressed receptors is confounded by the expression of those receptors anywhere in the body, not just the brain, let alone the CLA. This is further complicated by chemical decomposition of these ligands into derivatives with an increased binding affinity for non-specific receptors[140]. Targeted injection of

Cre-dependent AAVs into the CLA of Cre-expressing transgenic mice also presents hazards as transgene expression in the CLA is often accompanied by expression in nearby areas, such as dEN and cortical deep layers as noted above, thereby also preventing truly CLA-specific findings. These issues do, however, present an insight into the interaction between anatomy and physiology in the CLA that is informative for how results from such studies can be interpreted and expanded through the judicious use of more specific methods. Differences in the findings between studies using transgenic mice could be explained by both variations in experimental design and the activation or inactivation of genetically distinct CLA subpoplations. Therefore, it follows that findings in transgenic experiments are entirely valid and should be accompanied by a fine-grained dissection of CLA circuits to disambiguate which cells or structures may be involved.

In this section, I have circumscribed several modern difficulties in studying the CLA from anatomical and physiological perspectives. These include: variable definitions of CLA anatomy based on differences in interpretations between researchers using different experimental approaches, discrepancies in the presence and/or extent of intraclaustral circuitry, uncertainty surrounding whether single CLA neurons integrate or are selective for cortical input, and the constraints on interpreting the impact of CLA efferent activity in experiments using transgenic techniques alone. Several studies have recently demonstrated, however, the efficacy of leveraging the vast connectivity of the CLA using retrograde tracing, labeling, and expression techniques[34,45,110,131,141] to reliably and specifically ameliorate some of these issues. When combined with *in vitro*, *in vivo*, or transgenic technologies, retrograde strategies offer a powerful tool of defining, accessing, measuring, and perturbing CLA neurons. Below, I will discuss specific methods for doing each.

1.3 Methods in neuronal tract tracing

The first step in understanding a neural circuit is tracing its inputs and outputs — how is the flow of information organized by the connectivity of neurons in the

system? This question is typically answered through anatomical means in fixed tissue before using physiological or behavioral assays to probe network function. Tracing a network involves locating neurons both upstream and downstream of a target area and is of great importance in experimental and clinical settings[142].

Underpinning all neural tract tracing techniques is the axon[143] and the cytoplasmic flow of proteins, vesicles, nutrients, nucleic acids, mitochondria, and other materials mediated by the axoplasmic transport system[142,144,145]. Transport of substances can occur bidirectionally along the axon, anterogradely toward the presynaptic terminal or retrogradely toward the soma, with transport of exogenous substances usually being initiated by their uptake into lipid-lined endosomes via receptor-mediated fluid endocytosis[142,144]. Lateral spread through the lipid membrane is also possible for some compounds[146,147]. The direction a substance will flow once inside a cell is determined by the transport system it engages with[148]: organelles, enzymes, vesicles, mitochondria, and neurotransmitters can be transported anterogradely by kinesin-family proteins utilizing the microtubule scaffolds making up the cellular cytoskeleton while substances taken up by endocytosis, organelles, and proteins can be transported retrogradely to the soma by dynein-family proteins. Neural tract tracing leverages these biochemical mechanisms through the use of substances engineered to travel in one direction or another along an axon, typically from a site where the substance was injected directly into the brain and, in some cases, across the synaptic cleft to pre- or postsynaptic neurons. Below, I will briefly discuss a few of the methods in anterograde and retrograde neural tract tracing and note their relevance to experiments conducted here.

Anterograde tracing

Anterograde tracing, as noted above, tracks the movement of substances from the soma to the presynaptic terminal and is usually concerned with where the axons of a neuron project to. This is important and useful for several reasons, among which are understanding which cortices (and cortical layers) are projected to, the density with which axons innervate a given region, the approximate length of labeled axons,

and, in some cases, which cells or cell types are contacted explicitly. Though many techniques are available for anterograde neural tracing, I will focus predominantly on genetic and viral approaches here.

Of the modern anterograde tracing methods in neuroscience, the use of AAVs is among the most common. AAVs are non-toxic, relatively cheap, easy to use, and well-suited for a large variety of research and clinical applications[149,150]. These traits make them ideal for use in animal studies where anterograde tracing of axons from a whole region, a particular cell type, or even just a handful of cells is required. Below, I will discuss their biology, mechanisms of action, and utility for contemporary neuroscience research.

AAVs and recombinant AAVs (rAAVs) are viruses of the parvovirus family and carry small sequences of single-stranded DNA[150]. AAVs are capable of infecting multiple types of tissue but are not known to carry disease or illicit a pronounced immune response[150,151]. Unmodified AAV genomes contain two open reading frames, Cap and Ref, each of which are flanked by inverted terminal repeat sequences. Cap and Ref contain genes that encode proteins for constructing the 20 to 25 nm icosahedral capsid and for AAV replication, respectively. In experimental or gene therapy settings using AAVs, these sequences are typically deleted to prevent replication and the possibility of cell death and can be replaced with coding sequences up to the cloning capacity of the virus, typically genomes of less than 5 kb[150].

Capsid proteins make up capsomeres, the morphological subunits of the virus' capsid coat, and ultimately specify the viral serotype[152,153]. The serotype, the specific surface antigens displayed on the viral capsid coat, confers the tropism of the virus and is used in epidemiological classification of subspecies of microorganisms, such as viruses[153,154]. Eleven natural AAV serotypes, numbered AAV1 to AAV11, have been documented thus far, each able to infect particular types of tissue — rAAVs are engineered AAVs combining serotype properties from different AAVs to optimally maximize a particular tropism[154–156].

Among most AAV serotypes, cellular entry occurs by receptor-mediated endocytosis, a process requiring the binding of capsid proteins to cell-surface receptors, commonly specific AAV receptors (AAVR)[157], heparan sulfate proteoglycan (HSPG), or N/O-linked sialic acid in the cases of AAV2, 3, 4, and 5[151]. Once bound, intracellular signalling cascades rapidly initiate clatherin-dependent endocytosis of the receptor and virus. Efficiency of the uptake process can be enhanced for certain AAVs via the binding of coreceptors[151,153]. If a preferred receptor is expressed throughout the cell membrane, an AAV can theoretically bind and enter the cell anywhere, highlighting its usefulness in tract tracing studies. Once enclosed within an intracellular endosome, the virus is trafficked via a Rab protein-dependent process along the cellular cytoskeleton to the nucleus in a manner that is also influenced by viral serotype[151]. As such, AAVs have the capacity to travel through a neuron anterogradely or retrogradely or even transynaptically in some cases[150,156,158,159]. A recent study[160] used the anterograde transsynaptic infection properties of AAV1 to explore the behavioral ramifications of optogenetically stimulating input-defined populations of neurons in the superior colliculus. The authors noted the specific serotype and concentration-dependence of their findings, highlighting conventional difficulty of anterograde transsynaptic viral infection and the utility of their technique and AAVs in neural tract tracing.

AAVs escape the endosome once trafficked to the soma and enter the nucleus before shedding their capsid coat[151]. It is at this point that the potential of AAV technologies is realized as the genomic payload the AAV carries can encode any protein-coding sequence within the viral packaging capacity. Early studies using AAVs to deliver engineered constructs to neurons often did so by injection into the brains of transgenic animals[47,146,161,162] as a means of circumventing the need to breed animals expressing Cre-dependent[163] genes with animals expressing Cre recombinase under a cell type-specific promoter[4,164]. Later studies would introduce DNA sequences for fluorescently-labeled proteins[165,166] either alone or in a transgenic Cre-dependent design[18,45,47,164,167]. Once produced by the native cellular transcription and translation machinery, fluorescent proteins could be trafficked

anterogradely throughout the cell body, dendrites, and axon and visualized *in vitro* or *in vivo* with a number of light microscopy techniques[168].

Taken together, AAV and transgenic technologies offer powerful, efficient, and highly specific tools for anterograde neural tract tracing. In the next section, I will discuss retrograde tracing methods, some of which rely on these same genetic tools.

Retrograde tracing

Unlike anterograde neural tracing, retrograde tracing cannot currently be accomplished with a transgenic-only strategy in mammals, although progress in this field has been made recently in the fruit fly *Drosophila melanogaster*[169,170]. Contemporary methods in retrograde tracing, discussed in order hereafter, typically use one or a combination of inorganic fluorescent compounds, fluorophore-conjugated proteins, and/or viral methods.

Inorganic neuronal tracers have been held up as prime candidates for retrograde neural tracing for almost a half-century[171]. Whether conjugated to a fluorescent molecule or stained for in immunohistochemistry (IHC), they offer long-term, stable, and robust labeling of neurons[172]. Notable among them are hydroxystilbamidine (FluoroGold^{TM})[172], latex microbeads (retrobeads)[173], and carbocyanine lipophilic dyes such as DiI[147]. In the case of FluoroGold^{TM} and retrobeads, these substances can be taken up by cells via passive fluid endocytosis from an injection site into the brain, trafficked preferentially back to the soma along the axon, and stably remain stored in the cytosol or vesicles for weeks or months. In the case of DiI and other lipophilic dyes, these molecules embed themselves directly into the neuronal lipid membrane and passively diffuse along whatever part of the neuron they happen to be nearest, resulting in complete labeling of a neuron and its neurites. In this sense, lipophilic dyes are both retrograde and anterograde labels. Though not germane to this study, inorganic tracers are often compared to those discussed below in terms of efficacy, penetrance, brightness, and stability.

Protein substances are effective retrograde tracers and advantageous for their flexibility and ease of use. Horseradish peroixdase (HRP), eponymously named for the plant from which it is derived, has been known for centuries. HRP is a glycoprotein and metalloenzyme that catalyzes various oxidative reactions of chromogenic compounds to produce a detectable stain[174]. HRP was first observed to be a potent retrograde neuronal tracer in the early 1970s and sparked a wave of concentrated research on the use of biological substances in neuronal tract tracing[175,176]. One result of these efforts was the discovery that cholera toxin subunit B (CTB), the ganglioside-binding, non-pathogenic subunit of the toxin produced by *Vibrio cholerae*[177], retrogradely labeled neurons when isolated and injected into the brain. CTB demonstrated early on some advantages over several other methods of neural tracing, including: The ability to conjugate CTB to fluorophores that emit different wavelengths of light and use them together in combined experiments, the relative evenness of its signal in tissue, its low toxicity to cells, and its quick and specific uptake and transport via active endocytosis[178,179]. Given the breadth of CLA connectivity with cortex, several modern studies have effectively used CTB as a method for retrogradely labeling CLA cell bodies via their efferent projections[31,34,44,45].

Finally, viral vectors can be used to deliver DNA or fluorescent payloads retrogradely to the nuclei of target neurons. Several neurotropic virus species naturally exhibit retrograde transport as a part of their life cycle, including rabies[155], poliovirus[180], herpes simplex virus (HSV)[181], and certain serotypes of AAV. However, most viral systems are accompanied by certain drawbacks that might inhibit their versatility in experimental settings. For rabies, poliovirus, and HSV, a particular challenge is their potential for neurotoxicity, spread beyond a desired amount, and that they readily integrate into the host genome[149,182]. Traditional AAV serotypes have comparatively variable or weak retrograde transduction but low toxicity[47,150,159]. However, novel rAAVs have recently been engineered[48] with enhanced retrograde transduction efficiency using *in vivo* directed evolution. These new rAAV2-retro variants pass the cell membrane via mechanisms similar to traditional AAVs, allow

the same level of genetic access to neurons, support an improved genomic carrying capacity for specific promotor-driven sequences, and do so with greatly improved retrograde functionality[48,150]. Additionally, retro-AAV2 was shown to generalize across neural cell types, brain regions, and circuits. The advent of low-toxicity, high throughput retrograde rAAV technology has significantly bolstered options for retrograde labeling, neuronal tract tracing, and genetic delivery of protein actuators to upstream targets.

Anterograde and retrograde neuronal tract tracing are cornerstones of modern neuroscience research to the extent that a rigorous and sprawling subfield has arisen from them – connectomics. Neuronal tract tracing furnishes our understanding of neural circuits by bringing microscopically entangled structures into the realm of comprehensibility. In combination with physiological assays, which I will review in subsequent sections, neural tracing becomes a particularly potent tool.

1.4 Recording electrophysiological properties of neurons *in vitro*

The electrical properties of neurons allow for fast communication within the brain and for the emergence of the various computations performed by neural ensembles. The differential permeability of charged ion species[183] and their conductance across the cellular membrane underpins the action potential waveform, as shown in now classic electrophysiological studies of the squid giant axon performed in the mid-twentieth century[184–189]. The authors quantitatively reconstructed the action potential by correlating the conductance of ions such as sodium and potassium to the opening and closing of lipid-bound proteins known as ion channels, which selectively permit the flow of certain ion species in a voltage- and time-dependent manner.

Since that time, important insights and significant improvements have been made in electrophysiology with respect to the properties of neurons and the methods used to record them. Of these, there is perhaps no technique more fundamental

to single-cell electrophysiology than whole cell patch-clamp, developed some years after the modeling of the action potential waveform by Hodgkin and Huxley as a means to experimentally test their theory[190]. In the following section, I will review whole cell patch-clamp as a method for understanding intrinsic electrical properties of neurons, considerations for its use, and how patch-clamp electrophysiology can be used to differentiate neural cell types.

Whole cell patch-clamp

In principle, *in vitro* whole cell patch-clamp is a fairly straightforward procedure that can be expanded on in a variety of ways[190–192]. Briefly, cells from which recordings are to be made, whether cultured in a dish, tissue excised from living organisms, or simply ion channel-containing membranous vesicles, are bathed in an artificial salty solution meant to mimic the ionic properties of the extracellular environment in whole brains. Cells are approached with a micropipette open on one end that is filled with another electrolyte solution of a similar ionic content to the intracellular fluid. Importantly, this micropipette also contains a metal electrode connected to an electronic amplifier. An additional reference ground electrode sits in the bath solution to complete the pipette-cell-ground circuit. Cells are "patched" by direct apposition of the pipette to the cell surface, which is then ruptured through application of negative pressure, providing access to the intracellular environment. Once this is accomplished, either the voltage or the current of the cell can be "clamped" and kept nearly constant during recording while the other is allowed vary freely.

Voltage-clamp and current-clamp each offer useful capabilities for recording different aspects of the electrochemical dynamics and environment within and around a cell. Extracellular voltage-clamp was invented by Kenneth Cole and colleagues in 1947 and allowed for the clamping of the cellular membrane potential to a desired voltage via the iterative measurement and application of current by two electrodes in a feedback circuit[185,190]. In the context of modern whole cell patch-clamp, developed and refined by Neher and Sakmann in 1976-81[190–192], this technique is an extremely

powerful tool for characterizing the conductance of ion channels in a variety of experimental settings. Voltage-clamp is also useful for visualizing currents that arise from synaptic events, either those stimulated by presynaptic inhibitory or excitatory neurotransmitter release, or through the application of exogenous chemicals.

Current-clamp, by contrast, is a method for recording the voltage difference across a membrane by constantly injecting positive or negative current into the cell. In this setup, membrane voltage is allowed to fluctuate freely[191,193,194]. When no current is applied, the cellular membrane sits at its resting potential, determined by the electrochemical ion gradients and proportion of opened and closed channels across it[183,191]. Because voltage can vary in response to either endogenous or applied currents, the visualization of action potentials and other current-dependent attributes – intrinsic biophysical properties[195] – is made possible. While voltage-clamp can be used to understand the features of conductance exerted by ion channels on the neural membrane, current-clamp can be used to probe how the membrane potential characteristically responds to changes in conductance based on the number and type of ion channels it contains. Using these methods, one can capture an accurate idea of the intrinsic properties of neurons and the differences between them, differences that determine how a given neuron will integrate its inputs and the nature of its output.

Sorting neurons by intrinsic electrical properties

As alluded to above, groups of neurons can be defined by characteristic passive and active membrane properties, e.g. the intrinsic properties of a neuron based on its electroresponsiveness[195,196] to different current environments. This is typically accomplished using whole cell patch-clamp electrophysiology to drive changes in membrane potential by current injections of different sign, magnitude, and time course up to and exceeding the action potential threshold, usually by several fold[123,196,197]. Thus, by observing how a neuron responds to changes in current, one can infer intrinsic properties manifest in the shape of an action potential, the

temporal pattern of firing, and in the way a given neuron transforms synaptic inputs into spike output.

Classifying groups of neurons into distinct subpopulations by intrinsic biophysical properties can reveal aspects of the structure and function of a network. In addition, modern approaches to neuronal classification overlay a variety of datasets with intrinsic electrophysiology. For example, the geometrical (morphological) properties of recorded neurons and their location in the brain. This is achieved through an experimental approach in whole cell patch-clamp where the intracellular pipette is filled with an electrolytic solution containing a chemical dye or organic compound that diffuses into the cell during recording. *Post hoc* tissue fixation and IHC renders the compound visible in light microscopy, allowing neural morphologies to be procured and compared to electrophysiological attributes[74,123,198,199]. In a classic study, the dendritic and axonal arbors of cortical projection neurons and interneurons were reconstructed and mapped to intrinsic electrophysiological properties after whole cell recordings *in vitro*[123]. The authors found that the columnar location and morphology of neurons they recorded, as well as their synaptic partners, was reflected in their intrinsic electrical properties. Notably, the authors additionally demonstrated that subclasses of interneurons could be defined in this manner. Superimposing related information onto intrinsic electrophysiology in this way bolsters the available interpretations one can make about neurons and neural circuits.

The versatility of whole cell patch-clamp and the wealth of data it provides makes it a highly effective tool for describing the properties of neurons and the differences between them. When combined with genetic and biophysical methods, as I will explain in the next section, experimenters gain the ability to describe the properties and functionality of large, widely dispersed circuits of the nervous system.

1.5 *In vitro* circuit mapping with light

Mapping functional connectivity between distant regions of the mouse brain is difficult using *in vitro* whole cell patch-clamp methods alone, as these methods often require sectioning tissue that can sever presynaptic axons. Furthermore, the extent to which connectivity can be understood within a network is depleted with distance, as neurons tend to receive most of their local connections from within 200 μm of the soma[200]. When studying long-range neural circuits, as in the case of the CLA, there is a need for experimental tools to combat these limitations. Optogenetics, the use of genetically encoded opsin channel proteins to control the activity of specific groups of neurons with light, can be an especially effective work-around to slice-generated artifacts *in vitro*.

Francis Crick identified in 1979 the need to make sense of circuits in the mammalian brain by precisely controlling individual populations of neurons, later speculating that this could be accomplished with light[182,201]. During this same period, Oesterhelt and Stoeckenius discovered bacteriorhodopsins, light-sensitive single-component ion pumps found in the cell membranes of the microbe *Halobacterium halobium*[202]. The next several decades saw the slow expansion of opsin-based genetic technologies that would eventually marry with advances in optics and neuroscience, ultimately allowing optogenetic methods to be used in living organisms or tissue cultures to control ionic activity within neurons[182,203–207].

In the modern scientific context, optogenetic experiments proceed first, in general, by engineering a light-sensitive opsin protein with consideration given to features such as the wavelength to which it is maximally driven to conduct ions, the kinetics of how quickly it might do so, and to what cellular compartments it is localized to[208]. Next, opsins are expressed in neurons via viral[209] or transgenic[210,211] means. This then allows an experimenter to alter neural function simply by shining a light of the right frequency to drive currents through opsin channels expressed in the membrane[212,213]. These techniques combined offer unparalleled versatility through a relatively simple method of restricting gain or loss of function to individual brain

regions, cells, cell types, or projection-defined populations with precise temporal control.

Single-wavelength circuit mapping

The best studied and most popular opsin variants used in optogenetics are channelrhodopsin1 (ChR1), channelrhodopsin2 (ChR2), and the family of opsins similar to or engineered from them[182,214]. ChR are light-gated cation channels first discovered in the eyespot of green algae *Chlamydomonas reinhardtii*[205,215] and would later form the biophysical basis for thousands of optogenetic studies[182].

ChR mechanisms of action are directly tied to their molecular structure, from the strength and duration of their photocurrents to where they localize in a cellular membrane[214]. At the level of primary structure, all ChR (and most other rhodopsins) operate by the same process – absorption of a photon of (usually blue) light by the light-sensitive chromophore retinal, bound via a Schiff base to the H7 transmembrane subunit of the ChR protein. Photoabsorption and retinal isomerization induces conformational changes in the tertiary and quaternary structure of the ChR protein that prompt a shift from a closed channel state, to an open one, and eventually back to a closed state through light desensitization and further conformational shifts (the complete operation is known as the photocycle). The rate at which these steps occur, the types of ions that are permitted through the channel once open, and the wavelength of light that maximally drives the photocycle are subject to the primary structure of the ChR in question, the many varieties of which have useful experimental properties that I will explore in the next section.

Although which ChR to use is a matter of experimental design, most single-wavelength *in vitro* optogenetic circuit-mapping experiments utilize the membrane trafficking properties of conventional and modified ChR[216] to localize expressed opsins to specific compartments or the whole cell. Briefly, opsins are produced from the expression of viral or transgenic vectors in the soma of a genetically- or projection-defined population of neurons. Opsin proteins are then trafficked throughout the

cell through interactions with their C-terminal intracellular domain[217]. Patch-clamp recording experiments proceed via optogenetic photostimulation of opsin-expressing neurons. Because opsins can be trafficked to any given segment of membrane, including the axon terminal, *in vitro* whole cell patch-clamp experiments need not be confined to local circuits where the axon remains intact — severed axon terminals can still be stimulated to release neurotransmitter from synaptic vesicles onto the postsynaptic neuron under opsin-mediated presynaptic terminal depolarization. The experimental paradigm described here, known as ChR-assisted circuit mapping (CRACM)[218], has become an integral component of most circuit mapping experiments in neuroscience.

Dual-wavelength circuit mapping

Key to opsin activity within the membrane is the range of wavelengths of light over which they are maximally excited to open and conduct ionic currents (their excitation spectra). This property varies among opsins which can show maximal excitation to anywhere from blue to red light[214]. Two opsins used in the production of this thesis, originating from *Stigeoclonium helveticum* (Chronos) and *Chlamydomonas noctigama* (Chrimson), have ideally separated maximum excitation frequencies in the blue and red spectra, respectively[219], lending experimental usefulness to each in different settings. Using differentially excited opsins in concert, however, is less straightforward. Red-shifted opsins, like all opsins, still demonstrate some responsiveness to blue light, though the reverse relation among blue-shifted opsins is very weak. Previous studies have achieved specific excitation of dual-expressed opsins of different peak excitation wavelengths through rigorously titrated light power and opsin expression[219]. However, doing so under viral or transgenic paradigms is often challenging or prohibitive as expression of opsin proteins is difficult to control precisely.

One solution to this problem arises from the biophysics of ChR proteins mentioned earlier – repetitive or prolonged light exposure induces a dark-adapted, desensitized conformational state in which peak photocurrents are diminished or abolished[214]

and cannot be recovered for several seconds. Recently, this property has been exploited in experiments where opsins of red- and blue-shifted action spectra are expressed in different regions of the brain and their resulting convergence tested *in vitro* on post-synaptic neurons[220,221]. Experimenters in these studies employed a sequential stimulation scheme in which red-shifted light was used to activate, and then desensitize red-shifted opsins so that blue-shifted opsins could be activated independently. In each case, this method allowed the interrogation of two input streams to single neurons nearly simultaneously. Until blue-light responses can be eliminated among ChR derivatives, sequential dual-wavelength photostimulation represents a promising avenue for dissecting convergent circuits in the brain.

Together, single- and dual-wavelength circuit mapping *in vitro* are bedrock tools for investigating the physiology of neural circuits. Such investigations form the baseline from which more generalized observations or experiments can build upon. At a certain point, however, circuit knowledge must be translated into the context of animal experience — how does the architecture of a circuit inform perception or behavior? In the next section, I will discuss *in vivo* calcium imaging as a means of recording neural activity in awake mice.

1.6 *In vivo* recording of calcium activity

Circuits within the brain do not act in isolation but in concert with other pathways that together underpin all neural computation[222,223]. With this in mind, it is important to simultaneously record the activity of many neurons as it would occur in the brains of alive animals, e.g. *in vivo*. Historically, multi-neuron recording had been accomplished using microelectrodes that had been inserted into the brain, allowing for the recording of action potentials with high temporal accuracy[224,225]. Modern *in vivo* electrophysiology has rendered vastly superior electrodes capable of recording hundreds of neurons simultaneously[7] that, nevertheless, present certain challenges when drawing conclusions about neural activity. These include the inability to track the identity or precise location of recorded neurons in the brain,

complex analysis procedures[226], and is inflexibly limited to precise[227] or broad[228,229] stimulation regimes during recording.

In vivo calcium imaging[230] of neural activity circumvents these issues to record large populations of neurons with single-cell accuracy. This method grants the ability to record neural activity with light via the expression of a genetically engineered fluorescent molecule which undergoes a conformational state change after binding calcium, typically the result of the rapid flux of ions during an action potential[194,231]. GCaMP, the most widely used genetically encoded calcium indicator (GECI)[232], is a fusion protein of GFP (green fluorescent protein)[165], calmodulin (a calcium-binding protein), and a short peptide sequence from myosin light-chain kinase[233,234]. GCaMP can be stably expressed in neurons through viral[235] or transgenic[9] means, enabling repetitive experimentation with the same group of neurons within an animal. Although slower in the temporal domain than whole cell or *in vivo* electrophysiology due to the intracellular dynamics of calcium during and after the action potential[231], compensation takes form in the immense benefits provided by visualizing neural activity in alive and awake animals.

Imaging of GCaMP signal takes place during light microscopy, which leverages the difference in excitation and emission wavelengths of a fluorophore to excite GCaMP with one wavelength and then record activity emitted as another, longer wavelength using a camera or photomultiplier tube as a sensor[236]. This – known as single-photon microscopy – is useful when under low objective power or when spatial resolution is less important. However, due to the intrinsically photon-scattering nature of biological tissue, single-photon excitation is often less useful when precise localization of fluorescing cells is required and is specifically poor at doing so in the z-dimension, as photons liberated by the excitation beam can often originate beyond the focal plane. This problem is ameliorated in scanning microscopy, such as laser scanning confocal microscopy, in which the excitation beam samples only small sections of the specimen in sequence and emitted photons can be attributed to known regions by the detector[236]. However, confocal and scanning microscopy

are of limited use in *in vivo* mammalian neuroscience as the excitation spectra of most common calcium indicators like GCaMP require wavelengths of light that do not readily penetrate through more than a few hundred microns of brain tissue[237]. Instead, multiphoton absorption of longer, less easily scattered wavelengths, such as those in the far-red spectrum, allow for deep tissue penetration and a high signal-to-noise ratio. This technique, known as two-photon microscopy, produces photons of half the energy needed to excite a fluorophore, two of which are contrived to arrive simultaneously at the focal plane and combine their energies. Because the probability of this occurring is highly unlikely much beyond the limits of the focal plane, two-photon microscopy grants the ability to image neurons and their processes deeply in scattering tissue while being minimally invasive and delivering high-resolution, low-noise images.

Through the use of two-photon imaging of calcium dynamics in alive animals, it becomes possible to translate *in vitro* experiments on a given population of neurons or circuits into *in vivo* perception and behavior.

1.7 Summary

This text aims fill an important niche in CLA literature by applying the methods and ideas presented above to understanding the properties of CLA circuits. The CLA offers a unique insight into higher-order networks, the function for which has yet to be fully elucidated. At a fundamental level, the CLA is a case study in the long-range propagation of neural signals throughout the brain. Here, I use *in vitro* and *in vivo* methods to dissect CLA input and output streams, allowing for a detailed, cell-by-cell look into its anatomy and physiology, from which I perform comparative analyses on the resulting data. This work is a perspective on the organizing principles of the CLA that provides a mechanistic baseline for its proposed roles in the many facets of consciousness.

2

Anatomical & electrophysiological characterizations of the claustrum

Contents

As mentioned in the introduction, a thorough interrogation of CLA anatomy and physiology is necessary to draw functional conclusions about its activity, as the CLA comprises many spatially segregated and potentially non-overlapping input-output pathways[19,34,46]. This connectivity, however, can provide a useful baseline for understanding CLA gross architecture and cell types — a ground-truth marker not only for CLA identification on the whole, but also for an aspect of cellular identity, i.e. the projection target of a neuron. The RSP has been identified[46] in tracing experiments as having a unique relationship to the CLA — RSP receives innervation from CLA efferents but not at all from CLA-adjacent structures. This quality positions RSP as a prime candidate for specifically targeting the CLA. In

this way, CLA neurons can be retrogradely labeled for further investigation and compared on the basis of their projection identity.

Here, I expanded on a previously reported retrograde neuronal tract tracing method[177] for labeling the CLA[34,45] via stereotaxic injection of CTB into three different sites along the rostrocaudal axis of the RSP in mice. Machine learning-assisted image processing techniques were subsequently used to interpret the density and area comprised by CLA_{RSP} neurons labeled from the RSP injection that gave the highest number of labeled cells. Below, I present the spatial relationship of CLA_{RSP} neurons to each other and to the CLA overall before going on to describe the CLA intrinsic electrophysiological and morphological properties circumscribed by this projection-defined perspective.

2.1 Anatomical delineation of CLA_{RSP}

To understand how CLA neurons differentially innervate RSP, we injected wild-type (WT) C57BL6/J male mice with CTB488 (green; caudal), CTB555 (red; intermediate), CTB647 (blue; rostral) into three separate rostrocaudal locations along the RSP (n = 3 mice, Fig. 1a) based on coordinates obtained from the Franklin & Paxinos reference atlas[115]. Confocal microscopy imaging of 100 μm-thick coronal sections revealed that each injection strongly labeled highly overlapping populations of ipsilateral CLA neurons, distinct from the surrounding, unlabeled tissue (Fig. 1b,c). Dense cell body labeling was also noted in the ipsilateral anterior cingulate nucleus (ACA), contralateral RSP, and several ipsilateral thalamic nuclei including the ventrolateral thalamus and the laterodosal thalamus ventrolateral part (Fig. 1b). Sparser labeling could be found in contralateral ACA, contralateral thalamus, contralateral CLA, ipsilateral preoptic area, and ipsilateral nucleus of the diagonal band.

Comparison of CTB labeling in CLA between injection sites revealed that the caudal-most injection site reliably labeled the highest proportion of cells, followed by the intermediate and rostral injection sites, respectively (Fig. 1d-f). This was

especially true for the caudal regions of the CLA (51% of all labeled neurons) but less so for rostral regions where the proportion of labeled neurons from each site was roughly equivalent (33%, Fig. 1d). On the average, there were more CLA_{RSP} neurons labeled by their projection to caudal RSP across all slices ($p = 0.0005$ Mann-Whitney U test) than to the intermediate and rostral RSP, while there was no difference found between these latter two injections ($p = 0.17$; Fig. 1e). Across all slices and animals, caudally-projecting CLA_{RSP} neurons comprised 43% of all labeled CLA neurons (Fig. 1f). Additionally, the largest proportion of dual-labeled neurons projected to caudal and intermediate RSP (13%), while only a small number of counted neurons projected to all three RSP locations (4%).

Injection of retrograde neuronal tracers into the RSP consistently demonstrated that at least some CLA_{RSP} neurons could be found along the whole CLA length (as defined by other sources[4,18,115]). No gross differences in the dorsoventral or mediolateral localization of CLA_{RSP} were observed between injection sites (Fig. 1b,c,d). We chose the caudal-most RSP injection site for the remainder of the study due to the dense and highly specific labeling it yielded in CLA_{RSP} neurons.

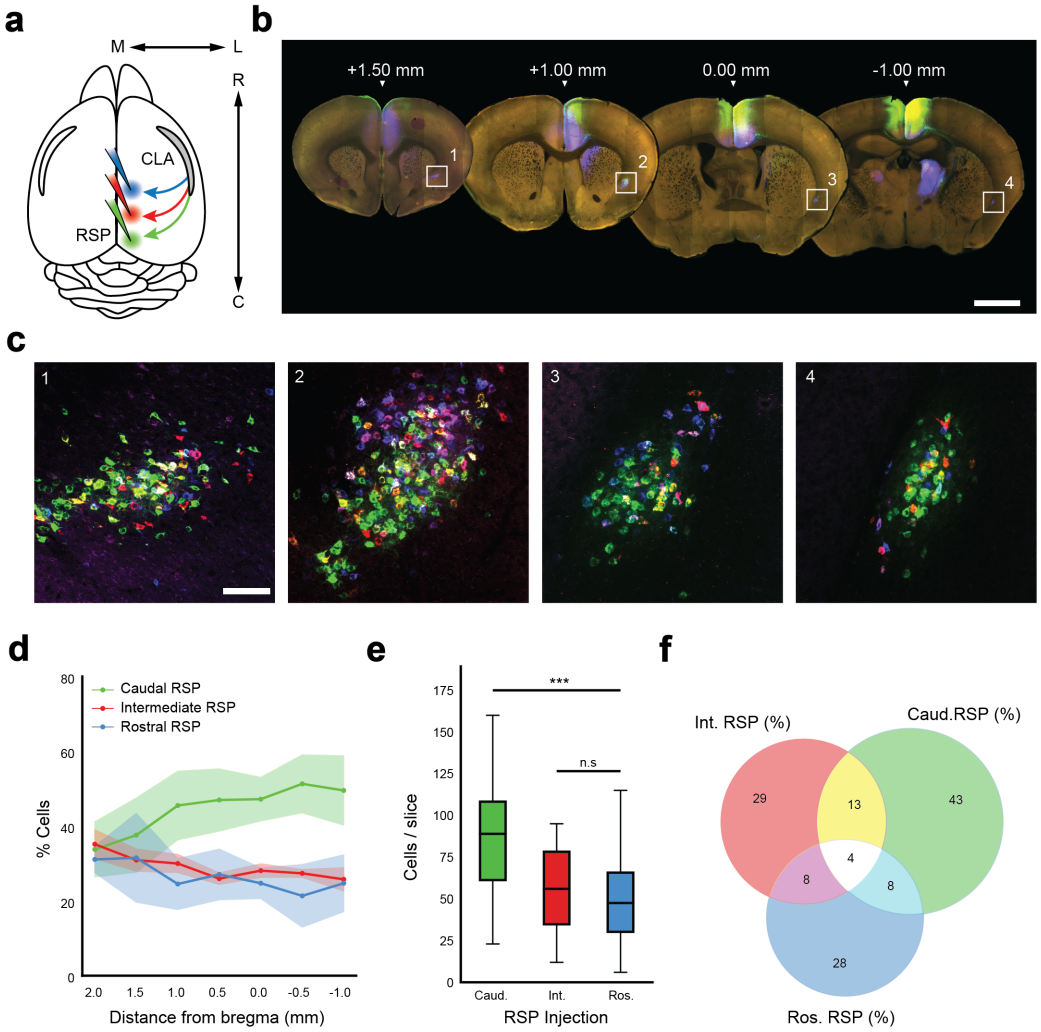

Figure 1: Retrograde tracers label CLA_{RSP}. **(a)** Schematic of the injection strategy using three CTB conjugates in different rostrocaudal regions of RSP. **(b)** Representative whole-slice images of a mouse brain spanning the approximate rostrocaudal axis of the CLA_{RSP}. **(c)** Insets of **b** of the CLA_{RSP}. **(d)** Proportion of neurons labeled from each injection site in **a-c**. Proportions normalized within each rostrocaudal section. Sections matched manually between animals (n = 3 mice). **(e)** Box-and-whisker plots displaying the range of cells labeled across slices in **d** for each injection site. **(f)** Caudal injections of CTB labeled the largest proportion of cells. Scale bars: **(b)** 1 mm, **(c)** 100 μm.

2.2 Comparison of CLA_{RSP} to known markers of CLA

We next compared known immunohistochemical markers of the CLA against retrograde labeling of CLA_{RSP} neurons to obtain a better understanding of the intraclaustral localization of CLA_{RSP} neurons. Calcium-binding proteins such as PV[31,32,80,99] and myelin basic protein (MBP)[19] have been previously shown to label

the CLA. PV-rich neuropil and a paucity in MBP labeling give both positive and negative stains for the CLA region. Thus, we chose these two markers against which we compared CLA_{RSP} neurons in a subset of slices from the CLA rostrocaudal axis (n = 3 mice, Fig. 2a).

As in our triple-retrograde experiments (Fig. 1), we found that injection of CTB into RSP labeled CLA neurons across the CLA rostrocaudal axis (Fig. 2b, *left*). We saw a similar trend for MBP (Fig. 2b, *center-left*) and PV (Fig. 2b, *center-right*) when each were labeled using IHC. MBP strongly labeled myelinated structures, such as the white matter of the external capsule, while PV showed bright expression in cell bodies and neuropil, specifically in the CLA and agranular insular cortex (AI). When these signals were overlaid (Fig. 2b, *right*), it became apparent that CLA_{RSP} neurons preferentially localized around the PV-rich plexus in the central CLA region as well as with the gap in fluorescence of the MBP stain. MBP+ fibers could be seen coursing above, around, and below the CTB/PV area but few if any axons appeared labeled by MBP within this same region.

Quantification of average fluorescence across the dorsoventral and mediolateral axes in the CLA region (Fig. 2c) further supported the qualitative observations described above. In the mediolateral case (Fig. 2, *left*), MBP fluorescence was high medially near the external capsule and waned laterally. PV and CLA_{RSP} fluorescence, however, were well-aligned and peaked where MBP signal tended to plateau at a low value. This relationship was, in general, preserved across the CLA rostrocaudal axis. The dorsoventral axis (Fig. 2c, *right*) showed a similar pattern — CTB and PV signals were tightly overlaid across the rostrocaudal axis. In caudal sections, the width of the CTB signal became narrower, indicating a decreased cross-sectional area occupied by CLA_{RSP} that will be addressed in the next section (Fig. 3). Interestingly, MBP signal peaked dorsally to the PV and CTB peaks, dropped to a minimum that was generally aligned to the CTB/PV peak, before rising again ventrally. The dorsal peak in MBP was less pronounced in caudal

sections and the MBP local minimum had a slight ventral offset from the CTB/PV peak in rostral sections.

CLA_{RSP} neurons were demonstrated to overlap with established markers for the CLA along the dorsoventral, mediolateral, and rostrocaudal axes. Based on current anatomical perspectives[19,32,34], CLA_{RSP} neurons were taken to represent a subpopulation of neurons in the ventral or "core" region of the CLA.

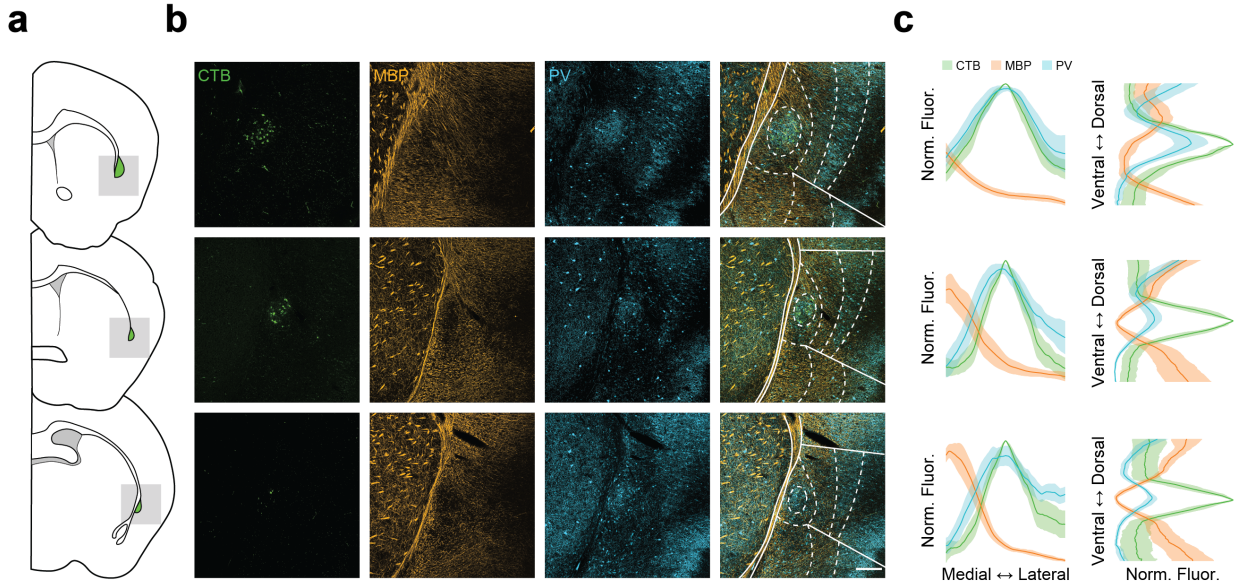

Figure 2: Canonical CLA markers align with CLA_{RSP}. (a) Schematic of tissue sections analyzed at representative rostrocaudal levels of the CLA. **(b)** CTB (green), MBP (orange), and PV (cyan) labeling in the region of the CLA from the shaded areas in **a**. Dashed lines in the right-most panels indicate approximate borders between CLA and other structures/layers. **(c)** Normalized average fluorescence traces for each label in **b** along the mediolateral (*left*) and dorsoventral (*right*) axes of the CLA (n = 6 mice). Anatomical boundaries based on those from the Allen Brain Atlas. Traces aligned to peak CTB signal. Scale bars: **(b)** 100 μm.

2.3 Modeling the spatial organization of CLA_{RSP}

Although CLA_{RSP} neurons have been shown to span the rostrocaudal axis of the CLA[34] (Fig. 1), it remains unclear how the spatial organization of individual CLA_{RSP} neurons changes across this plane. This is a relevant feature of CLA anatomy to understand, especially if there is a modular organization of inputs and outputs that occur along the height and length of the CLA, as has been

suggested[18,34,108,109]. Thus, we opted to investigate CLA_{RSP} structure in greater detail.

Serial coronal sectioning of thin (50 μm) slices of tissue followed by confocal imaging revealed in finer detail how the area comprised by CLA_{RSP} neurons varies with rostrocaudal position (n = 3 mice, Fig. 3a). Beginning rostrally, CLA_{RSP} neurons were dispersed over a large cross-section. Moving caudally, labeled neurons became more compact and occupied a smaller area overall, a finding that could be inferred from data presented elsewhere[34,45,107]. Few, if any, CLA_{RSP} neurons were seen rostral to 2.0 mm bregma and caudal to -1.0 mm bregma.

As noted already, a key difficulty in defining the CLA anatomically is precisely where to place boundaries that separate it from other structures. Historically, the parceling of brain regions has been done using plain structural boundaries (white matter, for instance) or based on data obtained from cytoarchitectural stains[115]. Here, I approached the problem of defining the CLA_{RSP} region in an automated fashion, using image processing and machine learning techniques to allocate CLA_{RSP} neurons to a delimited area (Fig. 3b). Confocal images of each slice across mice were preprocessed through signal denoising and normalization steps (see Ch.7: Materials & Methods). Images of the same section were then aligned to the center of mass (COM) of CTB signal and averaged, producing average images for each rostrocaudal coronal plane. An active contour model was then applied to each average image in turn, which produced the lowest energy, optimally smoothed contours of the CLA_{RSP} region.

As expected, contours taken from rostral sections were large and generally remained so until approximately 1.0 mm bregma before constricting considerably toward the caudal CLA pole (Fig. 3c). Analysis of the area comprised by the contours showed the CLA_{RSP} has a maximal cross-sectional area of 0.25 mm^3 and a minimum area of 0.05 mm^3, a five-fold difference across the length of the CLA. The inter-cell distance across this span reflected a tightening nucleus — CLA_{RSP} neurons became much more closely spaced in caudal sections, from an average of greater than 50

μm between cells in rostral areas to less than 25 μm in caudal areas (Fig. 3d, *left*). Interestingly, the sections of CLA containing the most CLA_{RSP} neurons centered about 1.0 mm bregma (Fig. 3d, *right*). This aligned the with general transition point between a less dense CLA rostrally to a more dense CLA caudally. Here, the use of retrograde labeling, confocal imaging, and techniques in image processing reveal the gross anatomical organization of CLA_{RSP} neurons.

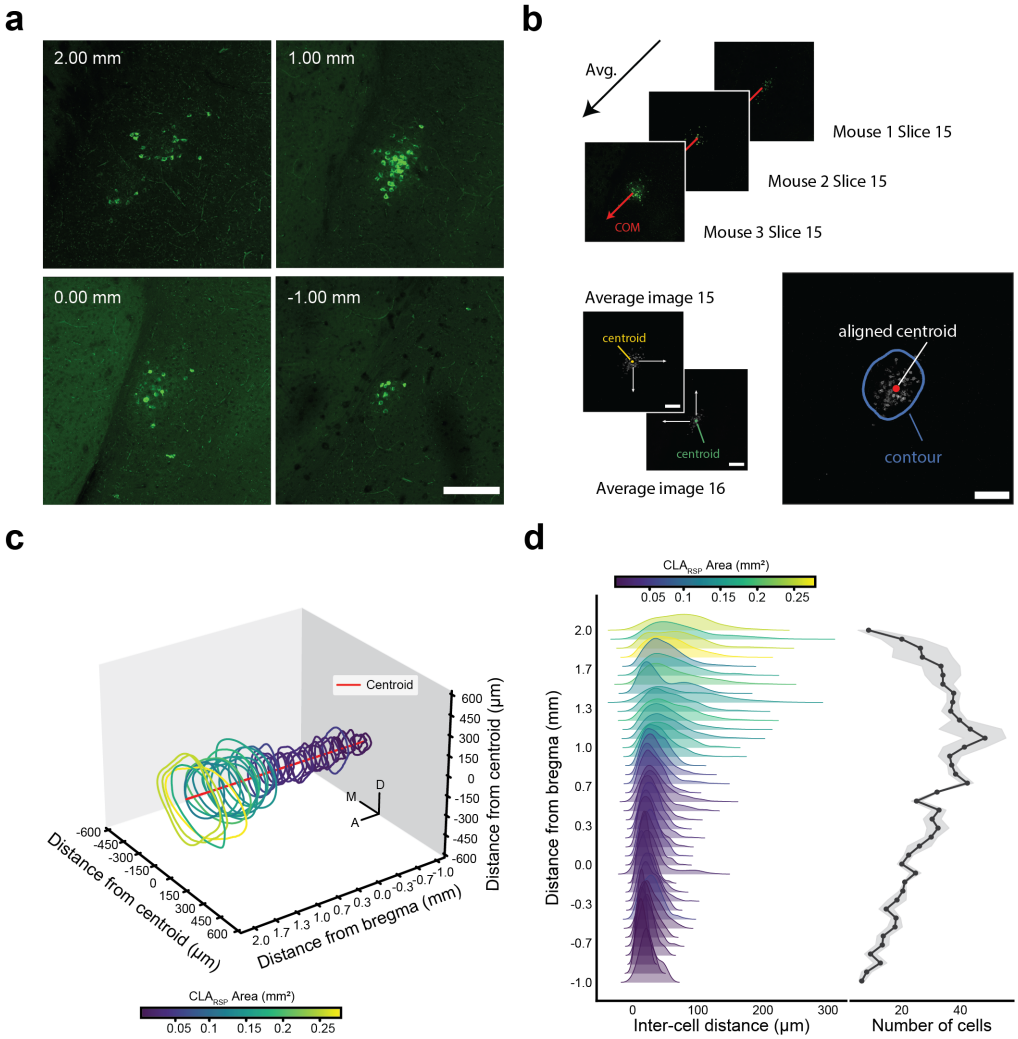

Figure 3: CLA_{RSP} varies in cell density and shape along the rostrocaudal axis. (a) Injection of CTB in caudal RSP labeled CLA neurons from bregma 2.00 mm to -1.00 mm (n = 3 mice). **(b)** Process for producing CLA_{RSP} area contours. Images of CLA in the same slice across mice are COM-aligned and averaged. Average images are then COM-aligned and contours are made for each average image. **(c)** Centroid-aligned contours from average images of the CLA. The cross-sectional area varied widely from rostral to caudal sections. **(d)** Cell density of CLA_{RSP} increased caudally. *Left*: Kernel density estimates of inter-cell distances across the CLA_{RSP} rostrocaudal axis, colored by contour area from **c**. *Right*: Average number of cells counted in all slices from **a-c**. Shaded region indicates the 95% confidence interval. Scale bars: **(a)** 200 μm, **(b)** 100 μm.

2.4 *In vitro* electrophysiological characterization

We repeated our retrograde labeling strategy to target both CLA_{RSP} neurons and non-CLA_{RSP} neurons for acute *in vitro* whole-cell patch clamp electrophysiology (Fig. 4a). CTB+ CLA_{RSP} neurons were readily apparent and were visualized during patching via a combination of transmitted and fluorescence microscopy (Fig. 4b). Electrophysiological profiles were collected using a standardized protocol that was scaled to the rheobase current of recorded neurons and intrinsic properties were collected (53 features; Table2.1, Fig. 4c). All patched neurons were subjected to rigorous automated and manual quality control to be included in the final dataset (n_{total} = 669 cells, n_{final} = 540 cells).

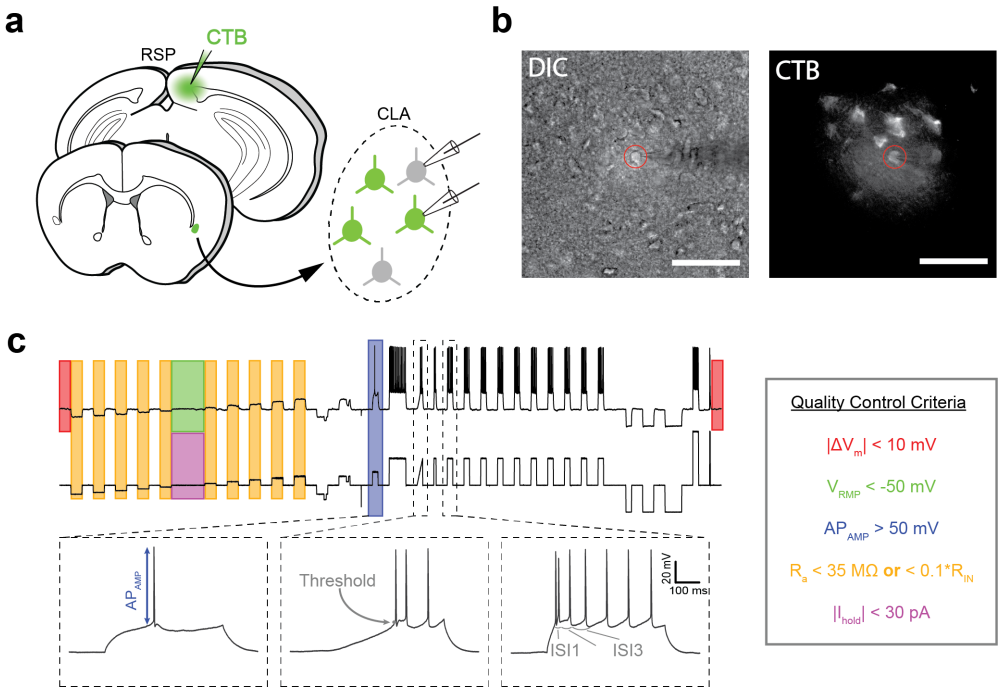

Figure 4: *In vitro* patching strategy. (a) Schematic of the *in vitro* whole cell patch-clamp strategy. CTB was injected into RSP to label CLA. CLA_{RSP} and non-CLA_{RSP} neurons were patched for intrinsic profiling. **(b)** Example transmitted light and CTB fluorescence images obtained *in vitro* of a patched neuron. **(c)** Example trace (top: voltage, bottom: current) and quality control criteria from a standardized intrinsic profile protocol used throughout all experiments. Insets show examples of metrics used in analysis. Quality criteria color-coded to regions from which they are extracted. Scale bars: **(b)** 100 μm, **(c)** 20 mV and 100 ms.

In line with previous accounts[105,130,238], we identified several subtypes of both putative excitatory (n_{EX} = 434) and inhibitory (n_{IN} = 106) neurons based on

intrinsic electrophysiological properties (Table2.1, Fig. 5a, *top*). Delineation of some electrophysiological subtypes was validated by statistical methods and by unsupervised clustering on a dimensionally reduced dataset (Fig. 5b-e). While a significant proportion of putative excitatory neurons were CTB+ and, by definition, CLA_{RSP} neurons, population-level homogeneity among this group impeded further separation using K-means clustering, an unsupervised method of cluster identification (Fig. 5d *right, center*). We additionally attempted clustering via hierarchical (Ward's) clustering and affinity propagation with similar results. The high degree of variability within the excitatory population extracted during dimensionality reduction, especially within key explanatory features such as the delay to spiking, threshold current, and resting membrane potential, confounded attempts to separate clusters. Rather, we relied on a number of intrinsic electrophysiological features – evident within the action potential wave-form for each cell – to define four excitatory cell subtypes (E1-4; Fig. 5b). E1, E2, and E3 could be divided by spike amplitude adaptation normalized from the first action potential where E1 monophasically declined, E2 increased to a plateau, and E3 showed a biphasic pattern, initially declining sharply before recovering slightly. E4 neurons showed a similar pattern to E3 but more pronounced and also could be differentiated from all others by the presence of an afterdepolarization potential (ADP, 3.1 +/- 2.2 mV, $p = 7.4 \times 10^{-9}$).

Putative interneurons, by contrast, could be easily categorized into four groups (high rheobase [HR], fast spiking [FS], low threshold [LT], irregular [IR]) using raw features (Fig. 5c) or unsupervised k-means clustering (average inhibitory silhouette score = 0.853, k = 4 clusters; Fig. 5d *right*, e). While hierarchical and affinity propagation clustering provided similar results to k-means, k-means clustering results were reported here for their superior separability. Interestingly, all clustering methods found a small continuity between FS and LT neural populations in low-dimensional space (Fig. 5d). FS cells were found to fire narrow spikes between 50-200 Hz, while LT cells had a low rheobase and high input resistance. Conversely, HR cells had a large rheobase and low input resistance with a significant delay-to-spike at

threshold. Finally, IR cells fired irregularly and very infrequently compared to other types. Electrophysiological feature comparisons between these cells additionally supported distinct subtypes that differed from excitatory cells (Fig. 5c), in line with cortical literature[74,75,123]. Surprisingly, a small subset of the neurons allocated to interneuron subtypes were found to be CTB+ during patching, suggesting either the presence of further excitatory subtypes mixed within our interneuron cohort or the presence of inhibitory projection neurons within the CLA. These cells, the majority of which were HR neurons, represented 23% of our putative inhibitory subtypes and 5% of total CLA neurons (Fig. 5a *bottom*).

Across all cells, E3 and E4 types were the most prevalent and, within excitatory neurons, the most likely to project to RSP (26% and 32% of all neurons, respectively; Fig. 5f). E1 neurons (18%) comprised a slightly smaller grouping, followed by E2, which made up the lowest proportion of excitatory neurons (5%). Interneurons were collectively 19% of all recorded neurons, a figure which comported with the proportion of inhibitory and excitatory neurons in the CLA reported in immunohistochemical studies[32,80].

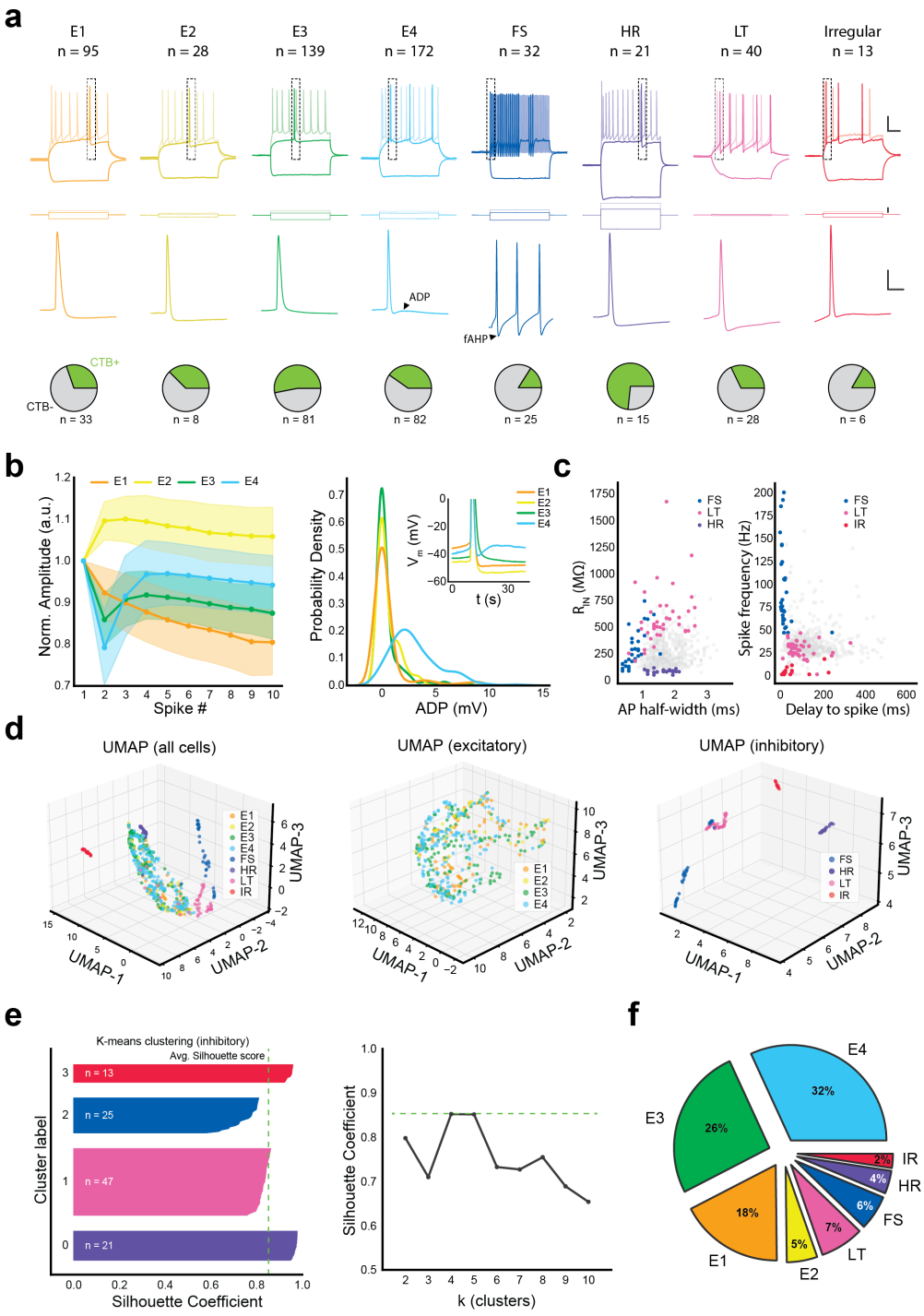

Figure 5: Electrophysiologically-defined cell types of the CLA. **(a)** *Top*: Representative intrinsic profiles of the eight CLA cell types found in *in vitro* electrophysiology. Top traces are from hyperpolarizing and depolarizing current injections at rheobase and 2x rheobase. Single spikes from the dashed black box in the top traces taken at rheobase. *Bottom*: proportion of patched neurons shown to be CTB+ during experimentation. **(b)** *Left*: Comparison of spike amplitude between excitatory types on the first ten spikes during 2x rheobase current injection, normalized to the amplitude of the first spike. *Right*: Kernel density estimate of ADP amplitude across CLA excitatory cell types. *Right, inset*: Example traces of ADP in E4 neurons compared to other types after a spike, aligned to 10 ms before spike onset. **(c)** *Left*: FS, LT, and HR types separated by input resistance and spike half-width. *Right*: FS, LT, and IR types were noticeably different in spike frequency at large current steps (5x rheobase). **(d)** Dimensionality reduction of electrophysiological features accurately separated manually-classified inhibitory, but not excitatory cell types. **(e)** K-means clustering and silhouette analysis of inhibitory neurons. **(f)** Proportion of CLA cell types across the dataset. Scale bars: **(a)** *top*: 20 mV and 100 ms, $top_{current}$: 200 pA, *middle*: 20mV and 10 ms.

Property	E1	E2	E3	E4	FS	HR	LT	IR
R_{in} (MΩ)	350 ± 136	401 ± 163	270 ± 112	310 ± 131	341 ± 189	110 ± 19	669 ± 298	231 ± 119
RMP (mV)	-70.1 ± 5.1	-67.4 ± 4.1	-70.6 ± 5.3	-70.5 ± 4.6	-66.0 ± 5.6	-75.4 ± 6.3	-66.5 ± 4.0	-69.7 ± 5.2
Thre. (mV)	-39.0 ± 5.4	-37.8 ± 4.8	-38.2 ± 5.0	-37.9 ± 4.1	-41.2 ± 7.6	-35.6 ± 3.8	-40.9 ± 5.6	-37.5 ± 5.5
Rheo. (pA)	79 ± 38	66 ± 35	109 ± 50	89 ± 42	97 ± 55	298 ± 65	36 ± 12	163 ± 96
fAHP (mV)	-12.3 ± 3.4	-11.3 ± 3.5	-9.6 ± 3.4	-6.5 ± 3.4	-18.2 ± 4.5	-9.3 ± 3.5	-13.2 ± 5.8	-8.7 ± 3.1
ADP (mV)	0.5 ± 1.7	0.5 ± 0.1	0.5 ± 1.19	3.1 ± 2.24	N/A	1.4 ± 2.2	N/A	N/A
$AP_{1/2}$ (ms)	1.8 ± 0.4	1.7 ± 0.2	1.9 ± 0.5	1.8 ± 0.5	0.8 ± 0.3	1.7 ± 0.4	1.7 ± 0.6	1.9 ± 0.6
Freq. (Hz)	38.9 ± 21.8	37.7 ± 12.4	33.2 ± 11.8	33.6 ± 13.5	93.2 ± 44.0	38.5 ± 10.8	28.8 ± 9.6	6.0 ± 4.9
AP_{max} (mV)	79.3 ± 9.2	68.2 ± 9.3	77.8 ± 9.9	74.9 ± 8.8	75.2 ± 11.8	81.8 ± 6.7	75.9 ± 9.2	83.0 ± 6.7
Spk_{delay} (ms)	188 ± 104	216 ± 106	152 ± 94	137 ± 68	24 ± 42	127 ± 87	99 ± 65	70 ± 75

Table 2.1: Select electrophysiological properties of CLA neurons. All values reported here as the mean ± the standard deviation. Abbreviations: R_{in} - input resistance, RMP - resting membrane potential, Thre. - spike threshold, Rheo. - rheobase current, fAHP - fast afterhyperpolarization potential, ADP - afterdepolarization potential, $AP_{1/2}$ - action potential half-width, Freq. - maximum recorded spike frequency, AP_{max} - maximum spike height at rheobase, Spk_{delay} - delay to spike onset.

2.5 Morphological reconstruction of CLA neurons

From our electrophysiological investigations, we filled and reconstructed 134 recovered morphologies for analysis of their features (33 morphological features; Table2.2 Fig. 6a), a recovery rate of approximately 25%. To be included in the dataset, morphologies were required to have accompanying quality-checked electrophysiology and pass manual inspection. Of this cohort, we were able to count spines along primary and secondary dendrites of 72 reconstructed neurons, approximately 54% of reconstructions. This group included neurons from each electrophysiological class which were categorized as either "spiny" or "aspiny" if dendritic spines were visible and countable or not (Fig. 6b). This distinction was taken as a proxy for excitatory and inhibitory neural cell types, respectively[123,198].

Our results recapitulated previous findings of predominantly spiny neurons in the CLA (81.9%; Fig. 6c) and a smaller (18.1%) group of aspiny neurons[99,103]. These proportions were in general accordance with those found in our *in vitro* intrinsic profiling (Fig. 5f). Within electrophysiologically-defined subtypes, E1-4 had spiny dendrites, consistent with them being excitatory neurons (Fig. 5, Fig. 6d, *top*). FS, HR, LT, and IR types were either aspiny or sparsely spiny in line with cortical GABAergic interneurons[198] (Fig. 6d, *bottom*). HR cells additionally had dense, branching dendritic arbors (Table 2.2) similar to that reported for neurogliaform cells[239]. These distinctions aside, CLA morphologies were highly variable in both general appearance and in coronal orientation (Fig. 6e,f). This said, most CLA neurons tended to avoid projecting medially, directly toward the capsule, many branched dorsally and ventrally while others projected outward laterally or retained most of their dendrites within the CLA itself (Fig. 6f). These patterns did not lead to useful cell type identification after dimensionality reduction and unsupervised clustering, however, and did not overlap with electrophysiological types either in a solely morphological dataset or in a combined electrophysiological dataset (Fig. 6e).

In summary, I demonstrated in this chapter the use of retrograde tracers in defining a subpopulation of claustrum neurons, how this method overlaps with previously defined markers for the CLA, and how the dimensions of this subpopulation changes across the rostrocaudal axis. Additionally, I showed that CLA neurons can be accurately grouped into several subpopulation that vary in both electrophysiological properties and projection target. Finally, I demonstrated the relative heterogeneity of CLA morphologies. These features of CLA anatomy and intrinsic physiology are important aspects, as I will show in the following chapters, when viewed in the light of CLA circuitry.

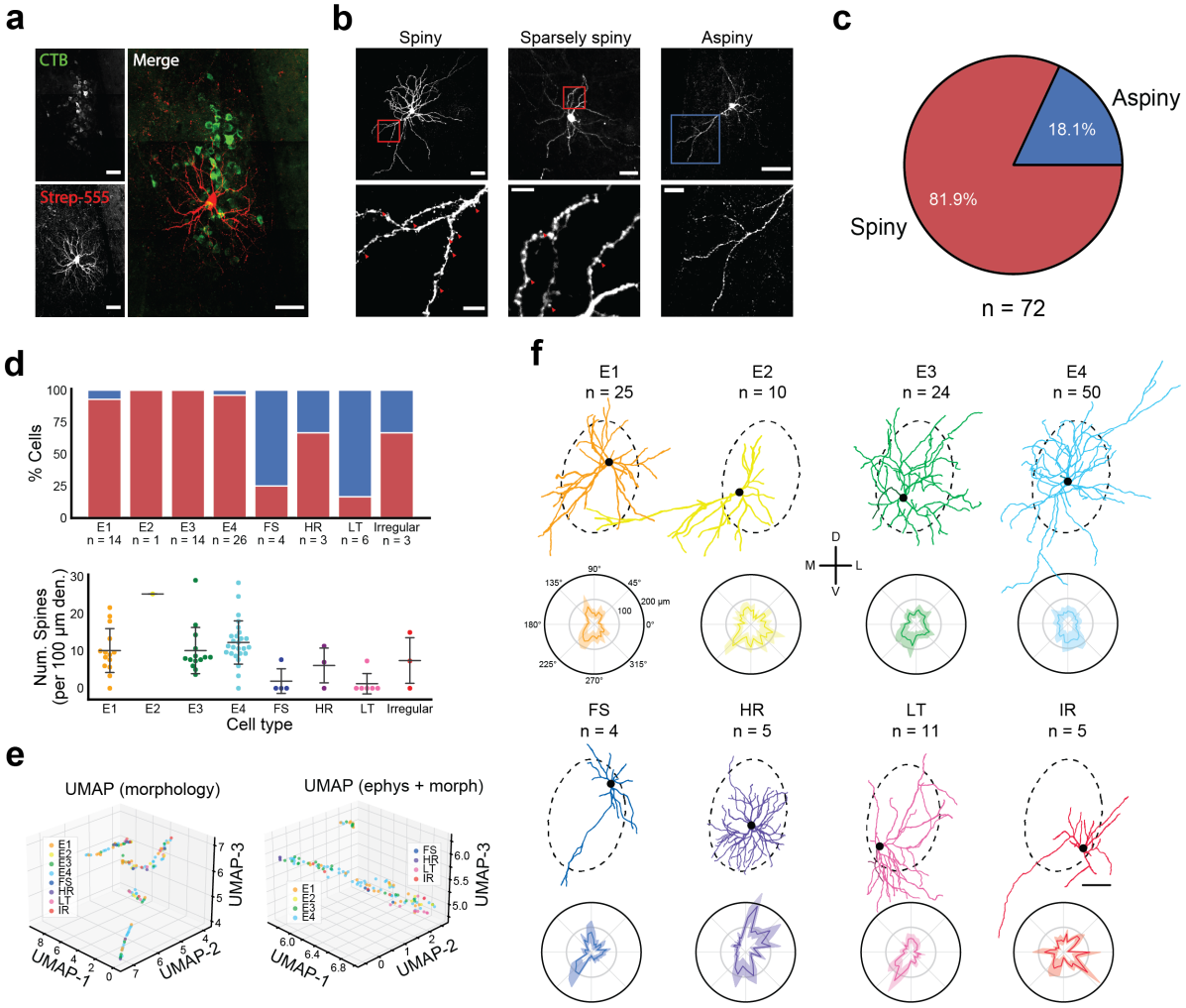

Figure 6: Dendritic morphology among CLA neurons is highly variable. **(a)** Confocal image of a patched neuron filled with biocytin and fluorescently labeled with streptavidin-555 in a field of CTB+ CLA_{RSP} neurons. **(b)** *Top*: Example morphologies of spiny, sparsely spiny, and aspiny neurons. *Bottom*: Insets of *top* showing the presence/absence of dendritic spines (red arrows). **(c)** 72/134 reconstructed neurons were of sufficient image quality to count spines. Shown here is the proportion of spiny and aspiny neurons in the morphological dataset. **(d)** Electrophysiologically-defined types displayed differences in spininess. *Top*: Percentage of cells in each cell type category found to be spiny or aspiny. Interneurons were typically aspiny or sparsely spiny. *Bottom*: Though some interneuron types had sparsely spiny cells, they were less spiny on average than excitatory types. **(e)** Morphologies across neuronal types were highly variable. *Left*: Dimensionality reduction of the morphological dataset found cells from each electrophysiological type in every cluster. Clustering and identification of types was not improved by overlaying the electrophysiological and morphological datasets in this case. **(f)** Example morphologies from each electrophysiological cell type. *Top*: morphologies localized to their approximate location relative to CLA_{RSP}. *Bottom*: Polar wedge analysis showing the average amount of dendritic length within each 10° polar bin. Scale bars: **(a)** 20 μm, **(b)** 50 μm, 10 μm,**(f)** 50 μm.

Property	E1	E2	E3	E4	FS	HR	LT	IR
#Den.	5 ± 2	6 ± 3	5 ± 1	6 ± 2	4 ± 2	6 ± 1	4 ± 2	6 ± 2
#Nodes	14 ± 8	15 ± 8	20 ± 11	19 ± 12	12 ± 7	29 ± 15	11 ± 6	16 ± 11
<Den.> (μm)	349 ± 253	473 ± 294	368 ± 192	427 ± 328	314 ± 144	409 ± 157	416 ± 235	519 ± 521
Max Den.$_{\text{order}}$	6 ± 2	8 ± 2	7 ± 2	7 ± 3	5 ± 2	9 ± 2	5 ± 1	7 ± 3
<Seg.> (μm)	50.3 ± 27.5	64.7 ± 23.0	43.0 ± 19.5	54.6 ± 18.1	46.5 ± 11.5	39.6 ± 6.5	68.1 ± 28.5	58.4 ± 20.7
ND (n/sholl)	3.7 ± 2.5	2.5 ± 1.5	5.3 ± 2.5	4.3 ± 2.7	3.0 ± 2.2	7.2 ± 5.5	2.4 ± 1.8	2.9 ± 1.9
Den.$_{\text{max}}$ (μm)	203 ± 129	298 ± 101	186 ± 99	236 ± 102	187 ± 76	210 ± 116	279 ± 126	284 ± 134
Len.$_{\text{max}}$ ($^\circ$)	20 ± 79	50 ± 94	10 ± 100	10 ± 100	0 ± 120	40 ± 60	340 ± 110	0 ± 120

Table 2.2: Select morphological properties of CLA neurons. All values reported here as the mean ± the standard deviation. Abbreviations: #Den. - number of primary dendrites, #Nodes - number of dendritic nodes, <Den.> - average dendritic length, Max Den.$_{\text{order}}$ - the highest order dendrite, <Seg.> - average dendritic segment length, ND - node density, Den.$_{\text{max}}$ - longest dendrite, Len.$_{\text{max}}$ - the polar bin of the longest dendrite.

3

In vitro investigations of intraclaustral circuitry

Contents

Intraclaustral connectivity likely underpins how the CLA is able to respond to cortical input[35,99] and subsequently drive cortical neurons through its efferent projections[110]. Yet surprisingly little is actually known about intraclaustral signalling due, in large part, to its famously sequestered location beneath the cortex. Previous work[99] has indicated that feed-forward inhibition is the primary motif at play within CLA circuits — cortical afferents jointly excite CLA projection neurons and local interneurons, which then, in turn, inhibit CLA projection neurons. CLA interneurons perform this function in a rapid and synchronized manner through extensive electrical synapses between them. In addition, the authors of this study found little evidence of excitatory-excitatory connectivity in coronal sections during dual-patch electrophysiological recordings. This finding would suggest that CLA circuits with the cortex, especially in anatomically distant parts of the CLA, are

non-overlapping and information relayed to different input domains of the CLA is not propagated through it.

Despite this, other studies using mostly anatomical methods (see, however, Orman, 2015) found evidence of such connectivity, confusing an already complex outlook on intraclaustral signalling[46,128,129]. Given the elongated structure of the CLA, there could plausibly be connectivity specified over the rostrocaudal axis that would be immeasurable in dual-patch recordings without the assistance of techniques to circumvent tissue sectioning-imposed experimental confounds. Thus, I set out to understand intraclaustral connectivity via a dual-retrograde approach to both label and perturb CLA_{RSP} neurons *in vitro*.

3.1 Dual-retrograde strategy for labeling and perturbing CLA activity

To resolve whether excitatory-excitatory connectivity exists – with implications for information transfer within the CLA – my colleagues and I returned to a retrograde neuronal tracing strategy using CTB injections into RSP as in Ch.2 (Fig. 7). In addition, we combined this injection with a retrograde Cre virus (retroAAV-Cre) in RSP and conditional viral expression of AAV-FLEX-ChrimsonR-tdTomato adjacent to CLA for specific labeling and opsin expression (Fig. 7a).

Imaging of fluorescence *in vitro* demonstrated incomplete overlap between CTB-labeled and opsin-expressing neurons in the CLA (Fig. 7b). This implied two experimental caveats: 1) that uptake and eventual labeling by CTB and retroAAV-Cre occurs with differential penetrance and 2) that the spread through tissue of AAV-FLEX-ChrimsonR-tdTomato occurs within a delimited range prior to experimentation, thus, only labeling a subset of neurons expressing retroAAV. This feature was confirmed in *post hoc* histology and confocal imaging (Fig. 7c). CTB, as in previous experiments, reliably labeled the CLA_{RSP} core all along the CLA rostrocaudal axis. AAV-ChrimsonR-tdTomato was visible in the soma of CLA_{RSP} neurons in regions approximately 200-400 μm from the injection site (1.00

mm rostral to bregma, see Table7.1). In rostral and caudal CLA regions, CLA_{RSP} neurons were labeled only by CTB and surrounded by a field of tdTomato+ CLA_{RSP} axons, presumably from cells whose soma was located nearer the CLA injection site. In caudal regions specifically, CLA_{RSP} axons appeared to avoid the CLA_{RSP} core labeled by CTB+ neurons almost entirely (Fig. 7c, *lower right*). This pattern was not observed in rostral CLA, though the region occupied by florescent axons was larger than in posterior regions, congruent with our modeling results (Fig. 3) and literature on CLA structure[18,19].

Because of the differential expression and labeling between AAV-ChrimsonR-tdTomato and CTB, we could address synaptic connectivity between separate subpopulations of CLA neurons – CLA_{RSP} and non-CLA_{RSP}. Further, because this method does not rely on intact axons to measure connection probability but simply whether a CLA neuron receives excitatory CLA input or not, we could record neurons at any point in the CLA irrespective of the soma location of presynaptic cells.

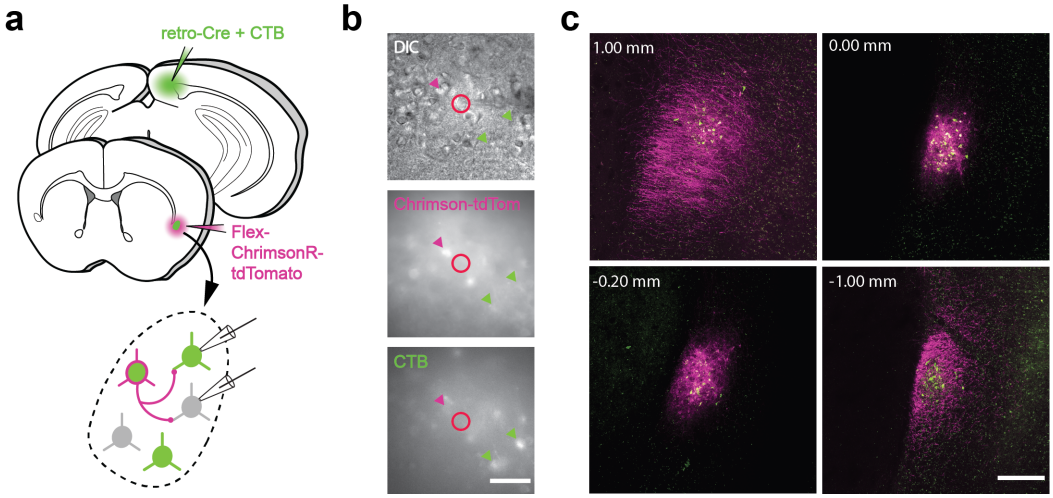

Figure 7: Dual-retrograde labeling in CLA_{RSP} **(a)** Schematic of the injection strategy retroAAV-Cre and CTB in RSP and AAV-FLEX-ChrimsonR-tdTomato in the CLA. **(b)** Example *in vitro* images taken using transmitted light and fluorescence microscopy. Green arrows: cells labeled only with CTB. Magenta arrows: cells labeled only with tdTomato. **(c)** 10X confocal microscopy images of CTB labeling and ChrimsonR-tdTomato expression at representative points along the length of the CLA. Somatic expression of ChrimsonR-tdTomato was generally restricted to the injection site. Axon labeling could be seen at rostral and caudal locations. Scale bars: **(b)** 50 μm, **(c)** 200 μm.

3.2 Neurons in CLA frequently form excitatory synapses

From the preparation described above, we tested synaptic connectivity in the CLA via whole cell patch-clamp electrophysiology. We used brief pulses of orange (595 nm) LED light to stimulate presynaptic axon terminals throughout the rostrocaudal length of CLA while recording from either CTB+ or CTB- CLA neurons (Fig. 8a). We found that we could evoke excitatory postsynaptic potentials (EPSPs) in the majority (69.5%; n = 32/46) of recorded CLA neurons, although only a small subset of these were CLA_{RSP} neurons (n = 4/11 CTB+ cells responsive; Fig. 8b). Examination of response magnitude and latency among responsive neurons (Fig. 8c) strongly suggest monosynaptic connectivity, as shown in studies of opsin kinetics[218]. Compared to the fast latency (0.69 ± 0.49 ms) of CLA neurons directly expressing opsin, monosynaptically-connected CLA neurons displayed longer latencies (4.9 ± 1.3 ms) that were nevertheless considered too short to have been evoked by a disynaptic connection. *In vitro* imaging of the soma location of recorded neurons with reference to the CLA_{RSP} core additionally indicated that neurons located outside the core but within the field of axonal labeling were more likely to respond to CLA_{RSP} input than neurons located within the core area (Fig. 8d).

We simultaneously acquired intrinsic electrophysiology from recorded neurons and found that both excitatory and inhibitory neuronal subtypes exhibited EPSPs in response to CLA optogenetic stimulation (Fig. 8e). Among inhibitory subtypes, FS neurons exhibited the highest frequency of receiving CLA input, while LT neurons received CLA input at rates comparable to that of excitatory types. Within the excitatory cell subtypes, E1 was more likely to receive local CLA input than E3 and E4 neurons, despite these latter two groups being the predominant subtypes in the CLA. In contrast to previous studies[99], we found that 66% of all responsive neurons were excitatory E1-4 neurons (Fig. 8f). It was additionally observed that projection target significantly modulated the likelihood of intraclaustral responsiveness (p =

0.01 Fisher Exact test; Fig. 8g) but that electrophysiological class, i.e. inhibitory or excitatory, did not (p = 0.45 Fisher Exact test; Fig. 8h).

These experiments collectively point to an extensive intraclaustral connectivity, engaging both excitatory and inhibitory neurons in a manner defined by efferent target. This further supports the idea that CLA contains the necessary circuitry to act as an integrative, excitatory hub for cross-modal associations.

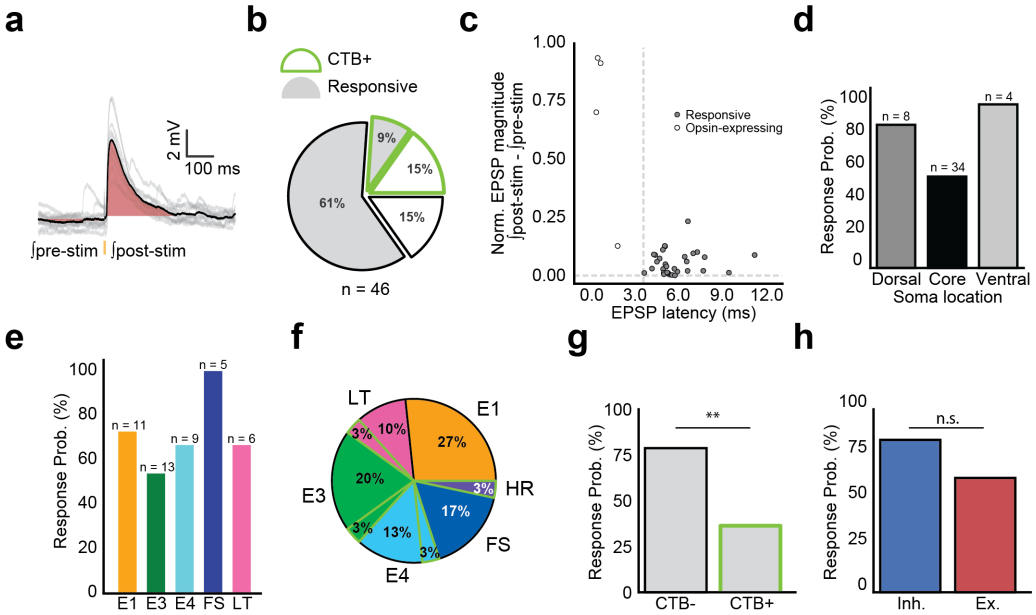

Figure 8: CLA_{RSP} communicate extensively within the CLA (a) Example postsynaptic excitatory potential in a CLA neuron in response to presynaptic CLA_{RSP} input. Shaded regions indicate the area under the curve used as a proxy for response magnitude. **(b)** Proportion of responsive and non-responsive cells in the CLA to CLA_{RSP} input. The majority of responsive cell were non-CLA_{RSP} neurons. **(c)** Comparison of response magnitude and latencies across responsive neurons. Compared to neurons directly expressing opsin, postsynaptic CLA neurons showed slower and weaker EPSPs. **(d)** CLA neurons were most likely to respond to presynaptic CLA_{RSP} input if the soma of the postsynaptic neuron was not located directly in the CLA_{RSP} core. **(e)** Response probability among CLA electrophysiological types. **(f)** Proportion of responsive neurons of each electrophysiological type. **(g)** CTB+ and CTB- neurons show a significant difference in response probability (p = 0.01, Fisher Exact test). **(h)** No difference was seen in response probability between excitatory and inhibitory types (p = 0.45, Fisher Exact test).

4

Single- and dual-wavelength optogenetic mapping of corticoclaustral circuits

Contents

In general, the broad connectome of the CLA is reciprocal with cortex[18], albeit with notable exceptions such as RSP, shown here (Fig. 1) and in other works[46]. CLA receives innervation from many, if not all cortical areas in mice[19], most densely from structures in the frontal lobe[18,19,35,39,109]. Regions of weakest innervation, curiously, appear to be those concerned with primary sensorimotor processing[35,108]. Furthermore, evidence from recent years indicates that the mouse CLA, similar to the CLA of monkeys[92,94] and cats[63,66], is functionally subdivided rostrocaudally[19] and dorsoventrally[109] into regions of innervation from different cortices. Physiological assays bear this out somewhat – neurons of a known projection identity tend to be more or less responsive to input from some cortices and not others[108], underpinning the existence of functional modules in the CLA defined by output target, as shown in

our intraclaustral experiments in Ch. 3. However, a compelling demonstration of the anatomical distribution of cortical axons in the CLA and their electrophysiological significance to a distinct CLA subpopulation has yet to be carried out. Moreover, it is completely unknown whether CLA neurons can be responsive to more than one input cortex at all. Are CLA neurons individually capable of multimodal processing and how does this intersect with cell type and axon/soma location within the CLA?

To answer these questions, I investigated the relationship of cortical inputs and CLA neuron activity *in vitro* using single- and dual-wavelength optogenetic input mapping. I used investigated a number of different cortical areas based on previously shown output modules to the same areas by retrograde neuronal tract tracing[34] (Table 4.1). I again returned to defining CLA_{RSP} neurons using CTB injections into RSP in order to retain anatomical and physiological knowledge of a known CLA neural subpopulation. Below, I describe my findings first in anatomical terms, then in the physiological significance of inputs from single cortices with an emphasis on the spatial organization of axons and CLA neurons. Finally, I use a dual-wavelength optogenetic stimulation strategy to map combinations of cortical inputs to the CLA cell types already delineated here (Ch. 2).

Cortical area	Abbreviation
Orbitofrontal area	ORB
Prelimbic area	PL
Anterior cingulate area, anterior part	ACAa
Primary motor area	MOp
Dorsal auditory area	AUDd
Anteromedial visual area	VISam
Entorhinal area, lateral part	ENTl

Table 4.1: Abbreviations of cortical areas used to assess corticoclaustral connectivity. From the Allen Institute Mouse Reference Atlas (see[4]).

4.1 Anterograde anatomical mapping of cortical afferents

Given the proposed role of CLA as a cortical network hub, we sought to better understand how cortical axons are arranged within the CLA. We again used a retrograde labeling method to distinguish CLA_{RSP}, now in tandem with anterograde viral expression of tdTomato (AAV-ChrismonR-tdTomato) in one of a range of afferent neocortical areas: frontal (ORB, PL, ACAa), motor (MOp), sensory (VISam, AUDd) and parahippcampal (ENTl) cortices (n = 3 mice/injection site, n = 21 mice total, Fig. 9a,b). Coronal sections from the rostral, intermediate , and caudal CLA (Fig. 9c) revealed variation in neocortical pyramidal cell axon innervation about the CLA_{RSP} region along the dorsoventral axis that were nevertheless stable rostrocaudally, proportional to CLA_{RSP} area (Fig. 9d).

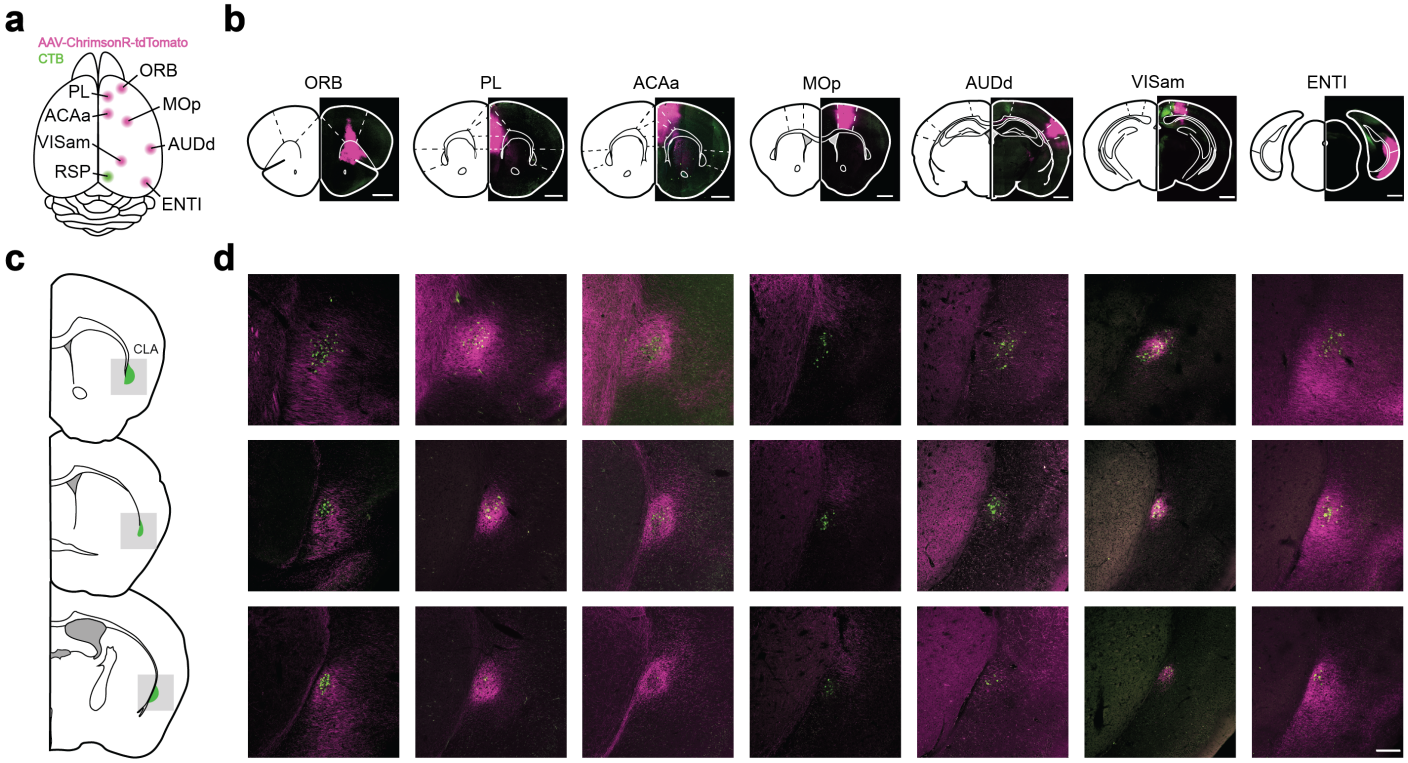

Figure 9: Mapping cortical afferents to CLA by anterograde and retrograde tracing. **(a)** Schematic of a mouse brain viewed from above, labeled with injection sites for AAV-ChrimsonR-tdTomato (magenta) and CTB (green). **(b)** Representative tissue sections and regional boundaries of injection sites in **a**. **(c)** Schematic of tissue sections used for analysis. **(d)** 10X magnification confocal microscopy images of cortical axons and CLA_{RSP} neurons in the CLA from the rostrocaudal locations depicted in **c**. Scale bars: **(a)** 1 mm, **(d)** 200 μm.

We next quantified axonal innervation in the CLA across mice to better to draw statistical conclusion about the spatial arrangement of cortical afferents with respect to CLA_{RSP}, our known regional anchor. For each injection experiment, images of fluorophore-labeled axons were aligned to CLA_{RSP} at 1.00 mm rostral to bregma across mice, averaged, and binned to a 15 μm $\times$ 15 μm pixel heatmap (Fig. 10a). From the qualitative appraisal given in Fig. 9, axons innervated distinct, but overlapping dorsoventral domains, indicative of a core-shell structure akin to previously reported domains seen in output neurons of CLA[34]. Thus, dorsal, core, and ventral regions were defined by the areas above and below the average contour of 1.00 mm rostral to bregma (Fig. 3), including the regions of labeling medial and lateral to the CLA_{RSP} "core" area (Fig. 10a, *left*). Axon fluorescence was normalized and compared between these regions (Fig. 10b).

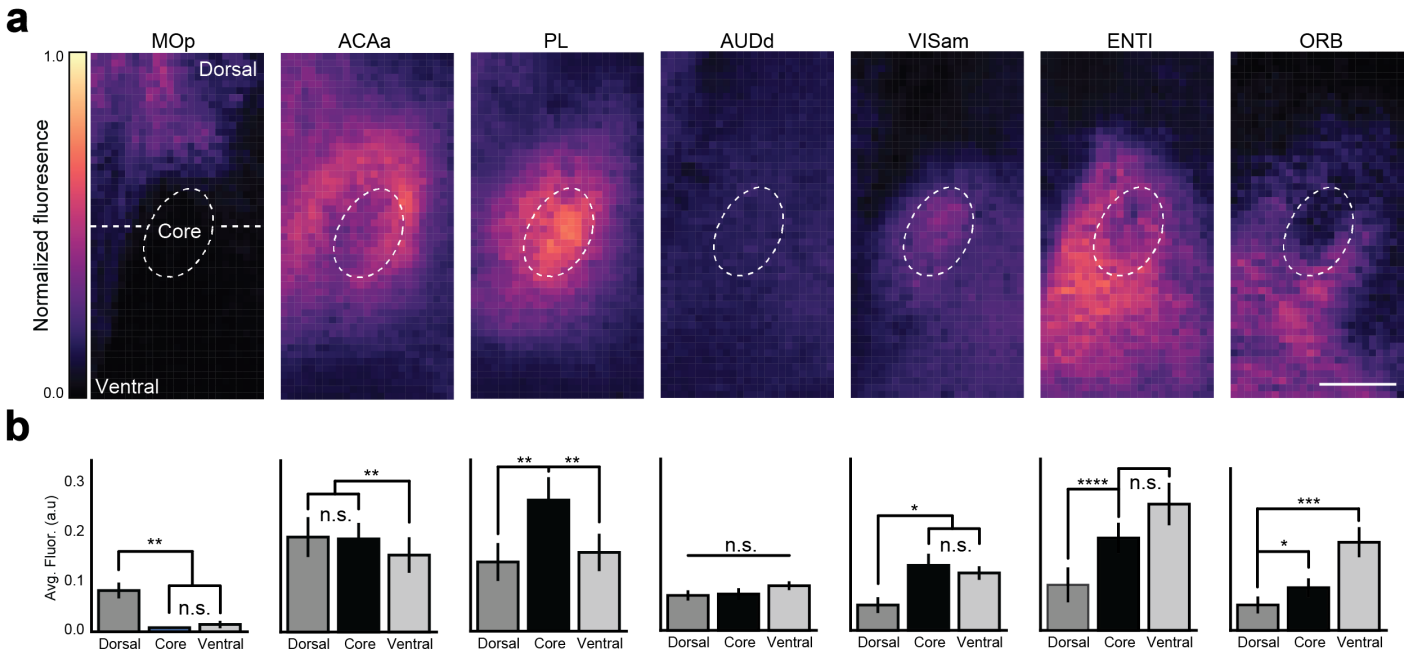

Figure 10: Afferent input to CLA from cortex forms a modular structure. **(a)** Average heatmaps of axonal fluorescence for each cortical site, arranged by projection to dorsal, core, then ventral CLA. Dorsal, core, and ventral regions of CLA appeared differentially innervated by cortex. Core region is the average contour of 1.00 mm bregma defined by CLA_{RSP}. Dorsal and ventral ares comprise image regions surrounding the CLA_{RSP} core. **(b)** Average regional fluorescence for each cortical area in the CLA in **(a)**. Scale bars: **(a)** 200 μm.

Distinct preferences in innervation along the dorsoventral axis could be observed between cortical areas, exemplified by the heatmaps for MOp, PL, and ORB. These

regions are congruent with those for both cortical afferents and CLA efferents found in other studies[34,109], validating the existence of discrete but overlapping CLA modules. In addition, several cortices innervated medially and laterally to CLA_{RSP}, including ACAa, ENTl, and ORB, further underscoring a core/shell arrangement of inputs to CLA centered about CLA_{RSP}.

These results highlighted potential functional modules of the CLA, arranged spatially. How these patterns of innervation might intersect with CLA neuron responsiveness, cell type, or projection identity remained to be seen.

4.2 Single-wavelength optogenetic input mapping

We next investigated the physiological significance of this innervation by optogenetically stimulating presynaptic cortical axon terminals while recording from post-synaptic CLA neurons *in vitro* (Fig 11a). We observed excitatory post-synaptic potentials (EPSPs) in CLA neurons in response to optogenetic stimulation of axons arising from every neocortical injection site (n = 175 cells, 40 animals).

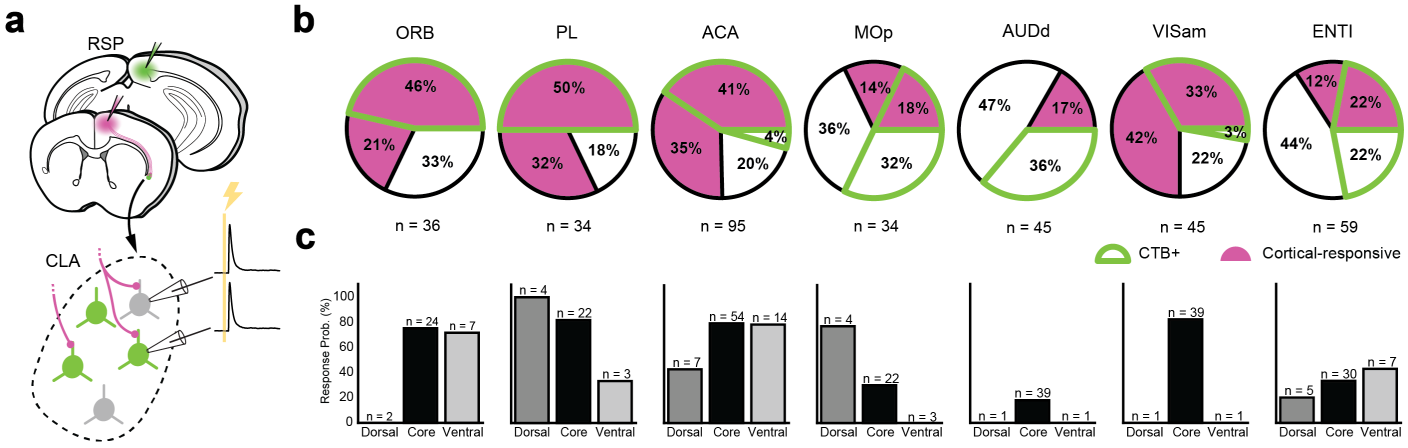

Figure 11: CLA neurons are mostly responsive to frontal cortical input. (a) Schematic of injection and patching strategy. Mice were injected with AAV-ChrimsonR-tdTomato (magenta) in cortex and CTB (green) in RSP. **(b)** Response proportions of CLA neurons for each injected cortical area. **(c)** Response probabilities for each injected cortical area in the CLA regions described in Fig. 10.

We found striking variability in the percentage of responsive CLA neurons when stimulating of axons from different cortical areas – PL and ACAa having the highest probability of evoking a response in both CLA_{RSP} and non-CLA_{RSP} neurons.

Stimulation of axons arising from sensorimotor areas such as AUDd and MOp had the lowest probability of evoking an EPSP with the notable exception of VISam. Further, CLA neurons were more likely to receive input from frontal cortical regions if they projected onward to RSP i.e. were CTB+. This relationship was weaker or absent in other areas, such as MOp and AUDd, suggesting differences in the input-output circuits of these CLA neurons. Additionally, the likelihood of a recording an EPSP in a CLA neuron for each input cortex was roughly congruent with the dorsoventral region of innervation for that cortex (Fig. 10): CLA neurons whose soma was located in the densest region of axonal innervation were generally more likely to respond with an EPSP (Fig. 11c). Results from these experiments further underscore the modularity of CLA anatomy and the interaction between input and output connectivity underlying the circuitry of CLA neurons.

4.3 Dual-wavelength optogenetic input mapping

One of the posited functions of CLA is to effect sensorimotor "binding" or information integration[21,22,29]. Given the distinct topography of input axons (Fig. 10) and spatial organization of projection targets[34] of the CLA, we next set out to test if single CLA neurons in mice are responsive to more than one cortical region and, therefore, support established models of CLA function. To do so, we sought to combine retrograde tracer injections into the RSP with a dual-color optogenetic strategy, injecting AAV-Chronos-GFP and AAV-ChrimsonR-tdTomato into combinations of the neocortical regions investigated in Ch.4.1-2. However, because of the notable optical cross-talk and excitation in response to blue light from red-shifted opsins noted earlier (Ch. 1.5), we first characterized a sequential stimulation strategy in mice expressing only one type of opsin in a single cortical area (PL; Fig. 12a).

Drawing from previously reported methodology[220,221] of dual-color optogenetic stimulation, we used prolonged orange light (595 nm, 500 ms) to desensitize ChrimsonR opsins and reveal independent blue light-sensitive (470 nm, 4 ms)

Chronos-expressing input (n = 6 mice, 21 cells; Fig. 12b). Doing so revealed that ChrimsonR could be successfully desensitized to blue light through prolonged orange light exposure prior to blue light onset, indicated by a sharp decrease in EPSP magnitude (Fig. 12c, *top*). Chronos opsins retained blue light responsiveness even after prolonged orange light exposure. Postsynaptic potentials to opsin photostimulation in both cases were fast (EPSP latency after 595 nm stimulation: 7.1 ± 1.6 ms, 470 nm: 6.1 ± 1.8 ms; Fig. 12d), indicating that these evoked responses were likely from monosynaptic innervation of CLA neurons by the injected cortex.

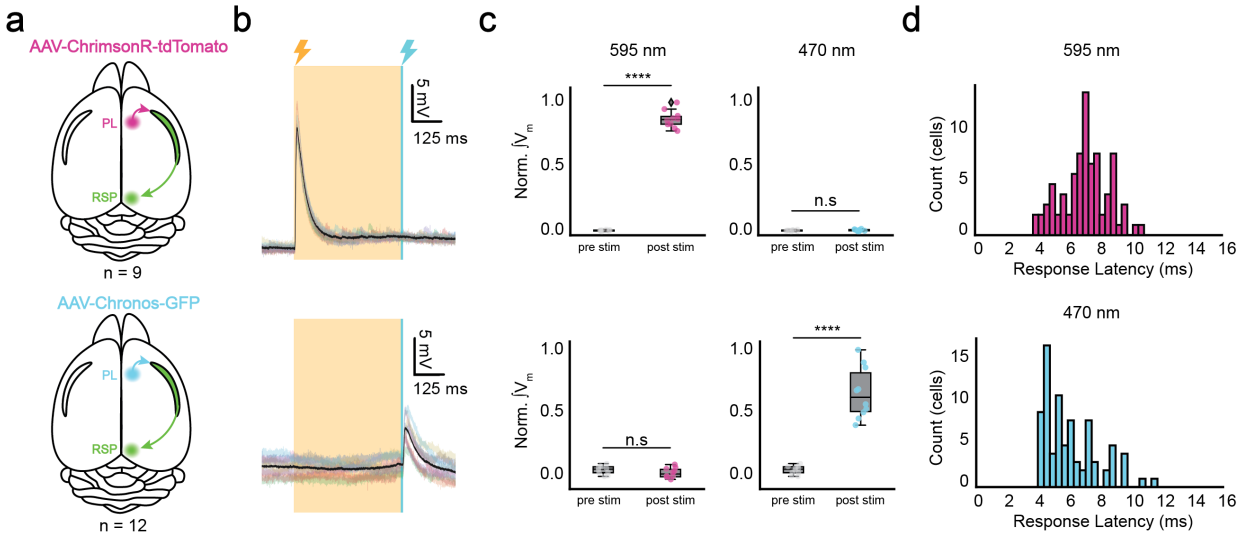

Figure 12: Opsin cross-talk can be eliminated through desensitization and sequential stimulation. **(a)** Injection strategy for control experiments in which only one of AAV-ChrimsonR-tdTomato or AAV-Chronos-GFP was injected into the prelimbic area (PL). **(b)** Example whole cell current-clamp recording of sequential photostimulation. ChrimsonR was successfully desensitized by exposure to prolonged 595 nm light. **(c)** Quantification of response magnitude, normalized to the maximum response within each condition of **b**. ChrimsonR-responsive neurons showed significant responses to 595 nm light ($p \leqslant 0.0001$) but not to 470 nm light after desensitization ($p \geqslant 0.05$). Chronos-responsive neurons showed significant responses to 470 nm light ($p \leqslant 0.0001$) but not to 595 nm light after desensitization ($p \geqslant 0.05$). **(d)** Response latencies for each opsin in all experiments to its peak excitation wavelength.

We next injected AAV-ChrimsonR-tdTomato and AAV-Chronos-GFP into combinations of upstream cortical areas previously characterized (Fig. 9, 10) and assessed the amount of co-innervation of either CLA_{RSP} or non-CLA_{RSP} neurons, i.e. integration of cortical input (Fig. 13a). Opsin-fluorophore expression was evident in axons localized in and around the region of CLA_{RSP} neurons during *in vitro* whole

cell patch-clamp recordings and *post hoc* histology (Fig. 13b). Using the sequential stimulation strategy (Fig. 12), we found CLA neurons displayed one of four response profiles: dual-responsive and integrating (Fig. 13c, *top*), single-cortex-responsive (Fig. 13c, *middle*), or no response (Fig. 13c, *bottom*).

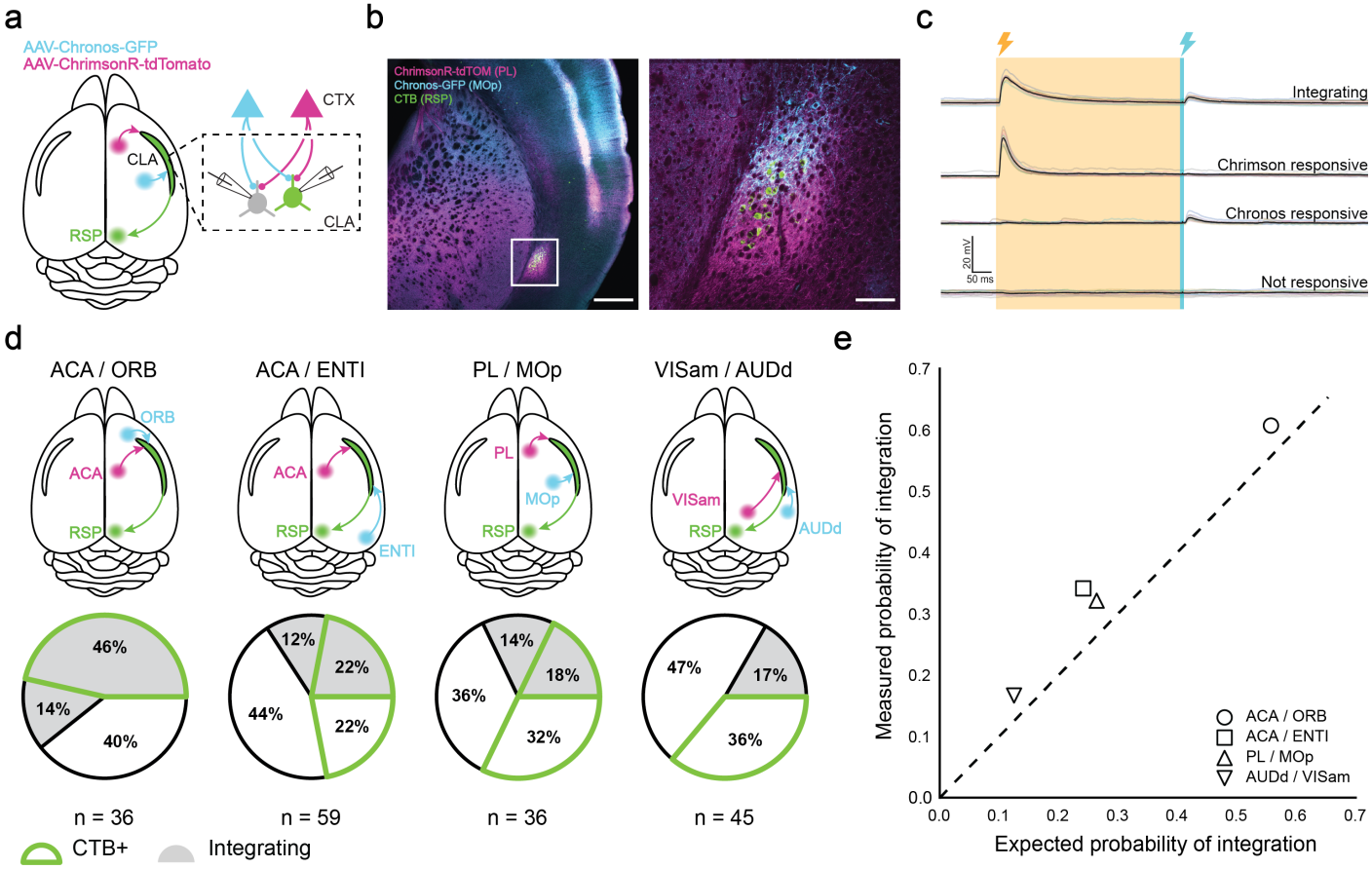

Figure 13: CLA neurons integrate cortical inputs. **(a)** Schematic of the injection and patching strategy for AAV-ChrimsonR-tdTomato and AAV-Chronos-GFP into different cortices of the same animal. **(b)** 4X (*left*) and 10X (*right*) magnification image of axons from PL (ChrimsonR, magenta) and MOp (Chronos, cyan) surrounding CLA_{RSP} neurons (CTB, green). **(c)** Sequential stimulation protocol elicits one four response types in CLA. **(d)** Dual-color optogenetics response and CTB proportions for cortices examined in Fig. 9-11 using the strategy in **c**. **(e)** Expected probability of integration compared to the measured probability *in vitro*. All combinations demonstrated a slightly higher probability during recording than expected. Scale bars: **(b)**,*left*: 500 μm, *right*: 200 μm.

Among all cortical combinations, CLA_{RSP} neurons were more likely to integrate inputs from frontal areas than they were from other areas, similar to our single opsin observations, although integration as a theme was constant throughout all examined pairs (n = 259 cells; Fig. 13d). Integration was most common between ACAa and ORB, while less so when only one or neither of the input cortices were located in

the frontal lobe, and lowest between VISam and AUDd. The measured probability of integration, however, was slightly higher than expected based on the probability of receiving inputs from each cortical area individually, implying integration among single CLA neurons in these experiments occurred at a likelihood higher than would be implied merely from coincidental con-innervation (Fig. 13e).

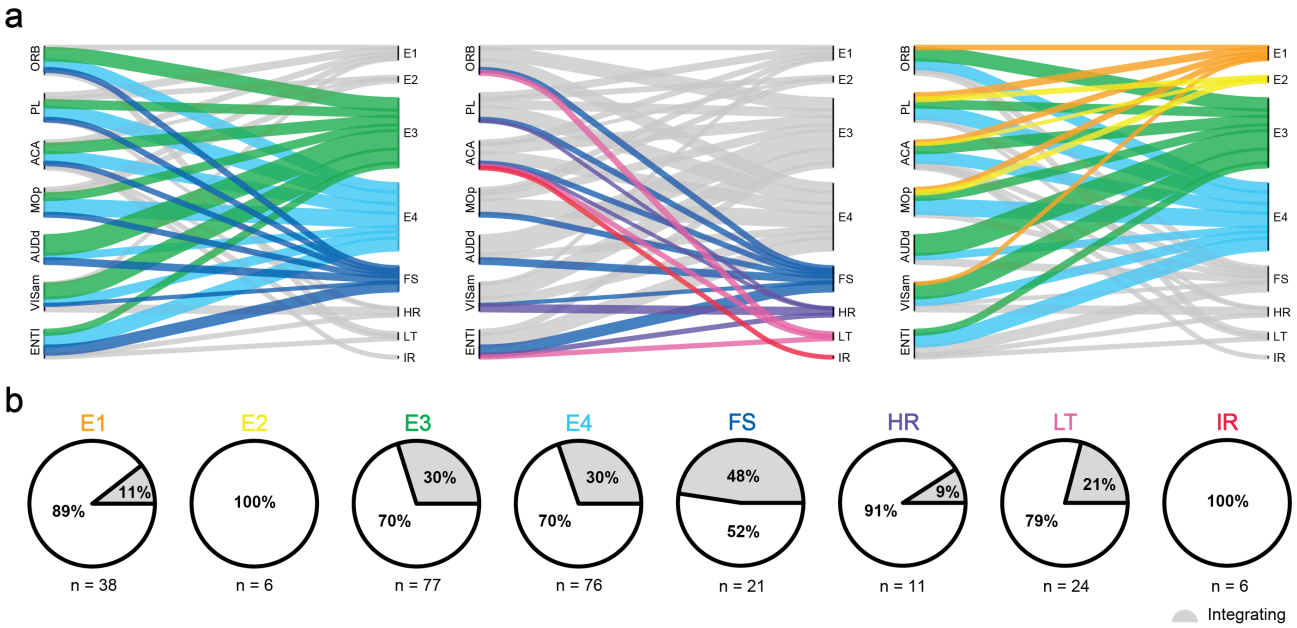

Figure 14: CLA neurons integrate inputs from cortex in a cell type-dependent manner. **(a)** River plots indicating the projection strength of each cortical area to each of the cell types as a proportion of cells showing EPSPs in response to optogenetic stimulation of cortical axons. *Left*: Only E3, E4, and FS neurons received input from all examined cortices. *Center*: Interneuron populations were targeted by different cortical areas to differing degrees. *Right*: Cortical areas displayed a bias for the excitatory types that they targeted. **(b)** Integration across CLA cell types recorded during dual-wavelength optogenetics experiments. E3, E4, and FS neurons were most likely to integrate cortical inputs.

With respect to the electrophysiological identities of CLA neurons themselves, we observed both striking and subtle differences in the proportion of innervation allocated by cortices to each cell type (Fig. 14). Overall, only E3, E4, and FS neurons received input from each examined cortical area, broadly implying these cells act as the main input domain for cortical afferents (Fig. 14a, *left*). Within the interneuron category, FS neurons received the bulk of cortical innervation (Fig. 14a, *center*), while IR neurons (n = 6) received innervation from just one cortex, ACAa. Interestingly, a large proportion of cortical inputs were given to interneuron classes

from ENTl (43%) and VISam (23%), indicating a functional specificity of afferents from these regions. Similarly, excitatory classes were differentially innervated by the cortex (Fig. 14a, *right*). For example, innervation of E3 neurons comprised 50% of all VISam inputs, while only 20% from MOp, despite 50% of MOp inputs being devoted to E4 neurons and 23% by VISam.

Taking innervation by more than one cortex into account, integration of cortical inputs appeared to be more prevalent in certain cell types (Fig. 14b). 30% of E3 and E4 neurons and 48% of all recorded FS interneurons were found to integrate cortical input, irrespective of the cortex in question. A large proportion of LT neurons were also found to integrate despite making up less than 10% of all neurons recorded. E1, E2, HR, and IR types showed little to no propensity for integrating any cortical inputs.

Our data suggest that CLA is broadly connected to neocortex overall and frontal and midline cortical areas in particular. We find that E3 and E4 neurons and FS interneurons are the most likely to integrate information from the cortex, while other excitatory and inhibitory cell types may participate in different circuits or have a dedicated and unitary region of input. These findings support the idea that CLA is a functionally diverse structure with integrative and modality-specific components.

5

In vitro and *in vivo* analysis of claustrocortical connectivity

Contents

Ascribing functionality to CLA circuits is typically done through exploration of its output to cortex. This has occurred in numerous ways experimentally and usually involves conditional expression of a genetic tool in and around the region of the CLA, such as a transgenically-encoded opsin or calcium indicator. In this way, CLA axons and cell bodies can be labeled, measured, and perturbed to understand where they localize, their activity, and the consequences of their in/activation. Pioneering studies in this area have demonstrated broad roles for CLA in global brain processes. Transgenic strategies in the CLA, for instance, have found that the CLA is most active during active behavior and not passive sensory stimulation[37], that the CLA aids in controlling attentional allocation with prefrontal cortex[39], is involved in behavioral state transitions[53,96,111], and that the CLA innervates midline cortices in a layer and region-specific manner[19,132,133] that typically elicits

feed-forward inhibition. However, while these studies can shed light on the general behavioral and cognitive processes the CLA has influence over, the lack of explicit specificity for CLA neurons in most transgenic strategies precludes CLA-specific findings.

We investigated the nature of CLA projections to cortex by returning to our retrograde injection strategy both *in vitro* and *in vivo* using conditionally-expressed opsins and fluorescent calcium indicators in CLA axons. This method is distinguished from similar studies[110,240,241] that employed retrograde strategies by our extensive characterization of the CLA_{RSP} subpopulation, lending a unique lens through we can understand the outputs of the CLA in the context of the neural types represented by a projection-defined subpopulation.

5.1 CLA_{RSP} axons differentially innervate cortex *in vitro*

To explore how CLA influences the neocortex we used retroAAV-Cre conditional expression of opsin in CLA_{RSP} neurons (Fig. 15a), focusing our analysis on ACA and RSP (Fig. 15b,c). In accordance with other studies[19], CLA_{RSP} axons could be seen distributed unevenly across layers in both regions (Fig. 15b). Cells in ACA or RSP were filled with biocytin during recording for *post hoc* analysis of their location within the cortical laminae (Fig. 15c). Axonal fluorescence from CLA neurons varied by cortical layer in these regions (Fig. 15d).

Whole-field optogenetic stimulation of CLA axons evoked both inhibitory postsynaptic currents (IPSCs) and excitatory postsynaptic currents (EPSCs) in cortical neurons during voltage-clamp at holding potentials of 0 mV and -70 mV, respectively (Fig. 15e,f). Observed EPSC latencies of 3 - 12 ms are in line with previous reports of monosynaptic connections studied using optogenetic approaches[218] (Fig. 15f). The longer latency to onset of IPSCs (7 - 15 ms) suggests recruitment of feed-forward inhibition by CLA neurons in both cortical areas, though some short latency IPSCs could be due to direct long-range inhibitory projections. However, IPSC latencies

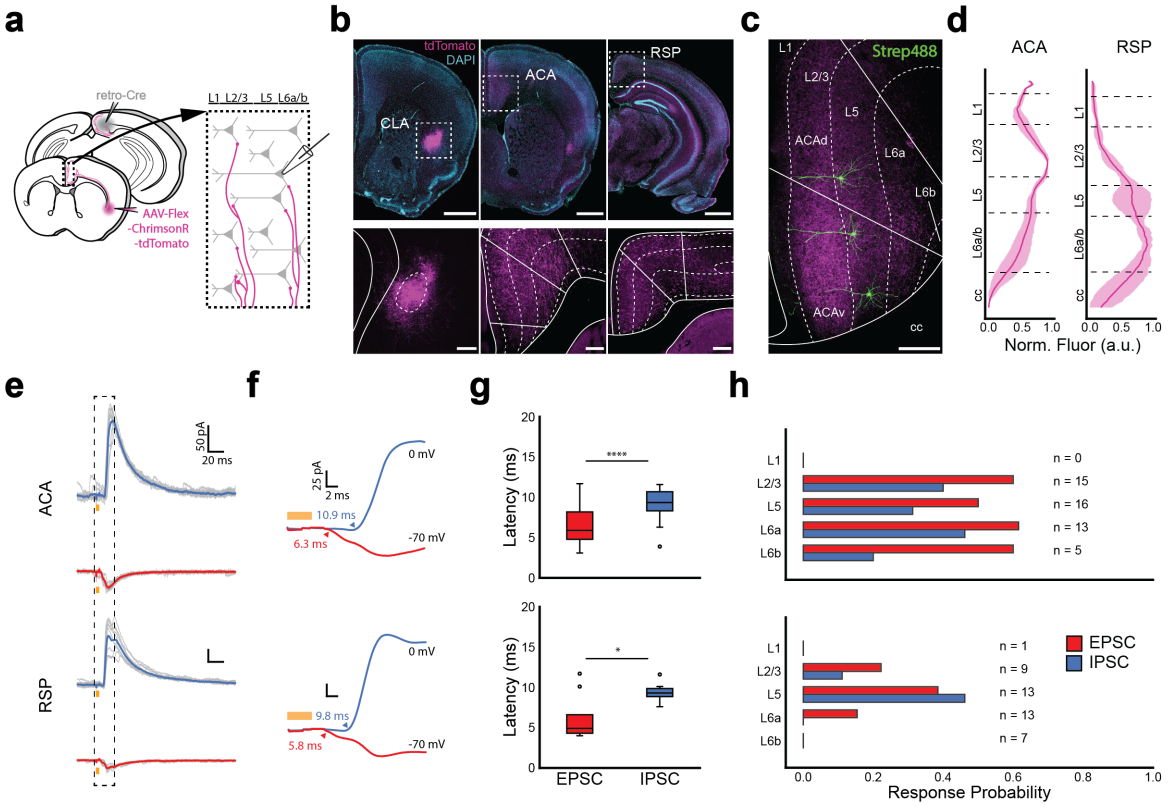

Figure 15: CLA afferents target cortices by layer. **(a)** Schematic of injection and patching strategy for assessing cortex responses to photostimulation of CLA axons. **(b)** Representative coronal sections of opsin expression in CLA cell bodies (left), ACA (middle), and RSP (right). **(c)** Example image of L5 pyramidal neurons patched in L5 of ACA. CLA axons were seen to have a clear laminar distribution. Layer definitions based on the Allen Brain Atlas. **(d)** Normalized CLA axonal fluorescence in ACA and RSP. **(e)** Example traces of IPSC (0 mV, blue trace) and EPSC (-70 mV, red trace) responses from a single neuron in both the ACA and RSP. **(f)** Mean IPSCs and EPSCs from **e** aligned to stimulus onset. **(g)** EPSC and IPSC latency for ACA (top) and RSP (bottom). EPSC and IPSC latency for ACA (top) and RSP (bottom). IPSC latency than EPSC latency in each area (ACA: p = 0.0006; RSP: p = 0.025). **(h)** PSC probability in cortical neurons sorted by the layer in which neurons were patched (n = 92 cells, 10 mice). Scale bars: **(b)** 1 mm (top), 200 μm (bottom); **(c)** 200 μm.

in both ACA and RSP were significantly later than EPSCs on average (ACA: p = 0.00005, RSP: p = 0.025), indicating that these connections were more likely disynaptic. The lack of obvious (low-latency) monosynaptic IPSCs in RSP, the existence of which is suggested by our earlier retrograde tracing (Ch. 5) could be due, in part, to tropism differences between CTB and retro-AAV2-Cre for retrograde uptake by projecting CLA neurons (see Ch. 1.3). Beyond this, it is possible the afferent inhibitory projections from CLA to cortex could be highly selective for cell type. A mechanistic explanation stemming from this could be that inhibitory

projections from CLA preferentially synapse onto local inhibitory neurons in the cortex. This could allow the CLA to flexibly release target areas or layers from inhibition while promoting feed-forward inhibition elsewhere.

PSCs could be evoked relatively evenly across most cortical layers of ACA with the ratio of inhibition to excitation increasing in deep layers (n = 49 cells, Fig. 15g, *top*). In RSP, we observed stronger responses in L5 neurons as compared to other laminae, especially inhibitory responses, though L2/3 and L6a exhibited a higher probability of excitation compared to inhibition (n = 43 cells, 15g, *bottom*). Overall, RSP exhibited excitation-to-inhibition ratios that were skewed toward superficial layers and somewhat to L6, while in ACA, the probability of excitation was loaded more heavily to deep layers. These experiments point to a complex interaction with target cortical areas that are both cortex and layer-dependent.

5.2 CLA axons carry diverse information to cortex *in vivo*

We next sought to understand what signals CLA conveys to the cortex *in vivo*. We injected mice with a retro-Cre virus in ACA and RSP and a Cre-dependent calcium indicator (AAV-FLEX-GCaMP7b) in the CLA. Mice were subsequently implanted with cranial windows centered above bregma for observation during two-photon calcium imaging (117 recordings from 7 animals including 1342 axon segments; Fig. 16a, *left*). Congruent with previous experiments, the expression of GCaMP7b was restricted to CLA neurons and axons from these neurons were visible in the cortex (Fig. 16b). GCaMP7b labeled axons were recorded throughout the cranial window.

During recording, mice were exposed to stimuli intended to evoke responses in different sensory modalities: a flash of light, stimulation of the whisker pad via a piezo-controlled paddle, and/or a complex auditory tone (Fig. 16a, *right*). Stimuli were randomized at 8-11 second intervals and interleaved with a “blank” period in which no stimulus was delivered (Fig. 16b). 47% of tested axons displayed

significant calcium transients to at least one stimulus modality during passive presentation and all modalities could evoke responses in at least some CLA axons (Fig. 16d,e). Interestingly, 85% of stimulus-responsive CLA axons were responsive to one or more multisensory combination, while only 15% of responsive axons were specific to unisensory stimuli (Fig. 16f). This result is consistent with our *in vitro* recordings that suggested input integration among CLA neurons was a common occurrence and/or that CLA neurons receive input from one cortex that contains neurons of mixed-selectivity (Fig. 13). Somatosensory stimuli (whisker) were the most likely to elicit changes in fluorescence, followed by light and then sound. The proportion of responsive axons tended to be highest when stimuli were combined (Fig. 16g).

These data collectively build on previous work aimed at understanding CLA activity in the cortex. CLA axons can carry signals derived from unimodal or multimodal sensory inputs and differentially innervate downstream targets depending on the cortical layer and cortical area in question. Moreover, based on axonal morphology shown in other works[19] and input mapping demonstrated here, it would seem that single CLA_{RSP} neurons appear to be capable of integrating diverse input information and then redistributing the transformed signal across the cortex.

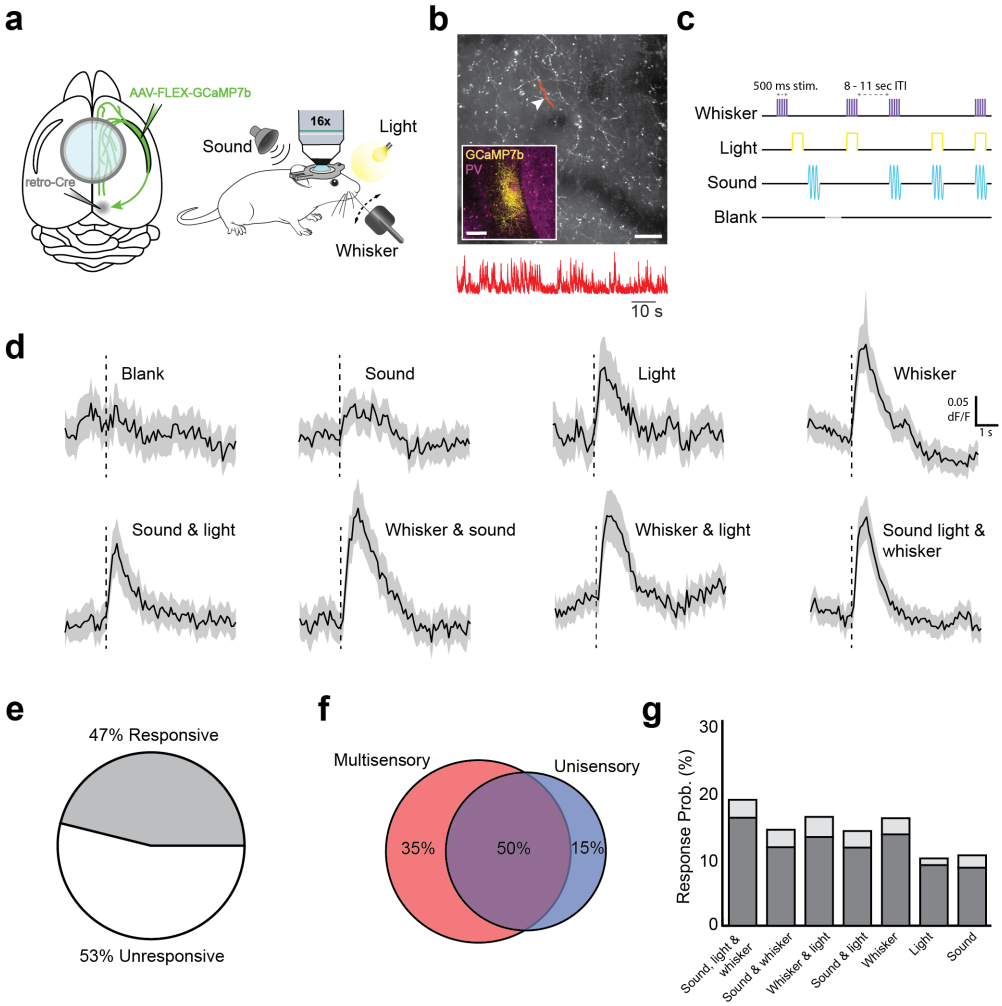

Figure 16: In vivo imaging of sensory-responsive CLA axons in cortex. (a, left) Schematic of injection strategy and window placement over bregma. **(a, right)** Schematic of *in vivo* recording strategy with symbols for stimuli (upper right: white-noise tone, upper left: LED light, lower left: whisker stimulator). **(b)** Example FOV above ACA with CLA axons expressing GCaMP7b. Highlighted area and arrow indicate the axon from which the red trace below was recorded. *Inset*: GCaMP7b expression in CLA from approximately 0.0 mm bregma. **(c)** Passive stimulation protocol using three stimulus modalities. Stimuli and combinations thereof were presented 8-11 s apart (randomized) with a fourth "blank" period where no stimulus was presented. **(d)** Average dF/F traces for each stimulus and combination type across all recorded axons (n = 7 mice, 1342 axons). **(e)** Proportion of all recorded axons displaying responses to any of the stimuli in d. **(f)** Some axons were modulated only by combinations of stimuli **(left)**, both single and multiple stimuli **(center)**, or only single stimuli **(right)**. **(g)** Percentage of all significantly activated axons responsive to each category and combination of stimuli. Light gray bars show the percentage exclusively responsive to each stimulus type. Scale bars: **(b)** 50 μm, 10 seconds; *Inset* = 200 μm.

6

Discussion

The CLA is one of the most densely connected regions of the mammalian brain[242] and has commensurately garnered attention over the long history of its study as a bilateral hub of cortical and subcortical network activity. Breakthrough work on the CLA in recent decades, spurred on many advances in genetic[9] and molecular[19,212,243] tools for measuring and perturbing CLA activity, has reshaped the perspective of this nucleus as an inscrutable "hidden space"[22] to an important player in global behavioral and cognitive functions. Modern hypotheses of CLA function posit that it is involved in processes ranging from sleep[30,53,96] to salience detection[25,99,241] to task engagement[97,110].

Recent studies have begun to address the lingering gaps in information on the nature of the CLA and have made critical insights into its cells and connectivity[108,130,132,244]. These include the disynaptic connectivity of cortical afferents onto CLA projection neurons and interneurons[99] to instantiate feed-forward inhibition, the functional modularity of CLA afferents and efferents[34,108], and the propensity for CLA projection neurons to contact cortical interneurons[131,133]. However, many questions remain, including how combinations of afferents from disparate cortices are arranged onto CLA cell types as well as the details of how the CLA connects to itself. These

unknowns are central to resolving the wider function of the CLA in brain activity as these details are the basic facts on which larger hypotheses are built.

This thesis has attempted to answer some of these remaining questions. First, our experimental preparation made use of CLA connectivity itself[34,46], allowing us to measure and perturb CLA activity *in vitro* and *in vivo*. Doing so provided us with the opportunity to base our conceptual paradigm around a subpopulation of CLA neurons of known projection identity and avoid experimental pitfalls that can come about due to CLA anatomy, location in the brain, and vague genetic delineation from cortex. Further, we defined this subpopulation anatomically and physiologically against other CLA neurons to build a framework from which we could interpret later experiments. Finally, we employed a variety of experimental techniques, including *in vitro* whole cell patch-clamp electrophysiology, optogenetics, immunohistochemistry, neural tract tracing, and *in vivo* calcium imaging to broaden our perspective on the organizing principles of CLA cell types and circuitry.

By exploiting CLA projections to RSP using a retrograde labeling approach, we identified several electrophysiological CLA cell types and assessed their role in corticoclaustral, intraclaustral, and claustrocortical circuits. Our results show that individual CLA neurons integrate diverse information from across the cortex, participate in specific intraclaustral networks, and are capable of broadcasting sensory-related information to the cortex in a region- and layer-specific manner.

6.1 Defining CLA anatomy & physiology

A key difficulty in researching CLA neurons is defining the CLA itself. By using a retrograde tracing strategy in the RSP, we could label and assess a delimited region and subpopulation of CLA neurons[34,46,107]. The RSP is uniquely positioned for use in this technique as it does not receive inputs from structures around the CLA but receives dense innervation from the CLA itself. We found that CLA_{RSP} neurons span the rostrocaudal axis of the CLA and align with previously identified markers of the CLA "core"[31,32,80,243].

We found that retrograde tracing using CTB differentially labeled CLA neurons based on the rostrocaudal injection site in the RSP. Caudal RSP injections tended to label more CLA neurons. Moreover, the low proportion of dual- or triple-labeled CLA_{RSP} neurons in tri-CTB investigations is surprising; other reports in which the full axonal arbor of CLA neurons were reconstructed[19,245,246] show widely branching processes that appear to cover all three injected RSP zones. Given this, one would expect the proportion of triple-labeled neurons to exceed just 4%, reported here. These results may be explained by a number of factors. Firstly, the buildup of more than one CTB in a neuron may be toxic and induce cell death, lowering the apparent proportion of neurons labeled. Secondly, this thesis was not selective for a particular transgenic cell type as were other reconstruction studies —it is possible that highly branching CLA neurons are idiosyncratic to a particular transgenic line. Additionally, because CTB selectively binds gangliosides residing on the surface of the cell membrane[177], only exposed, non-myelinated axonal segments would take up the tracer. Fibers of passage from highly branching CLA axons would likely not take up CTB unless damaged or exposed in some other way. Finally, differences in tracer labeling could reflect different projection pathways from the CLA to the RSP. It is known that the CLA contains several different projection motifs to cortex[19] —the apparent low proportion of co-labeled cells could arise from populations of CLA_{RSP} with different projection patterns.

Analysis of cell density and CLA_{RSP} area in retrograde tracing experiments found significant variability across the rostrocaudal axis of the CLA. Importantly, we showed that a steep transition in the CLA_{RSP} cross-sectional area occurs as the number of retro-labeled CLA_{RSP} neurons peaked. This transition, therefore, represents a notable change in CLA_{RSP} cell density and could indicate the border between two CLA functional modules, described elsewhere[18,19,63]. Significant in this finding is that CLA_{RSP} neurons persist through this transition, despite changes in their spatial organization. These results, in combination with those from our other experiments, offers comprehensive perspective on CLA_{RSP} organization that

proved useful in assessment of the physiological features of the CLA in later experiments.

Disparate accounts have been reported of CLA neurons' intrinsic electrophysiological properties, which poses a challenge when trying to determine the role of CLA neuronal subtypes in brain activity[98,99,130,247]. From our perspective, this disparity could arise from uncertainty over which group of CLA neurons is being recorded between studies. Retrograde labeling of CLA_{RSP} proved useful for targeted investigations of CLA electrophysiology *in vitro* using a standardized protocol[197,199]. From our recordings across a large population of both CLA_{RSP} and non-CLA_{RSP} neurons, it was evident that a heterogeneous mix of spiny, excitatory neurons and aspiny, inhibitory neurons exist in the CLA. These broad categories could be further subdivided into smaller subgroups consisting of four electrophysiological types in each. Similar to the cortex[10], excitatory neurons were found to be relatively homogeneous from an unsupervised clustering perspective but could nevertheless be differentiated by their AP waveforms and variability in their tendency to project to RSP.

Though direct comparisons are difficult, the E1, E3, and E4 subtypes shown here resembled the excitatory cell types found in another study[130]. Based on the spike waveform, our E1 excitatory type appears most similar to the PN1 group of this study, with both groups showing a striking monophasic adaptation in spike amplitude during prolonged current injections. PN1 cells were also found to have one of the lowest rates of retrograde labeling from cortex, congruent with E1 neurons shown in Fig. 5. Further, their PN2 and PN3-5 subtypes closely matched our E3 and E4 cells, respectively. In the former comparison, both PN2 and E3 neurons displayed biphasic spike amplitude adaptation patterns without the presence of an ADP. In the latter, PN3-5 and E4 neurons also demonstrated this pattern but with an ADP of various sizes.

Only E2 neurons were apparently absent from the excitatory types of Graf et al (2020). However, this could potentially be explained by differences in sample size

and methodology between our two studies: if E2 neurons comprise roughly 5% of all CLA neurons, as shown here, then Graf et al would have recorded from approximately 16 of these neurons (N = 326 recorded cells) had they solely injected RSP with retrograde tracer. Instead, they injected a variety of cortices with tracer, including lateral orbital (LO) and primary motor (MOp) cortices. It is possible that E2 does not project to these other locations or that the CLA modules retro-labeled by projections to these areas was different from that of CLA_{RSP}, thereby biasing cell-targeting during patching (see Fig. 10 and[34]). These factors together would have potentially lowered the likelihood that the E2 neural subtype would be retro-labeled and recorded from. Finally, what few E2 neurons they may have recorded would likely have been allocated to another, larger group.

With respect to inhibitory neurons, low within-group and high between-group variability accurately distinguished subtypes using unsupervised methods. Many of these inhibitory interneuron subtypes are similar to those observed in the neocortex[248]. In addition, we found multiple lines of evidence indicating the existence of a substantial subpopulation of inhibitory projection neurons, which have also been observed in prefrontal cortex, amygdala, hippocampal areas, entorhinal cortex, and the subplate[249–255]. However, this finding has yet to be confirmed by other independent studies. Graf et al (2020), in fact, specifically does not find retrogradely labeled CLA inhibitory neurons as confirmed by IHC[130]. Differences between their study and ours may again be explained by differences in methodology: uptake and transport of CTB and the fluorescent latex microbeads used in Graf et al may occur by different means that may bias findings to particular subsets of CLA neurons. In addition, their smaller sample size of retrogradely labeled neurons (n = 44/326 cells, 13.5%) compared to ours (n = 118/284 cells of known CTB status, 41.5%) suggests lower penetrance of the retrograde label using their method. Adjusting the proportion of projection inhibitory neurons reported here (9% of retrogradely labeled neurons) using the rate of labeling in their study, Graf et al would have expected to see less than four (3.7) retrogradely labeled inhibitory neurons across their dataset. Given this, it is possible that projection inhibitory neurons could

have been miscategorized in their study. As the largest group of such neurons in our findings are HR inhibitory neurons, which bear some similarity to excitatory substypes, Graf et al may have grouped the few projection inhibitory neurons they may have seen into excitatory clusters.

If a cohort of CLA inhibitory neurons are indeed long-range projecting, this not only highlights the similarity of the CLA to other forebrain structures that also display this trait[113] but additionally suggests previously unconsidered functional possibilities for it. These putative monosynaptic inhibitory inputs may provide another route by which CLA exerts a direct suppressive influence on the cortex (see also below).

6.2 CLA circuitry within & without

Hypotheses that position the CLA as affecting synchronization[23,24], cross-modal processing[256,257], or integration[22,29] implicitly rely on a substantive intraclaustral excitatory network to link projection neurons across its considerable length. Conflicting evidence thus far has not been able to deliver a satisfying answer to whether such connectivity exists and, if so, with what specificity[46,99,128,129,247]. Here, we used a dual-retrograde and conditional opsin expression strategy to understand if such connections are present in the CLA. We found that excitatory connections are quite common in the CLA and broadly target most CLA excitatory and inhibitory types. Moreover, these connections are highly likely to be monosynaptic in this case because of the low likelihood of local (within-slice) excitatory connections that could be initiated by opsin stimulation to produce a disynaptic connection, as seen in other studies[99]. That is, due to slicing artifacts, any disynaptic connection would necessitate an intact axon of a local neuron presynaptic to the recorded cell and opsin-mediated synaptic release onto this neuron enough to drive it to spike. Additionally, we observed that this connectivity was less biased toward inhibitory types than previously thought[99], but was influenced more by the output target of postsynaptic CLA neurons. Data obtained here offer critical insights into the

types of computations the CLA is capable of performing given its extensive internal excitatory connectivity. From an functional perspective, these findings suggest that the CLA could perform computations ranging from coincidence detection to winner-take-all input integration where CLA modules responsive to various cortices compare input salience via recurrent excitation and reinforce or temporally synchronize those that induce stronger drive in CLA neurons.

Much like CLA efferents[34], we found that cortical projections to CLA arrange into modules along the dorsoventral axis. Interestingly, certain cortices such as ORB and ACAa "cupped" CLA_{RSP} both medially and laterally in addition to dorsally or ventrally. Physiological investigations of cortical input revealed that CLA_{RSP} neurons are more likely to respond to frontal cortical regions than non-CLA_{RSP} neurons. CLA_{RSP} neurons were also more likely than non-CLA_{RSP} neurons to respond to motor and association cortices. Surprisingly, however, we found that CLA neurons, especially non-CLA_{RSP} neurons, were far more likely to respond to secondary visual cortex input *in vitro*, more so than has been reported in primary sensory cortices[35,108]. These findings both confirm the deep ties between CLA and frontal areas associated with top-down cognitive functions and suggest higher responsiveness to more highly processed sensory information.

The patterning of cortical axons in the CLA of mice is simultaneously segmented, with identifiable dorsal, core, and ventral modules, while also forming an overlapping gradient[109] that blends input streams to CLA neurons. From an anatomical perspective, we thought it very likely that CLA neurons in mice instantiate multimodal integration at the level of single cells given the overlap of cortical afferents within it, despite previous reports of unisensory modules in the CLA of cats and monkeys[63,66,92]. To test whether this was the case, we used a dual-color optogenetic input mapping strategy to assess the responsiveness of CLA_{RSP} neurons and non-CLA_{RSP} neurons to more than one cortical area *in vitro*[258]. Our findings demonstrate that individual CLA neurons are frequently responsive to multiple different inputs. This was especially true for CLA_{RSP} neurons when the

cortices in question were both frontal, while the balance of responsiveness shifted to non-CLA_{RSP} neurons when other cortical areas were involved.

What this "integration" means, at the level of a single neuron, however, is open to interpretation when using this methodology. Due to the overlapping action spectra of ChrimsonR and Chronos opsins and the differences in the photocurrents they elicit (see Ch. 1.5), it was not possible to assess whether coincident inputs from any two cortical areas was additive or subtractive, linear or non-linear, especially as pharmacological control of inhibitory tone was not accounted for. As such, these experiments confirm that neurons within the CLA of mice are, at least, less selective than those seen in monkeys[92] and that dual-response to cortical input is highly dependent on projection target and cell type. Future experiments might eliminate inhibitory currents using gabazine and tightly control the photocurrents elicited by Chronos and Chrimson in order to indirectly understand how postsynaptic CLA neurons may be transforming inputs temporally coincident inputs from cortex.

Our final set of experiments sought to investigate the regional and laminar differences of CLA innervation of the cortex as well as the types of sensory-related information CLA axons convey to their cortical targets. Recent *in vivo* electrophysiological evidence points toward differences in excitatory and inhibitory tone elicited by excitation of CLA cell bodies that varies by cortical area and layer[110,133]. Other studies in single cortical regions find more uniform responses to CLA inputs, generally inhibitory[97,132], although electrophysiological studies in cats have found more variable or bidirectional responses in visual cortices[259,260]. We chose to investigate CLA_{RSP} connections to ACA and RSP *in vitro* and *in vivo* – ACA for the dense connectivity it shares with CLA (and CLA_{RSP}) and RSP for the known properties of neurons that project there. From *in vitro* studies, we found that CLA axons innervate the cortical layers of ACA and RSP differently. The ratio of excitatory and inhibitory response probabilities in ACA neurons slightly favored excitation and was generally equal across layers in ACA but higher overall in deep layers. Supragranular and deep (L6a) layers of RSP were excited by CLA input

whereas L5, by contrast, was more likely to be inhibited than other layers relative to excitation. These results demonstrate the CLA exhibits a variable influence over cortical function that is both region- and layer-dependent.

Our *in vivo* calcium imaging experiments concurrently confirmed that axons of CLA_{RSP} neurons can carry representations of sensory stimuli to cortical regions. Moreover, we found CLA axons were frequently responsive during stimulation, implying the CLA actively participates during the processing of sensory information. This finding contrasts with recent studies in mice[37,38] in which CLA neurons were infrequently responsive to sensory stimulation *in vivo*. The disparity between these results may be explained by methodological differences. Both studies used different methods of labelling CLA neurons: Ollerenshaw et al used a transgenic line (Gnb4) while Chevée et al optotagged neurons based on their projections to somatosensory cortex. While the Chevée et al study used a similar retrograde labelling strategy, they likely still targeted a different subpopulation of CLA neurons[34]. Additionally, both studies also used different techniques to record neural activity. Ollerenshaw et al used calcium imaging to record responses in CLA neurons directly, requiring the implantation of a GRIN lens, which may reduce the transmission of inputs to the CLA. Chevée et al used less invasive extracellular electrophysiological recordings, but this required *post-hoc* confirmation of CLA identity that cannot precisely map each recorded neuron back onto its exact location in the tissue. Finally, we observe the strongest responses to whisker stimulation with a paddle in mice with all whiskers intact, which neither Ollerenshaw et al nor Chevée et al incorporated into their studies (Chevée et al used single whisker stimulation).

6.3 Limitations & future work

Through the course of this exploration into the CLA, my colleagues and I have sought to ameliorate common confounds present in other studies through the diligent use of specific and reliable methods for making the CLA experimentally tractable. Despite these efforts, we nevertheless acknowledge the imperfectness of our approach,

which I duly summarize below along with avenues for avoiding these issues and expanding on our findings in future research.

Firstly, although retrograde labeling and expression methods are cleaner in many respects than transgenic or Cre recombinase-dependent technologies in terms of specificity, they are by no means immune from a bevy of experimental pitfalls that must be noted here. When using such specific methods, the obvious drawback is a lack of penetrance — CLA neurons project widely across the cortex[19] and are rarely limited to a single projection target. As such, using projection-based strategies usually labels only a subset of a subset of CLA neurons. Therefore, thematic claims of CLA circuitry must be understood through this delimited perspective. Subsequent work in this area would do well to combine these methods in order to access different CLA subpopulations simultaneously to invoke a more nuanced view of how projection targets of CLA neurons and their intrinsic properties might be overlaid.

Concerning the delineation of CLA neural cell types, the classic peril arises here that has been described as the "lumpers vs. splitters"[261] dilemma. Often, the demarcations between biological states exist more for our own conceptual convenience than they do in reality. This is reflected in the difficulty of defining excitatory neurons along only a small number of features or even an experimental method[10]. Often times, for biological relevance to emerge from collected data, the most important considerations end up being what is both experimentally convenient and experimentally realistic. Therefore, the categorizations of CLA neurons used here surely represent reality, but only along select facets of it. CLA research conducted in studies hereafter would benefit from a collated database from which a community-wide consensus of cell types can drive further exploration of their attributes and differences.

Difficulties arising from classifying interneuron subtypes could be ameliorated in a more straightforward way. As mentioned above (Ch. 2), discerning specific types of interneurons, even in CLA, can be accomplished via IHC against known

markers, such as PV, SOM, NPY. Future work in delineating CLA interneurons should prioritize confirming the identity of such neurons through whole cell patch-clamp, morphological analysis, and IHC. It is possible through such analysis that some inhibitory neurons found here would be more suited to a putative excitatory class.

Concerning the designation of a subpopulation of inhibitory neurons as cortical-projecting, specifically, the answer is far less clear. While the use of retrograde tracers, in this case CTB, is extremely powerful, it can be prone confounds. It is possible that CTB+ inhibitory neurons found here could have received the label through some indirect means. For example, the rupturing of a projecting excitatory CLA neuron could then release CTB into the extracellular space that is later taken up by non-projecting local inhibitory neurons. Careful confirmation of labeling through post-hoc IHC and more thorough investigations of potentially inhibitory post-synaptic currents promoted by CLA afferents in cortex could help resolve this issue.

The integrative properties of CLA neurons described above do not necessarily imply that the CLA, or even most CLA neurons, are receiving inputs from all areas of cortex, has as been shown in the anatomical literature and in our own. For example, olfactory signals are noticeably absent from CLA inputs and are directed, instead, to dEN. However, recent thinking of CLA anatomy and functionality[243] indicates that the CLA forms a "claustrum complex" with the dEN and deep layers of adjacent cortex – these structures being both genetically and anatomically related. It's possible that some larger functional group including these structures could mediate a much wider range of processes in the brain. Therefore, future work should investigate the CLA, dEN, and other structures individually as well as components of a broader system. For example, anatomical and functional connectivity between the CLA and dEN remains poorly understood and could provide a much broader perspective on both. Conceptually, *in vivo* experiments using olfactory cues could test this functionally through manipulation of CLA-projecting dEN neurons, and

vice versa. Should these connections exist and inter-CLA-dEN carry olfactory signals, then integration of olfactory signals should be observable in the CLA only in the presence of an intact and active dEN. Experiments like these would further the argument of CLA as an integrative hub as well as member of the larger complex.

Finally, we offer here a unique view of the internal workings of CLA circuits by describing the robust excitatory innervation between CLA neurons of different projection identities. However, this is is by no means a complete view. The CLA is undoubtedly a more complex structure than has been described here and has been modified and expanded upon countless ways between species over evolutionary time. The use of retrograde labeling and expression methods allowed us to delve into this circuitry but future work using finer tools and strategies may be able to parse it even further. It remains unclear exactly how intraclaustral circuitry is specified between definitive functional modules (for instance, between visual and motor domains) and intense focus on this aspect of CLA organization will be essential to divining how top-down information from the cortex is transformed by local CLA computations. To this end, electrophysiological tools and high-resolution serial confocal or electron microscopy together could prove extremely powerful. In the opinion of the author this particular aspect of the CLA is perhaps one of the greatest challenges, but among the most rewarding of enterprises, remaining in unraveling how the CLA could be represented in the neural correlates of conscious perception and cognition.

6.4 Summary

This thesis finds that the CLA, specifically CLA_{RSP}, participates in a complex circuit with both the cortex and other CLA neurons that is specified by intrinsic electrophysiological type and efferent projection target. CLA neurons are broadly capable of synthesizing a wide range of cortical inputs at the level of single neurons, a finding that supports the idea of CLA acting as a cortical network hub. The

presence of a robust internal network of excitatory CLA neurons additionally supports the view that the CLA performs local computations. These computations then differentially influence downstream cortical processing in a regional- and layer-specific manner, which may then depend on the specific CLA output modules that are active at the time. The fast monosynaptic connections investigated in this study could give rise to cortical synchronization or oscillations through these integrative and cross-modular CLA networks. Finally, the fundamentally integrative nature of the claustrum at the anatomical and functional levels may provide crucial neural substrates for a diverse and computationally powerful set of roles for brain function.

7

Materials and Methods

Contents

7.1 Animal usage

Animal procedures were subject to local ethical approval and adhered to the United Kingdom Home Office (Scientific Procedures) Act of 1986. Male and female C57BL/6J or Nkx2.1Cre;Ai9 mice were used in these experiments. Mice were

between 3-4 weeks of age when surgery was performed.

7.2 Surgical Procedures

Cortical and claustral injections of viruses and/or retrograde tracers were performed in mice aged p22–40. Briefly, mice were anesthetized under 5% isoflurane and placed in a stereotaxic frame before intraperitoneal injection of 5 mg/kg meloxicam and 0.1 mg/kg buprenorphine. Animals were then maintained on 1.5% isoflurane and warmed on a heating pad at 37°C for the duration of the procedure. The scalp was sterilized with chlorhexidine gluconate and isopropyl alcohol (ChloraPrep). Local anesthetic (bupivacaine) was applied under the scalp two minutes prior to making the initial incision. The scalp was then incised along the midline and retracted in order to expose the skull, which was then manually leveled between bregma and lambda. Target regions were found using coordinates derived from the Paxinos & Franklin Mouse Brain Atlas (3rd ed.)[115] and marked onto the skull manually (see Table 7.1 for coordinates). Craniotomies were performed using a dental drill (500 μm tip) at 1-3 sites above the cortex. Craniotomies were made exclusively in the right hemisphere unless otherwise noted. Pulled injection pipettes were beveled and back-filled with mineral oil before being loaded with one or more of the following: AAV1-Syn-ChrimsonR-tdTomato (Chrimson, 2.10e+13 gc/mL, 250 nL, Addgene #59171-AAV1), AAV5-Syn-FLEX-rc[ChrimsonR-tdTomato] (FLEX-Chrimson, 1.20e+13 gc/mL, 250 nL, Addgene #62723-AAV5), AAVrg-hSyn-Cre-WPRE-hGH (retro-Cre, 2.10e+13 gc/mL, 80 nL, Addgene #105553-AAVrg), AAV1-Syn-Chronos-GFP (Chronos, 2.90e+13 gc/mL, 250 nL, Addgene #59170-AAV1), AAV-syn-FLEX-jGCaMP7b-WPRE (FLEX-GCaMP7b, 1.90e+13 gc/ml, 250 nL, Addgene, Addgene #104493-AAV1), Cholera Toxin Subunit B (Recombinant) Alexa Fluor™ 488/555/647 Conjugate (CTB-488/555/647, 0.1% wt/vol, 80 nL, ThermoFisher C34775/C34776/C34778). Pipettes were lowered to the surface of the pia at the center of the craniotomy and zeroed before being lowered into the brain. The pipette was allowed to rest two minutes prior to injection of substances, at which point injection took place at 5-10 μl/sec. Pipettes were allowed to rest for

ten minutes after injection. The incision was sutured with Vicryl sutures and sealed with Vetbond (3M) after all craniotomies and injections had been made. Mice were then transferred to a fresh cage and allowed to recover. Mice were supplied with edible meloxicam jelly during post-op recovery for additional analgesia.

Mice to be implanted with cranial windows first received intracranial injections as described above. Once fully recovered from the injection surgery, mice were re-anesthetized for window implantation. Surgical preparation, anesthesia, analgesia, and recovery procedures were the same as for intracranial injection surgeries. Following sterilization of the scalp, a section was removed. The skull was then cleaned to remove the periosteum. An aluminum headplate with an imaging-well centered on bregma was then secured in place with dental cement (Super-Bond C&B, Sun-Medical). A 4 mm circular craniotomy centered on bregma was then drilled. After soaking in saline, the skull within the craniotomy was removed. The craniectomy was then flushed with sterile saline to clean any bleeding. A durotomy was then performed over the right hemisphere. A cranial window composed of a 4 mm circular coverslip glued to a 5 mm circular coverslip was pressed into the craniotomy and sealed with cyanoacrylate (VetBond) and dental cement. Mice were then allowed to recover fully before any further experimental procedures.

Table 7.1: Stereotaxic injection coordinates. Dorsoventral coordinates measures from pia.

Target Area	AP (mm)	ML (mm)	DV (mm)
CLA	1.0	3.4	-2.7
RSPr	-1.75	0.50	-1.00
RSPi	-2.25	0.50	-1.00
RSPc	-3.00	0.50	1.00
ACAa	1.34	0.30	-1.25
ACAp	0.11	0.25	0.90
PL	1.50	0.60	-1.80
ORB	2.50	1.20	-1.80
MOp	0.60	1.50	-0.75
ENTl	-4.30	3.50	2.25
VISam	-2.70	1.50	-0.50
AUDd	-2.12	3.75	-0.50

7.3 *In vitro* slice preparation

Acute coronal brain slices (300 μm thick) were prepared from tracer- and/or virus-injected mice (average age at time of experimentation = p52). Slices from virus-injected mice were prepared exclusively 3-5 weeks post-injection. Mice were deeply anesthetized with 5% isoflurane and transcardially perfused with ice cold NMDG ACSF of the following composition: 92 mM N-Methyl-D-Glucamine (NMDG), 2.5 mM KCl, 1.25 mM NaH_2PO_4, 30 mM $NaHCO_3$, 20 mM HEPES, 25 mM glucose, 2 mM thiourea, 5 mM Na-ascorbate, 3 mM Na-pyruvate, 0.5 mM $CaCl_2 \cdot 4H_2O$ and 10 mM $MgSO_4 \cdot 7H_2O$, 12 mM N-acetyl-cysteine (NAC), titrated pH to 7.3–7.4 with concentrated hydrochloric acid, 300-310 mOsm. The brain was then extracted, mounted, and sliced in ice cold NMDG ACSF on a Leica VT1200s vibratome or a Vibratome 3000 vibratome. Slices were incubated in NMDG solution at 34°C for 12-15 minutes before being transferred to room temperature HEPES holding ACSF of the following composition for 45-60 minutes before experimentation began: 92

mM NaCl, 2.5 mM KCl, 1.25 mM NaH_2PO_4, 30 mM $NaHCO_3$, 20 mM HEPES, 25 mM glucose, 2 mM thiourea, 5 mM Na-ascorbate, 3 mM Na-pyruvate, 2 mM $CaCl_2 \cdot 4H_2O$ and 2 mM $MgSO_4 \cdot 7H_2O$, 12 mM NAC, titrated pH to 7.3–7.4 with concentrated hydrochloric acid, 300-310 mOsm. All solutions were continuously perfused with 5% CO_2/95% O_2 from 20 minutes prior to use.

7.4 Cell identification & electrophysiological recording

Individual slices were transferred to a submersion chamber continuously superfused with bath ACSF of the following composition: 119 mM NaCl, 2.5 mM KCl, 1.25 mM NaH_2PO_4, 24 mM $NaHCO_3$, 12.5 mM glucose, 2 mM $CaCl_2 \cdot 4H_2O$ and 2 mM $MgSO_4 \cdot 7H_2O$, titrated pH to 7.3–7.4 with concentrated hydrochloric acid, 300-310 mOsm, held at 32°C, and perfused with 5% CO_2/95% O_2 for 20 minutes prior to use. Neurons were visualized with a digital camera (Hammamatsu ORCA-Flash4.0 V3 C13440) and imaged under an upright microscope (Sutter Instruments) using 10X (0.3 NA, Olympus) and 40X (0.8 NA, Zeiss) objective lenses and transmitted infrared light or epifluorescence in various wavelengths.

CLA neurons were identified in acute slices by one of several methods. First, in the majority of experiments, neurons were patched within the subregion of retrogradely labeled somas following CTB injection in the RSP. Additionally, in most experiments we also used fluorescently-labeled corticoclaustral axons from two different sources to further identify the CLA. In a small subset of experiments in Nkx2.1-Cre;Ai9 animals, we were also able to visualize a tdTomato-labeled dense plexus of fibers in the CLA that matches with previous identifications of the CLA relying on a dense plexus of parvalbumin-positive fibers[31,34,80,99].

Borosilicate glass pipettes (4-8 MΩ, 1-3 μm tip outer diameter) were pulled using a Narishige PC-10 two-step puller with steps at 65.1°C and 44.2°C and filled with an intracellular solution for electrophysiological recordings of one of the following

compositions: 1) 128 mM K-Gluconate, 10 mM HEPES, 4 mM NaCl, 5 mM Mg-ATP, 0.3 mM Li_2-GTP, 2 mM $CaCl_2$, 8.054 mM biocytin, pH 7.2, 285–290 mOsm. 2) 110 mM Gluconic acid, 40 mM HEPES, 5 mM $MgCl_2$, 0.2 mM EGTA, 2 mM ATP, 0.3 mM GTP, 5 mM lidocaine, 8.054 mM biocytin, pH 7.2 with CsOH, 285–290 mOsm.

Whole-cell patch-clamp recordings were made in single neurons using a Multi-Clamp 700B amplifier (Molecular Devices) in current-clamp mode and controlled with custom protocols in PackIO[262]. Briefly, neurons were approached in voltage-clamp (0 mV) with intracellular solution back-filled pipettes under positive pipette pressure and 40X magnification. Negative pressure was applied once a small dimple in the membrane could be seen and was held (-60 mV) until >1 GΩ seal had formed, after which the seal was broken and recording began. Recordings were low-pass filtered at 10 kHz and digitized at 10 or 20 kHz. Results were not corrected for the -14 mV liquid junction potential during current-clamp experiments and the -0.69 mV junction potential in voltage-clamp experiments. The chloride reversal potential in each case was -72 mV and -65 mV, respectively.

To be included for further analysis, patched neurons needed to pass a number of quality-control criteria during recording of intrinsic profiles. These included $R_{access}<$ 35 MΩ or $<$ 20% of R_{input}, relative action potential amplitude at rheobase $>$ 50 mV and a absolute amplitude above 0 mV, I_{hold} $>$ -30 pA, absolute drift from baseline (measured from the beginning of the recording) $<$ 10 mV, and a resting membrane potential $<$ -50 mV.

In most cases, only one CLA neuron was patched per slice to prevent ambiguity during morphological reconstruction. Once recordings were complete, neurons were allowed to fill with biocytin for up to 30 minutes, after which the pipette was withdrawn from the tissue and slices were transferred to 4% paraformaldehyde (PFA).

7.5 Optical system for *in vitro* visualization / photostimulation

The optical system used for *in vitro* visualization and photostimulation combined blue (Thorlabs M470L4), orange (Thorlabs M595L3), and far-red (Thorlabs M625L3) LED paths. Briefly, orange and far-red LED paths were combined via a 50/50 beamsplitter (Thorlabs BSW10R), then passed through a blue/red combining dichroic mirror (Thorlabs DMLP505R). Light was then passed down onto the sample through either a RGB dichroic mirror (Laser2000 FF409/493/573/652-Di02-25x36) for epifluorescence visualization or a "cold" mirror (Thorlabs FM03R) for photostimulation. Tissue was visualized via 850 nm light transmitted through a condenser mounted beneath the slice chamber (Thorlabs M850L3). Incident and reflected light passed through excitation (Semrock FF01-378/474/554/635-25) and emission (Semrock FF01-432/515/595/730-25) filters while in RGB visualization mode.

7.6 Optical system for *in vivo* visualization of CLA axons

All two-photon imaging was performed using a Bruker Ultima 2P+ two-photon microscope controlled by Prairie View software, and a femtosecond-pulsed, dispersion-corrected laser (Chameleon, Coherent). Imaging was performed using a Nikon 16X 0.8 NA water immersion lens. The lens was insulated from external light using a custom 3D printed cone connected to a flexible rubber sleeve. A wavelength of 920 nm and 50 mW power on sample was used for visualizing GCaMP. An imaging rate of 30 Hz and a 512 × 512 pixel square field of view (FOV) were used for all recordings. FOVs were selected across the right side of the cranial window. The approximate coordinates of the center of the FOV relative to bregma ranged from: AP -1.2 mm to +1.3 mm; ML mm +0.3 mm to +1.5 mm; DV -0.03 mm to -0.3 mm.

7.7 *In vivo* sensory stimulation

Once mice had completely recovered from surgery, and after allowing sufficient time for viral expression (> 3 weeks), mice were assessed for GCaMP7b labeled axons in the cortex. Animals were first acclimated to head fixation under the microscope. Next, GCaMP7b expression levels were assessed by eye. Animals in which no GCaMP7b labeled axons could be found in the cranial window were excluded from future experiments. Animals with GCaMP7b labeled axons in the cortex were then used for multisensory stimulation experiments.

Sensory stimuli were delivered using a data acquisition card (National Instruments) and PackIO software. Briefly, custom MATLAB (MathWorks) code was used to generate voltage traces. These traces were then used by PackIO to output timed voltage from the data acquisition card to a white light LED (Thorlabs), a piezoelectric whisker stimulator (Physik Instrumente), and a speaker (Dell). Stimuli lasted 500ms. A complex tone, white LED light, and an oscillating paddle adjacent to the whisker pad were used for auditory, visual, and tactile stimulation respectively. The light stimulus consisted of a flash of white light, the auditory stimulus of a complex sound, and the tactile stimulus of a paddle moving vertically within the mouse's right-hand whiskers.

During each experiment, mice were first head-fixed under the microscope. Imaging was performed in an enclosed hood to minimize visual stimuli, and white noise was used to obscure extraneous sounds. The surface of the cranial window was leveled relative to the imaging plane using a tip-tilt stage (Thorlabs). During each imaging session, FOVs with visible axon expression were selected manually. In the unisensory-only cohort, mice were presented with 60 randomly interleaved stimulus presentations separated by randomly generated 8-11 second inter-trial intervals. These 60 stimuli were randomly drawn from 4 trial types: sound, light, whisker, and blank. In the uni- and multisensory cohort, mice were presented with 120 stimuli randomly drawn from 8 trial types: sound alone; light alone; whisker alone; sound and light; sound and whisker; light and whisker; sound, light, and whisker; and

blank. During blank trials, no stimuli were delivered. The order and the precise number of each trial type were randomly generated each day. After all stimuli were delivered, a new FOV was then selected and the sensory stimulation was repeated. Imaging FOVs were selected based on visible axon expression and were drawn from across the extent of the cranial window. Care was taken to avoid recording from the same axon twice on a given day. However, as axons were only visible when active, and given the contorted and branched shape, separate regions of interest may have included the same axons.

The first round of unisensory data collection involved 5 mice, of which 1 was excluded due to unrecoverable histology (not shown). The second round of data collection involved 7 mice, of which 1 was excluded due to unrecoverable histology (not shown), and two were excluded due to off-target expression in cortex. Two animals were used in both data sets of which one was excluded due to unrecoverable histology (not shown).

7.8 Photostimulation of ChrimsonR & Chronos

In experiments where opsin-expressing viruses were injected into either the cortex or CLA, a number of different optogenetic photostimulation protocols were used. Briefly, 470/595 nm LEDs were used to deliver light pulses (4 ms or 500 ms) through a 40X objective lens. LED power on the sample was titrated to the minimum power required to elicit a response in each cell. 470 nm LED power under the objective lens ranged between 0.069 mW and 3.99 mW and was typically 0.6 mW. 595 nm LED power under the objective lens ranged between 0.61 mW and 4.4 mW and was typically 1.22 mW. With the exception of dual-color sequential stimulation, all light pulses were separated by 10s to allow sufficient time for opsins to resensitize.

For dual-color sequential photostimulation, contributions of each cortical presynaptic input axon expressing either Chrimson or Chronos were assessed separately by photostimulation with 470 or 595 nm light pulses (4 ms). To disambiguate 470 nm-evoked Chrimson responses from 470 nm-evoked Chronos responses, 595 nm

light was pulsed for 500 ms followed immediately by a brief 4 ms 470 nm pulse in order to desensitize Chrimson opsins expressed in presynaptic terminals before Chronos stimulation. All photostimulation experiments were repeated ten times and averaged.

For experiments in which FLEX-Chrimson was expressed directly in CLA neurons via retro-Cre injection into RSP, non-expressing CLA neurons were patched and stimulated using 595 nm light (4ms) at both 0.1 Hz. 595 nm light was typically set at 1.22 mW power on sample. The same protocol was used during voltage-clamp recording of cortical neurons in response to CLA axon stimulation.

7.9 Morphological recovery

Patched tissue was fixed in 4% PFA for 2 hours or overnight as described above. Sections were then removed from PFA and washed 3 x 5 minutes in 0.01M PBS. Sections were then transferred to 0.25% PBST and allowed to incubate in streptavidin for at least three days (1:500 Streptavidin, Alexa Fluor™ 488/647 conjugate, ThermoFisher S11223/S21374). Tissue was then washed 3 x 5 minutes in 0.01M PBS, mounted, coverslipped, and imaged as described below.

7.10 Perfusion & tissue sectioning

Mice were deeply anesthetized with 5% isoflurane before receiving an overdose of pentobarbital via intraperitoneal injection. Mice were then transcardially perfused with 0.01M phosphate buffered saline (PBS), followed by 4% paraformaldehyde (PFA). The brain was then extracted and allowed to fix in 4% PFA overnight. Brains were then moved to 0.01M PBS and mounted for sectioning on a Leica VT1000s vibratome. Slices were sectioned coronally to 50 μm or 100 μm thickness and placed in 0.01M PBS before immunohistochemistry and mounting or stored in tissue freezing solution (TFS, 45% 0.01M PBS, 30% ethylene glycol, 25% glycerol) at -20°C for up to three years.

7.11 Immunohistochemistry & imaging

Mice were perfused and sections were collected as above. Sections were first washed 3 x 5 minutes 0.01M PBS before permeabilization in 0.01M PBS and 0.5% TritonX (PBST) for 2 x 10 minutes. Sections were then blocked for 90 minutes in PBST and 5% normal goat or donkey serum at room temperature, after which they were incubated in primary antibody (mouse anti-MBP 1:500, Merck NE1019, RRID:AB_604550; rabbit anti-PV 1:400–500, Swant PV27a, RRID:AB_2631173; chicken anti-GFP 1:2500, AVES GFP-1020, RRID: AB_10000240) for at least 48 hours at 4°C. The slices were then washed 3 x 5 min in 0.5% PBST followed by incubation in secondary antibodies (goat anti-mouse Alexa Fluor 405 1:500, Invitrogen A31553, RRID:AB_221604; goat anti-rabbit Alexa Fluor 488 1:500, Invitrogen A11034, RRID:AB_2576217; donkey anti-rabbit Alexa Fluor 594 1:500, Jackson ImmunoResearch 711-585-152, RRID:AB_2340621; Donkey anti-chicken Alexa Fluor 488 1:500, Jackson ImmunoResearch 703-545-155, RRID:AB_2340375) for 3 hours. Finally, tissue was washed in 0.01M PBS for 3 x 5 minutes, then mounted and coverslipped.

Once dry, whole slice and CLA images were taken at 4X and 10X magnification (UPlanSApo, 0.16 and 0.4 NA) on an Olympus FV3000 laser scanning confocal microscope. For recovered morphologies, images were taken on the above microscope or on a Zeiss LSM710 confocal laser scanning microscope at 20X magnification and tiled across the z-axis, or on a custom 2p microscope at 16X magnification (Coherent Vision-S laser, Bruker 2PPlus microscope, Nikon 16X 0.8 NA objective). Slices and morphologies were not corrected for tissue shrinkage as a result of fixation.

7.12 Data Analysis & Availability

All analyses were performed with custom routines using Python 3.7.9 and open source packages unless otherwise stated. All processed data and the functions used to generate the figure panels in this study are available upon request from the author.

Electrophysiological analysis

Intrinsic electrophysiological recordings taken in current clamp mode were passed through a series of automated quality-controls before features were calculated and stored for later cell-typing analysis. All extracted feature data is available from the author upon request.

Neurons that passed quality-controls were first sorted manually based on their intrinsic profiles at threshold and 2x threshold current injection. Excitatory and inhibitory neurons were classified together, then independently classified into further subgroups. Automated classification involved a preprocessing step in which the electrophysiological dataset was standardized for feature and for every cell. Principal component analysis (PCA) was then used to reduce the dimensionality of the standardized dataset, producing a neurons $\times$ components matrix, the first three components of which accounted for greater than 85% of the explained variance in the dataset. All components were used in uniform manifold approximation and projection (UMAP), the data from which was plotted and clustered using k-means clustering. Clusters were compared via silhouette analysis and the average silhouette score across samples was used as an indicator of how well unsupervised methods had identified which value of k best represented electrophysiological groups.

Due to poor separation among subclasses of excitatory neurons using the above method, we compared manually sorted groups of excitatory neurons using a select set of electrophysiological features. Values for each feature between groups were compared using non-parametric Mann-Whitney U test and corrected for multiple comparisons with a false-discovery rate of 10% (Benjamini-Hochberg). Feature comparisons for which the correlation between the features was high ($r > 0.7$; e.g. spike rise time and spike rise rate) were ignored for this analysis.

For *in vitro* optogenetic mapping experiments, ten trials for each cell were recorded and averaged. Response magnitudes relative to baseline were calculated as the difference in the integral of the post-stimulus (30 ms after stimulus offset) and

pre-stimulus (30 ms before stimulus onset) periods. Significant responses in current-clamp and voltage-clamp modes were taken as those exceeding three and five standard deviations from the average baseline period, respectively, and validated manually and by Mann-Whitney U tests that were corrected for multiple comparisons via Benjamini-Hochberg false discovery rate analysis with an alpha of 10%. Latencies for significant and non-significant responses were found manually.

Expected probabilities were defined as:

$$p(expected) = p(event_1 + event_{1+2}) * p(event_2 + event_{1+2}) \tag{7.1}$$

Two-photon calcium imaging analysis

Calcium imaging data was preprocessed using Suite2P to automatically segment axonal regions of interest (ROIs)[263]. For the unisensory-only cohort, axonal regions of interest (ROIs) were selected by hand using ImageJ. For the uni- and multisensory cohort, axonal ROIs were automatically selected using Suite2P. Automatically generated ROIs were then curated manually. ROIs were selected based on their morphology and activity traces. We computed $\Delta F/F$ for each axon using the equation:

$$\Delta F/F = (F - \bar{F})/\bar{F} \tag{7.2}$$

where:
$\bar{F}$ = The mean of F across time through the entire session.

For axonal ROIs selected by suite2P, F was first corrected for neuropil fluorescence by subtracting $0.7 * F_{\mathrm{Neu}}$. After calcium traces were exported from Suite2P, all analyses were carried out using custom MATLAB code. Calcium traces were plotted using the gramm software package[264].

Extracted calcium signals were then analyzed to identify axon segments that significantly responded to one or more sensory modalities. First, the calcium signal from 2 seconds before to 6 seconds after stimulus onset was averaged for all

presentations of a given trial type (i.e. whisker alone, whisker and sound) for each axon segment in each FOV. Significantly responsive axon segments were identified by using a non-parametric Mann-Whitney U test to compare the signal in the 1 second before and after stimulus onset. Multiple comparisons correction was performed using the Benjamini-Hochberg false discovery rate analysis with an alpha of 1%.

Morphological reconstruction analysis

Images of filled neurons were processed using ImageJ (v1.8.0_172), then uploaded to the software Neurolucida 360 (MBF) and used as a template for semi-automated, user-guided reconstruction in three dimensions. Neurolucida Explorer (MBF Bioscience) was used to extract a range of dendritic, somatic, and axonal properties from neuronal reconstructions. All cell data was compiled into an online morphological dataset that is available from the authors upon request.

Confocal image analysis

All images used for quantitative analysis in this study were imaged on a confocal microscope at 10X magnification (see Immunohistochemistry & imaging section above for details). Cell counts and cell coordinates were collected and analyzed using ImageJ and custom JavaScript macros. Comparisons between cell counts from injection cites were done using Mann-Whitney U tests, corrected for multiple comparisons by Bonferroni correction. Inter-cell distances were calculated as the smallest euclidean distance between cell somas. Fluorescence traces (**Fig. 2**) were produced by aligning CLA images across mice (n = 6) to the max CTB signal, cropped to the same area, and rotated along the external capsule. Images were then normalized and averaged along the horizontal and vertical axes. The fluorescence profiles were processed in Python and smoothed using a Gaussian filter. The intensity of the signal for each indicator was scaled using min-max normalization.

Contours generated from confocal images of CTB+ neurons in the CLA (n = 3 mice) were made via morphological snakes[265,266] of average images. Briefly, confocal images of the CLA taken from 50 μm-thick sections were thresholded using Otsu's method[267]. A binary erosion algorithm[268] was applied to thresholded images to remove noise from small, punctate autofluorescence above threshold in each image. Processed images was then multiplied by their original counterparts to create denoised, native fluorescence intensity images of CTB+ CLA neurons. Images of the same slice across mice were grouped based on the Paxinos & Franklin Brain Atlas and the Allen Brain Atlas[4,115]. Each image in a group representing a single coronal plane was normalized and aligned to the center of mass (COM) of fluorescence before being averaged into a single image. After generation of these average images for each AP plane, the border of the CLA as defined by CTB+ neurons was found by initializing an ellipse about the COM of CLA fluorescence to act as a boundary for morphological snake active contours. These contours evolve in time and are pulled toward object boundaries until the energy functions reach their minimum. Area for each contour was calculated as the integral for the closed contour path.

Confocal images of cortical axons innervating the CLA were prepared as above and COM-aligned to the CTB signal in the CLA across mice for a given cortical injection (n = 3 mice/injection site). Axonal fluorescence from each image was normalized and averaged to 15 μm x 15 μm bins and displayed as a heatmap.

To determine the amount of dorsal/core/ventral fluorescence within the CLA of each injection experiment, the CLA contour at the AP position of the analyzed image was used as a mask for the core. Dorsal and ventral masks were taken as the regions in the image above and below the core, including medial and lateral regions above and below ½ the core height. Image masks were multiplied to each processed and normalized image within an injection experiment set and fluorescence from that region was averaged pixel-wise. Regional fluorescence was then averaged across mice to obtain a comparison of dorsal, core, and ventral axon fluorescence in the CLA

from each cortical area. Values for each region were compared using independent t-test. Multiple comparisons correction was performed using the Benjamini-Hochberg false discovery rate analysis with an alpha of 10%.

Bibliography

1. Adolphs, R. The unsolved problems of neuroscience. *Trends in Cognitive Sciences* **19,** 173–175 (2015).
2. Markram, H. Seven challenges for neuroscience. *Functional Neurology,* 7.
3. Harris, J. A. *et al.* Hierarchical organization of cortical and thalamic connectivity. *Nature* **575,** 195–202 (2019).
4. Wang, Q. *et al.* The Allen Mouse Brain Common Coordinate Framework: A 3D Reference Atlas. *Cell* **181,** 936–953.e20 (2020).
5. Steinmetz, N. A., Zatka-Haas, P., Carandini, M. & Harris, K. D. Distributed coding of choice, action and engagement across the mouse brain. *Nature* **576,** 266–273 (2019).
6. Siegle, J. H. *et al.* Survey of spiking in the mouse visual system reveals functional hierarchy. *Nature* **592,** 86–92 (2021).
7. Steinmetz, N. A. *et al.* Neuropixels 2.0: A miniaturized high-density probe for stable, long-term brain recordings. *Science* **372** (2021).
8. Campagnola, L. *et al.* Local connectivity and synaptic dynamics in mouse and human neocortex. *Science* **375** (2022).
9. Daigle, T. L. *et al.* A Suite of Transgenic Driver and Reporter Mouse Lines with Enhanced Brain-Cell-Type Targeting and Functionality. *Cell* **174,** 465–480.e22 (2018).
10. Gouwens, N. W. *et al.* Classification of electrophysiological and morphological neuron types in the mouse visual cortex. *Nature Neuroscience* **22,** 1182–1195 (2019).
11. Gouwens, N. W. *et al.* Integrated Morphoelectric and Transcriptomic Classification of Cortical GABAergic Cells. *Cell* **183,** 935–953.e19 (2020).
12. Sawa, A. & Snyder, S. H. Schizophrenia: Diverse approaches to a complex disease. *Science* **296,** 692–695 (2002).
13. Song, J. & Kim, J. Degeneration of dopaminergic neurons due to metabolic alterations and Parkinson's disease. *Frontiers in Aging Neuroscience* **8,** 1–11 (2016).
14. Patru, M. C. & Reser, D. H. A new perspective on delusional states - Evidence for claustrum involvement. *Frontiers in Psychiatry* **6,** 1–14 (2015).
15. Zeng, X. S., Geng, W. S., Jia, J. J., Chen, L. & Zhang, P. P. Cellular and molecular basis of neurodegeneration in Parkinson disease. *Frontiers in Aging Neuroscience* **10,** 1–16 (2018).
16. Stoker, T. B. & Greenland, J. C. *Parkinson's Disease* (2018).
17. Milardi, D., Bramanti, P., Milazzo, C., Finocchio, G., Arrigo, A., Santoro, G., Trimarchi, F., Quartarone, A., Anastasi, G. & Gaeta, M. Cortical and subcortical connections of the human claustrum revealed in vivo by constrained spherical deconvolution tractography. *Cerebral Cortex* **25,** 406–414 (2015).

18. Wang, Q. *et al.* Organization of the connections between claustrum and cortex in the mouse. *Journal of Comparative Neurology* **525,** 1317–1346 (2017).
19. Wang, Q. *et al.* Regional and cell type-specific afferent and efferent projections of the mouse claustrum. *bioRXiv* (2022).
20. Kappers, A., Huber, C. & Elizabeth Caroline, C. The Comparative Anatomy of the Nervous System of Vertebrates, including Man. *Nature* **139,** 650–651 (1937).
21. Edelstein, L. R. & Denaro, F. J. The claustrum: a historical review of its anatomy, physiology, cytochemistry and functional significance. *Cellular and molecular biology* **50,** 675–702 (2004).
22. Crick, F. & Koch, C. What is the function of the claustrum? *Philosophical Transactions of the Royal Society B: Biological Sciences* **360,** 1271–1279 (2005).
23. Smythies, J., Edelstein, L. & Ramachandran, V. Hypotheses relating to the function of the claustrum. *Frontiers in Integrative Neuroscience* **6,** 1–16 (2012).
24. Smythies, J., Edelstein, L. & Ramachandran, V. Hypotheses relating to the function of the claustrum II: Does the claustrum use frequency codes? *Frontiers in Integrative Neuroscience* **8,** 2012–2014 (2014).
25. Mathur, B. N. The claustrum in review. *Frontiers in Systems Neuroscience* **8,** 1–11 (2014).
26. Sperner, J., Sander, B., Lau, S., Krude, H. & Scheffner, D. Severe transitory encephalopathy with reversible lesions of the claustrum. *Pediatric Radiology* **26,** 769–771 (1996).
27. Meletti, S., Slonkova, J., Monti, G., Specchio, N., Krupa, P., Pietrafusa, N., Berankova, D. & Bar, M. Claustrum damage and refractory status epilepticus following febrile illness. *Neurology* (2015).
28. Koubeissi, M. Z., Bartolomei, F., Beltagy, A. & Picard, F. Electrical stimulation of a small brain area reversibly disrupts consciousness. *Epilepsy and Behavior* **37,** 32–35 (2014).
29. Vidyasagar, T. R. & Levichkina, E. An integrated neuronal model of claustral function in timing the synchrony between cortical areas. *Frontiers in Neural Circuits* **13,** 1–8 (2019).
30. Atilgan, H., Doody, M., Oliver, D. K., McGrath, T. M., Shelton, A. M., Tracey, I., Vyazovskiy, V. V., Manohar, S. G. & Packer, A. M. Human leisions and animal studies links the claustrum to perception, salience, sleep, and pain. *Brain* (2022).
31. Druga, R., Chen, S. & Bentivoglio, M. Parvalbumin and calbindin in the rat claustrum: An immunocytochemical study combined with retrograde tracing from frontoparietal cortex. *Journal of Chemical Neuroanatomy* **6,** 399–406 (1993).
32. Real, M. Á., Dávila, J. C. & Guirado, S. Expression of calcium-binding proteins in the mouse claustrum. *Journal of Chemical Neuroanatomy* **25,** 151–160 (2003).
33. Watakabe, A., Ohsawa, S., Ichinohe, N., Rockland, K. S. & Yamamori, T. Characterization of claustral neurons by comparative gene expression profiling and dye-injection analyses. *Frontiers in Systems Neuroscience* **8,** 1–14 (2014).
34. Marriott, B. A., Do, A. D., Zahacy, R. & Jackson, J. Topographic gradients define the projection patterns of the claustrum core and shell in mice. *Journal of Comparative Neurology* **529,** 1607–1627 (2021).
35. White, M. G., Panicker, M., Mu, C., Carter, A. M., Roberts, B. M., Dharmasri, P. A. & Mathur, B. N. Anterior Cingulate Cortex Input to the Claustrum Is Required for Top-Down Action Control. *Cell Reports* **22,** 84–95 (2018).

36. Terem, A., Gonzales, B. J., Peretz-Rivlin, N., Ashwal-Fluss, R., Bleistein, N., del Mar Reus-Garcia, M., Mukherjee, D., Groysman, M. & Citri, A. Claustral Neurons Projecting to Frontal Cortex Mediate Contextual Association of Reward. *Current Biology* **30,** 3522–3532.e6 (2020).
37. Ollerenshaw, D. R., Davis, J., McBride, E. G., Shelton, A., Koch, C. & Olsen, S. R. Anterior claustrum cells are responsive during behavior but not passive sensory stimulation. *bioRxiv,* 2021.03.23.436687 (2021).
38. Chevée, M., Finkel, E. A., Kim, S.-J., O'Connor, D. H. & Brown, S. P. Neural activity in the mouse claustrum in a cross-modal sensory selection task. *Neuron,* 1–16 (2021).
39. Fodoulian, L., Gschwend, O., Huber, C., Mutel, S., Leone, R., Renfer, J.-R., Ekundayo, K., Rodriguez, I. & Carleton, A. The claustrum-medial prefrontal cortex network controls attentional set-shifting. *bioRxiv,* 2020.10.14.339259 (2020).
40. Hubel, D. H. & Wiesel, T. N. Receptive fields, binocular interaction and functional architecture in the cat's visual cortex. *The Journal of Physiology* **160,** 106–154 (1962).
41. Poggio, G. F. & Poggio, T. The analysis of stereopsis. *Annual Review of Neuroscience* **VOL. 7,** 379–412 (1984).
42. Katz, L. C. & Shatz, C. J. Synaptic activity and the construction of cortical circuits. *Science* **274,** 1133–1138 (1996).
43. Akerman, C. J., Smyth, D. & Thompson, I. D. Visual Experience before Eye-Opening and the Development of the Retinogeniculate Pathway. *Neuron* **36,** 869–879 (2002).
44. Kitanishi, T. & Matsuo, N. Organization of the claustrum-to-entorhinal cortical connection in mice. *Journal of Neuroscience* **37,** 269–280 (2017).
45. Zingg, B., Dong, H.-W., Tao, H. W. & Zhang, L. I. Input-output organization of the mouse claustrum. *Journal of Comparative Neurology* **526,** 2428–2443 (2018).
46. Zingg, B., Dong, H. W., Tao, H. W. & Zhang, L. I. Input–output organization of the mouse claustrum. *Journal of Comparative Neurology* **526,** 2428–2443 (2018).
47. Kaspar, B. K. *et al.* Adeno-associated virus effectively mediates conditional gene modification in the brain. *Proceedings of the National Academy of Sciences of the United States of America* **99,** 2320–2325 (2002).
48. Tervo, D. G. R. *et al.* A Designer AAV Variant Permits Efficient Retrograde Access to Projection Neurons. *Neuron* **92,** 372–382 (2016).
49. Vicq-d"Azyr, F. (.-1. Traité d"anatomie et de physiologie, avec des planches coloriées représentant au naturel les divers organes de l"homme et des animaux. Dédié au Roi par M. Vicq d"Azyr,... Tome 1er, 409.
50. Johnson, J. I. & Fenske, B. A. History of the Study and Nomenclature of the Claustrum. *The Claustrum: Structural, Functional, and Clinical Neuroscience,* 1–27 (2014).
51. Puelles, L., Kuwana, E., Puelles, E., Bulfone, A., Shimamura, K., Keleher, J., Smiga, S. & Rubenstein, J. L. Pallial and subpallial derivatives in the embryonic chick and mouse telencephalon, traced by the expression of the genes Dlx-2, Emx-1, Nkx-2.1, Pax-6, and Tbr-1. *Journal of Comparative Neurology* **424,** 409–438 (2000).
52. Wang, W. Z. *et al.* Comparative aspects of subplate zone studied with gene expression in sauropsids and mammals. *Cerebral Cortex* **21,** 2187–2203 (2011).

53. Norimoto, H. *et al.* A claustrum in reptiles and its role in slow-wave sleep. *Nature* **578,** 413–418 (2020).
54. Buchanan, K. J. & Johnson, J. I. Diversity of spatial relationships of the claustrum and insula in branches of the mammalian radiation. *Annals of the New York Academy of Sciences* **1225,** 30–63 (2011).
55. Baizer, J. S., Sherwood, C. C., Noonan, M. & Hof, P. R. Comparative organization of the claustrum: What does structure tell us about function? *Frontiers in Systems Neuroscience* **8,** 1–10 (2014).
56. Butler, A. B., Molnár, Z. & Manger, P. R. Apparent Absence of Claustrum in Monotremes: Implications for Forebrain Evolution in Amniotes. *Brain, Behavior and Evolution* **60,** 230–240 (2002).
57. Carinna M. Torgerson Andrei Irimia, S. M. G. & Horn, J. D. V. The DTI Connectivity of the Human Claustrum Carinna. *Human Brain Mapping* **4,** 827–838 (2015).
58. Krimmel, S. R., White, M. G., Panicker, M. H., Barrett, F. S., Mathur, B. N. & Seminowicz, D. A. The human claustrum is functionally connected to cognitive networks and involved in cognitive control. *bioRxiv* **32008181,** 1–23 (2018).
59. Druga, R. Cortico-claustral connections. I. Fronto-claustral connections. *Folia morphologica* **14,** 391–399 (1966).
60. Druga, R. Cortico-claustral connections. II. Connections from the parietal, temporal and occipital cortex to the claustrum. *Folia morphologica* **16,** 142–149 (1968).
61. Narkiewicz, O. Degenerations in the claustrum after regional neocortical ablations in the cat. *The Journal of Comparative Neurology* **123,** 335–355 (1964).
62. LeVay, S. & Sherk, H. The visual claustrum of the cat. I. Structure and connections. *Journal of Neuroscience* **1,** 956–980 (1981).
63. Olson, C. R. & Greybiel, A. M. Sensory maps in the claustrum of the cat. *Nature* (1980).
64. Wilhite, B. L., Teyler, T. J. & Hendricks, C. Functional relations of the rodent claustral-entorhinal-hippocampal system. *Brain Research* **365,** 54–60 (1986).
65. Vakolyuk, N. I., Kosterina, A. V. & Shlumukova, A. R. Spontaneous electrical activity of the claustrum. *Neurophysiology* **12,** 113–120 (1980).
66. LeVay, S. & Sherk, H. The visual claustrum of the cat. II. The visual field map. *Journal of Neuroscience* **1,** 981–992 (1981).
67. Sherk, H. & LeVay, S. The visual claustrum of the cat. III. Receptive field properties. *Journal of Neuroscience* **1,** 993–1002 (1981).
68. Kowiański, P., Dziewiatkowski, J., Kowiańska, J. & Moryś, J. Comparative anatomy of the claustrum in selected species: A morphometric analysis. *Brain, Behavior and Evolution* **53,** 44–54 (1999).
69. Ashwell, K. W. S., Hardman, C. & Paxinos, G. The Claustrum Is Not Missing from All Monotreme Brains. *Brain, Behavior and Evolution* **64,** 223–241 (2004).
70. Day-Brown, J. D., Slusarczyk, A. S., Zhou, N., Quiggins, R., Petry, H. M. & Bickford, M. E. Synaptic organization of striate cortex projections in the tree shrew: A comparison of the claustrum and dorsal thalamus. *Journal of Comparative Neurology* **525,** 1403–1420 (2017).
71. Brennan, E. K., Jedrasiak-Cape, I., Kailasa, S., Rice, S. P., Sudhakar, S. K. & Ahmed, O. J. Thalamus and claustrum control parallel layer 1 circuits in retrosplenial cortex. *eLife* **10,** 1–42 (2021).

72. Jones, E. Viewpoint: the core and matrix of thalamic organization. *Neuroscience* **85,** 331–345 (1998).
73. Parvizi, J. & Damasio, A. R. Differential distribution of calbindin D28k and parvalbumin among functionally distinctive sets of structures in the macaque brainstem. *The Journal of Comparative Neurology* **462,** 153–167 (2003).
74. Kawaguchi, Y. & Kubota, Y. GABAergic cell subtypes and their synaptic connections in rat frontal cortex. *Cerebral Cortex* **7,** 476–486 (1997).
75. Butt, S. J., Fuccillo, M., Nery, S., Noctor, S., Kriegstein, A., Corbin, J. G. & Fishell, G. The temporal and spatial origins of cortical interneurons predict their physiological subtype. *Neuron* **48,** 591–604 (2005).
76. The Petilla Interneuron Nomenclature Group (PING). Petilla terminology: nomenclature of features of GABAergic interneurons of the cerebral cortex. *Nature Reviews Neuroscience* **9,** 557–568 (2008).
77. Cowan, R. L., Wilson, C. J., Emson, P. C. & Heizmann, C. W. Parvalbumin-containing gabaergic interneurons in the rat neostriatum. *The Journal of Comparative Neurology* **302,** 197–205 (1990).
78. Reynhout, K. & Baizer, J. S. Immunoreactivity for calcium-binding proteins in the claustrum of the monkey. *Anatomy and Embryology* **199,** 75–83 (1999).
79. Celio, M. R. Calbindin D-28k and parvalbumin in the rat nervous system. *Neuroscience* **35,** 375–475 (1990).
80. Real, M. Á., Dávila, J. C. & Guirado, S. Immunohistochemical localization of the vesicular glutamate transporter VGLUT2 in the developing and adult mouse claustrum. *Journal of Chemical Neuroanatomy* **31,** 169–177 (2006).
81. Mumoli, L., Labate, A., Palamara, G., Sturniolo, M. & Gambardella, A. Reversible symmetrical external capsule hyperintensity as an early finding of autoimmune encephalitis. *Neurological Sciences* **35,** 1147–1149 (2014).
82. Shintaku, M., Kaneda, D., Tada, K., Katano, H. & Sata, T. Human herpes virus 6 encephalomyelitis after bone marrow transplantation: Report of an autopsy case. *Neuropathology* **30,** 50–55 (2010).
83. Hiraga, A., Watanabe, O., Kamitsukasa, I. & Kuwabara, S. Voltage-gated Potassium Channel Antibody-associated Encephalitis with Claustrum Lesions. *Internal Medicine* **53,** 2263–2264 (2014).
84. Hwang, K. J., Park, K.-C., Yoon, S. S. & Ahn, T.-B. Unusual Lesion in the Bilateral External Capsule Following Status Epilepticus: A Case Report. *Journal of Epilepsy Research* **4,** 88–90 (2014).
85. Shiihara, T., Kato, M., Ichiyama, T., Takahashi, Y., Tanuma, N., Miyata, R. & Hayasaka, K. Acute encephalopathy with refractory status epilepticus: Bilateral mesial temporal and claustral lesions, associated with a peripheral marker of oxidative DNA damage. *Journal of the Neurological Sciences* **250,** 159–161 (2006).
86. Randerath, J., Finkel, L., Shigaki, C., Burris, J., Nanda, A., Hwang, P. & Frey, S. H. Does it fit? – Impaired affordance perception after stroke. *Neuropsychologia* **108,** 92–102 (2018).
87. Snider, S. B., Hsu, J., Darby, R. R., Cooke, D., Fischer, D., Cohen, A. L., Grafman, J. H. & Fox, M. D. Cortical lesions causing loss of consciousness are anticorrelated with the dorsal brainstem. *Human Brain Mapping* **41,** 1520–1531 (2020).

88. Chau, A., Salazar, A. M., Krueger, F., Cristofori, I. & Grafman, J. The effect of claustrum lesions on human consciousness and recovery of function. *Consciousness and Cognition* **36,** 256–264 (2015).
89. Bota, M., Sporns, O. & Swanson, L. W. Architecture of the cerebral cortical association connectome underlying cognition. *Proceedings of the National Academy of Sciences of the United States of America* **112,** E2093–E2101 (2015).
90. Crick, F. & Koch, C. Towards a neurobiological theory of consciousness. *Seminars in the neurosciences* **2,** 263–275 (1990).
91. Pearson, R. C. A., Brodal, P., Gatter, K. C. & Powell, T. P. S. The organization of the connections between, the cortex and the claustrum in the monkey. *Brain Research,* 7 (1982).
92. Remedios, R., Logothetis, N. K. & Kayser, C. Unimodal responses prevail within the multisensory claustrum. *Journal of Neuroscience* **30,** 12902–12907 (2010).
93. Remedios, R., Logothetis, N. K. & Kayser, C. A role of the claustrum in auditory scene analysis by reflecting sensory change. *Frontiers in Systems Neuroscience* **8,** 1–8 (2014).
94. Reser, D. H., Richardson, K. E., Montibeller, M. O., Zhao, S., Chan, J. M., Soares, J. G., Chaplin, T. A., Gattass, R. & Rosa, M. G. Claustrum projections to prefrontal cortex in the capuchin monkey (Cebus apella). *Frontiers in Systems Neuroscience* **8,** 1–10 (2014).
95. Mathur, B. N., Caprioli, R. M. & Deutch, A. Y. Proteomic analysis illuminates a novel structural definition of the claustrum and insula. *Cerebral Cortex* **19,** 2372–2379 (2009).
96. Narikiyo, K., Mizuguchi, R., Ajima, A., Shiozaki, M., Hamanaka, H., Johansen, J. P., Mori, K. & Yoshihara, Y. The claustrum coordinates cortical slow-wave activity. *Nature Neuroscience* **23,** 741–753 (2020).
97. Atlan, G. *et al.* The Claustrum Supports Resilience to Distraction. *Current Biology* **28,** 2752–2762.e7 (2018).
98. Shibuya, H. & Yamamoto, T. Electrophysiological and morphological features of rat claustral neurons: An intracellular staining study. *Neuroscience* **85,** 1037–1049 (1998).
99. Kim, J., Matney, C. J., Roth, R. H. & Brown, S. P. Synaptic organization of the neuronal circuits of the claustrum. *Journal of Neuroscience* **36,** 773–784 (2016).
100. Feil, S., Valtcheva, N. & Feil, R. in *Gene Knockout Protocols* FEBRUARY, 15–27 (2009).
101. Kim, J. C., Cook, M. N., Carey, M. R., Shen, C., Regehr, W. G. & Dymecki, S. M. Linking genetically-defined neurons to behavior through a broadly applicable silencing allele. *Neuron* **63,** 305 (2009).
102. Asrican, B. *et al.* Next-generation transgenic mice for optogenetic analysis of neural circuits. *Frontiers in Neural Circuits* **7,** 1–24 (2013).
103. Braak, H. & Braak, E. Neuronal types in the claustrum of man. *Anatomy and Embryology* **163,** 447–460 (1982).
104. Hur, E. E. & Zaborszky, L. Vglut2 afferents to the medial prefrontal and primary somatosensory cortices: A combined retrograde tracing in situ hybridization. *Journal of Comparative Neurology* **483,** 351–373 (2005).
105. Spahn, B. & Braak, H. Percentage of projection neurons and various types of interneurons in the human claustrum. *Cells Tissues Organs* **122,** 245–248 (1985).

106. Watakabe, A. In situ hybridization analyses of claustrum-enriched genes in marmosets. *Journal of Comparative Neurology* **525,** 1442–1458 (2017).
107. Erwin, S. R., Bristow, B. N., Sullivan, K. E., Marriott, B., Wang, L., Clements, J., Lemire, A. L., Jackson, J. & Cembrowski, M. S. Spatially patterned excitatory neuron subtypes and circuits within the claustrum. *bioRxiv* (2021).
108. Chia, Z., Augustine, G. J. & Silberberg, G. Synaptic Connectivity between the Cortex and Claustrum Is Organized into Functional Modules. *Current Biology* **30,** 2777–2790.e4 (2020).
109. Atlan, G., Terem, A., Peretz-Rivlin, N., Groysman, M. & Citri, A. Mapping synaptic cortico-claustral connectivity in the mouse. *Journal of Comparative Neurology* **525,** 1381–1402 (2017).
110. Atlan, G. *et al.* Claustral Projections to Anterior Cingulate Cortex Modulate Engagement with the External World. *bioRxiv,* 2021.06.17.448649 (2021).
111. Niu, M. *et al.* Claustrum mediates bidirectional and reversible control of stress-induced anxiety responses. *Science Advances* **8,** eabi6375 (2022).
112. Smith, J. B., Alloway, K. D., Hof, P. R., Orman, R., Reser, D. H., Watakabe, A. & Watson, G. D. The relationship between the claustrum and endopiriform nucleus: A perspective towards consensus on cross-species homology. *Journal of Comparative Neurology* **527,** 476–499 (2019).
113. Bruguier, H. *et al.* In search of common developmental and evolutionary origin of the claustrum and subplate. *Journal of Comparative Neurology* **528,** 2956–2977 (2020).
114. Watson, C. & Puelles, L. Developmental gene expression in the mouse clarifies the organization of the claustrum and related endopiriform nuclei. *The Journal of Comparative Neurology* **525,** 1499–1508 (2017).
115. Franklin, K. B. J. & Paxinos, G. *The mouse brain in stereotaxic coordinates* 3. ed (Elsevier, AP, Amsterdam, 2008).
116. Dillingham, C. M., Mathiasen, M. L., Frost, B. E., Lambert, M. A. C., Bubb, E. J., Jankowski, M. M., Aggleton, J. P. & O'Mara, S. M. The Anatomical Boundary of the Rat Claustrum. *Frontiers in Neuroanatomy* **13,** 53 (2019).
117. White, M. G., Cody, P. A., Bubser, M., Wang, H. D., Deutch, A. Y. & Mathur, B. N. Cortical hierarchy governs rat claustrocortical circuit organization. *Journal of Comparative Neurology* **525,** 1347–1362 (2017).
118. Hoerder-Suabedissen, A. & Molnár, Z. Molecular Diversity of Early-Born Subplate Neurons. *Cerebral Cortex* **23,** 1473–1483 (2013).
119. Obst-Pernberg, K., Medina, L. & Redies, C. EXPRESSION OF R-CADHERIN AND N-CADHERIN BY CELL GROUPS AND FIBER TRACTS IN THE DEVELOPING MOUSE FOREBRAIN: RELATION TO THE FORMATION OF FUNCTIONAL CIRCUITS, 29 (2001).
120. Dillingham, C. M., Jankowski, M. M., Chandra, R., Frost, B. E. & O'Mara, S. M. The claustrum: Considerations regarding its anatomy, functions and a programme for research. *Brain and Neuroscience Advances* **1** (2017).
121. Gehrlach, D. A., Weiand, C., Gaitanos, T. N., Cho, E., Klein, A. S., Hennrich, A. A., Conzelmann, K.-K. & Gogolla, N. A whole-brain connectivity map of mouse insular cortex, 25 (2020).
122. Nunez, A., Amzica, F. & Steriade, M. Electrophysiology of cat association cortical cells in vivo: intrinsic properties and synaptic responses. *Journal of Neurophysiology* **70,** 418–430 (1993).

123. Kawaguchi, Y. Groupings of nonpyramidal and pyramidal cells with specific physiological and morphological characteristics in rat frontal cortex. *Journal of Neurophysiology* **69,** 416–431 (1993).
124. Rahman, F. E. & Baizer, J. S. Neurochemically defined cell types in the claustrum of the cat. *Brain Research* **1159,** 94–111 (2007).
125. Fernández-Miranda, J. C., Rhoton, A. L., Kakizawa, Y., Choi, C. & Álvarez-Linera, J. The claustrum and its projection system in the human brain: a microsurgical and tractographic anatomical study: Laboratory investigation. *Journal of Neurosurgery* **108,** 764–774 (2008).
126. Wang, H.-P., Spencer, D., Fellous, J.-M. & Sejnowski, T. J. Synchrony of Thalamocortical Inputs Maximizes Cortical Reliability. *Science* **328,** 106–109 (2010).
127. Douglas, R. J., Koch, C., Mahowald, M., Martin, K. A. C. & Suarez, H. H. Recurrent Excitation in Neocortical Circuits. *Science* **269,** 981–985 (1995).
128. Smith, J. B. & Alloway, K. D. Interhemispheric claustral circuits coordinate sensory and motor cortical areas that regulate exploratory behaviors. *Frontiers in Systems Neuroscience* **8,** 1–14 (2014).
129. Orman, R. Claustrum: a case for directional, excitatory, intrinsic connectivity in the rat. *Journal of Physiological Sciences* **65,** 533–544 (2015).
130. Graf, M., Nair, A., Wong, K. L., Tang, Y. & Augustine, G. J. Identification of mouse claustral neuron types based on their intrinsic electrical properties. *eNeuro* **7,** 1–29 (2020).
131. Jackson, J. Attention: Noisy Networks Are Tuned Out by the Claustrum. *Current Biology* **28,** R937–R939 (2018).
132. Jackson, J., Karnani, M. M., Zemelman, B. V., Burdakov, D. & Lee, A. K. Inhibitory Control of Prefrontal Cortex by the Claustrum. *Neuron* **99,** 1029–1039.e4 (2018).
133. McBride, E. G., Gandhi, S. R., Kuyat, J. R., Ollerenshaw, D. R., Arkhipov, A., Koch, C. & Olsen, S. R. Influence of claustrum on cortex varies by area, layer, and cell type. *bioRxiv,* 1–25 (2022).
134. Ferguson, S. M. & Neumaier, J. F. Grateful DREADDs: Engineered receptors reveal how neural circuits regulate behavior. *Neuropsychopharmacology* **37,** 296–297 (2012).
135. Zhu, H. & Roth, B. L. DREADD: A chemogenetic GPCR signaling platform. *International Journal of Neuropsychopharmacology* **18,** 1–6 (2015).
136. Zhu, H., Aryal, D. K., Olsen, R. H., Urban, D. J., Swearingen, A., Forbes, S., Roth, B. L. & Hochgeschwender, U. Cre-dependent DREADD (Designer Receptors Exclusively Activated by Designer Drugs) mice: Conditional DREADD Mice. *genesis* **54,** 439–446 (2016).
137. Roth, B. L. DREADDs for Neuroscientists. *Neuron* **89,** 683–694 (2016).
138. Vardy, E. *et al.* A New DREADD Facilitates the Multiplexed Chemogenetic Interrogation of Behavior. *Physiology & behavior* **176,** 139–148 (2015).
139. MacLaren, D. A., Browne, R. W., Shaw, J. K., Radhakrishnan, S. K., Khare, P., España, R. A. & Clark, S. D. Clozapine N-oxide administration produces behavioral effects in long-evans rats: Implications for designing DREADD experiments. *eNeuro* **3** (2016).
140. Manvich, D. F., Webster, K. A., Foster, S. L., Farrell, M. S., Ritchie, J. C., Porter, J. H. & Weinshenker, D. The DREADD agonist clozapine N-oxide (CNO)

is reverse-metabolized to clozapine and produces clozapine-like interoceptive stimulus effects in rats and mice. *Scientific Reports* **8,** 3840 (2018).
141. Chevée, M., Finkel, E. A., Kim, S.-J., O'Connor, D. H. & Brown, S. P. Neural activity in the mouse claustrum in a cross-modal sensory selection task. *Neuron* **110,** 486–501.e7 (2022).
142. Morecraft, R. J., Ugolini, G., Lanciego, J. L., Wouterlood, F. G. & Pandya, D. N. in *Diffusion MRI* 359–399 (Elsevier, 2014).
143. Oztas, E. Neuronal Tracing. *Neuroanatomy* **2** (2004).
144. Weiss, P. & Hiscoe, H. B. Experiments on the mechanism of nerve growth. *Journal of Experimental Zoology* **107,** 315–395 (1948).
145. Kandel, E. R., Schwartz, J. H., Jessell, T. M., Siegelbaum, S. A. & Hudspeth, A. J. *Principles of Neural Science* (2013).
146. Bruce, L., Christensen, M. & Fritzsch, B. Electron microscopic differentiation of directly and transneuronally transported DiI and applications for studies of synaptogenesis. *Journal of Neuroscience Methods* **73,** 107–112 (1997).
147. Honig, M. G. & Hume, R. I. Dil and DiO: versatile fluorescent dyes for neuronal labelling and pathway tracing. *Trends in Neurosciences* **12,** 333–341 (1989).
148. Brown, A. Axonal transport of membranous and nonmembranous cargoes. *Journal of Cell Biology* **160,** 817–821 (2003).
149. Betley, J. N. & Sternson, S. M. Adeno-Associated Viral Vectors for Mapping, Monitoring, and Manipulating Neural Circuits. *Human Gene Therapy* **22,** 669–677 (2011).
150. Haggerty, D. L., Grecco, G. G., Reeves, K. C. & Atwood, B. Adeno-Associated Viral Vectors in Neuroscience Research. *Molecular Therapy - Methods & Clinical Development* **17,** 69–82 (2020).
151. Ding, W., Zhang, L., Yan, Z. & Engelhardt, J. F. Intracellular trafficking of adeno-associated viral vectors. *Gene Therapy* **12,** 873–880 (2005).
152. Lidmar, J., Mirny, L. & Nelson, D. R. Virus shapes and buckling transitions in spherical shells. *Physical Review E* **68,** 051910 (2003).
153. Wu, Z., Asokan, A. & Samulski, R. J. Adeno-associated Virus Serotypes: Vector Toolkit for Human Gene Therapy. *Molecular Therapy* **14,** 316–327 (2006).
154. Grimm, D. & Kay, M. From Virus Evolution to Vector Revolution: Use of Naturally Occurring Serotypes of Adeno-associated Virus (AAV) as Novel Vectors for Human Gene Therapy. *Current Gene Therapy* **3,** 281–304 (2003).
155. Callaway, E. M. Transneuronal circuit tracing with neurotropic viruses. *Current Opinion in Neurobiology* **18,** 617–623 (2008).
156. Harris, J. A., Wook Oh, S. & Zeng, H. Adeno-Associated Viral Vectors for Anterograde Axonal Tracing with Fluorescent Proteins in Nontransgenic and Cre Driver Mice. *Current Protocols in Neuroscience* **59** (2012).
157. Pillay, S. *et al.* Adeno-associated Virus (AAV) Serotypes Have Distinctive Interactions with Domains of the Cellular AAV Receptor. *Journal of Virology* **91,** 1–17 (2017).
158. Kuypers, H. & Ugolini, G. Viruses as transneuronal tracers. *Trends in Neurosciences* **13,** 71–75 (1990).
159. Castle, M. J., Gershenson, Z. T., Giles, A. R., Holzbaur, E. L. & Wolfe, J. H. Adeno-Associated Virus Serotypes 1, 8, and 9 Share Conserved Mechanisms for Anterograde and Retrograde Axonal Transport. *Human Gene Therapy* **25,** 705–720 (2014).

160. Zingg, B., lin Chou, X., gang Zhang, Z., Mesik, L., Liang, F., Tao, H. W. & Zhang, L. I. AAV-Mediated Anterograde Transsynaptic Tagging: Mapping Corticocollicular Input-Defined Neural Pathways for Defense Behaviors. *Neuron* **93,** 33–47 (2017).
161. Anton, M. & Graham, F. L. Site-specific recombination mediated by an adenovirus vector expressing the Cre recombinase protein: a molecular switch for control of gene expression. *Journal of Virology* **69,** 4600–4606 (1995).
162. Rohlmann, A., Gotthardt, M., Willnow, T. E., Hammer, R. E. & Herz, J. Sustained sotnatic gene inactivation by viral transfer of Cre recotnbinase. **14,** 4 (1996).
163. McLellan, M. A., Rosenthal, N. A. & Pinto, A. R. Cre- *lox* P-Mediated Recombination: General Principles and Experimental Considerations: Cre- *lox* P-Mediated Recombination. *Current Protocols in Mouse Biology* **7,** 1–12 (2017).
164. Oh, S. W. *et al.* A mesoscale connectome of the mouse brain. *Nature* **508,** 207–214 (2014).
165. Chalfie, M., Tu, Y., Euskirchen, G., Ward, W. W. & Prasher, D. C. Green Fluorescent Protein as a Marker for Gene Expression. *Science* **263,** 802–805 (1994).
166. *Fundamentals of Fluorescence Imaging* 1st ed. (ed Cox, G.) (Jenny Stanford Publishing, 2019).
167. Zingg, B. *et al.* Neural networks of the mouse neocortex. *Cell* **156,** 1096–1111 (2014).
168. Yuste, R. Fluorescence microscopy today. *Nature Methods* **2,** 902–904 (2005).
169. Ni, L. Genetic Transsynaptic Techniques for Mapping Neural Circuits in Drosophila. *Frontiers in Neural Circuits* **15,** 749586 (2021).
170. Huang, T.-h., Niesman, P., Arasu, D., Lee, D., De La Cruz, A. L., Callejas, A., Hong, E. J. & Lois, C. Tracing neuronal circuits in transgenic animals by transneuronal control of transcription (TRACT). *eLife* **6,** e32027 (2017).
171. Lanciego, J. L. & Wouterlood, F. G. A half century of experimental neuroanatomical tracing. *Journal of Chemical Neuroanatomy* **42,** 157–183 (2011).
172. Köbbert, C., Apps, R., Bechmann, I., Lanciego, J., Mey, J. & Thanos, S. Current concepts in neuroanatomical tracing. *Progress in Neurobiology* **62,** 327–351 (2000).
173. Katz, L. C., Burkhalter, A. & Dreyer, W. J. Fluorescent latex microspheres as a retrograde neuronal marker for in vivo and in vitro studies of visual cortex. *Nature* **310,** 498–500 (1984).
174. Norita, M. Demonstration of bilateral claustro-cortical connections in the cat with the method of retrograde axonal transport of horseradish peroxidase. *Archivum Histologicum Japonicum = Nihon Soshikigaku Kiroku* **40,** 1–10 (1977).
175. Kristensson, K. & Olsson, Y. Uptake and retrograde axonal transport of peroxidase in hypoglossal neurones: Electron microscopical localization in the neuronal perikaryon. *Acta Neuropathologica* **19,** 1–9 (1971).
176. LaVail, J. H. & LaVail, M. M. Retrograde Axonal Transport in the Central Nervous System. *Science* **176,** 1416–1417 (1972).
177. Stoeckel, K., Schwab, M. & Thoenen, H. ROLE OF GANGLIOSIDES IN THE UPTAKE AND RETROGRADE AXONAL TRANSPORT OF CHOLERA AND TETANUS TOXIN AS COMPARED TO NERVE GROWTH FACTOR AND WHEAT GERM AGGLUTININ. *Brain Research* **132,** 273–285 (1977).

178. Luppi, P.-H., Fort, P. & Jouvet, M. Iontophoretic application of unconjugated cholera toxin B subunit (CTb) combined with immunohistochemistry of neurochemical substances: a method for transmitter identification of retrogradely labeled neurons. *Brain Research* **534,** 209–224 (1990).
179. Conte, W. L., Kamishina, H. & Reep, R. L. Multiple neuroanatomical tract-tracing using fluorescent Alexa Fluor conjugates of cholera toxin subunit B in rats. *Nature Protocols* **4,** 1157–1166 (2009).
180. Ohka, S., Yang, W.-X., Terada, E., Iwasaki, K. & Nomoto, A. Retrograde Transport of Intact Poliovirus Through the Axon via the Fast Transport System. *Virology* **250,** 67–75 (1998).
181. Ugolini, G., Kuypers, H. & Simmons, A. Retrograde transneuronal transfer of Herpes simplex virus type 1 (HSV 1) from motoneurones. *Brain Research* **422,** 242–256 (1987).
182. Yizhar, O., Fenno, L. E., Davidson, T. J., Mogri, M. & Deisseroth, K. Optogenetics in Neural Systems. *Neuron* **71,** 9–34 (2011).
183. Goldman, D. E. POTENTIAL, IMPEDANCE, AND RECTIFICATION IN MEMBRANES. *Journal of General Physiology* **27,** 37–60 (1943).
184. Hodgkin, A. L. & Katz, B. The effect of sodium ions on the electrical activity of the giant axon of the squid. *The Journal of Physiology* **108,** 37–77 (1949).
185. Hodgkin, A. L., Huxley, A. F. & Katz, B. Measurement of current-voltage relations in the membrane of the giant axon of *Loligo*. *The Journal of Physiology* **116,** 424–448 (1952).
186. Hodgkin, A. L. & Huxley, A. F. The components of membrane conductance in the giant axon of *Loligo*. *The Journal of Physiology* **116,** 473–496 (1952).
187. Hodgkin, A. L. & Huxley, A. F. The dual effect of membrane potential on sodium conductance in the giant axon of *Loligo*. *The Journal of Physiology* **116,** 497–506 (1952).
188. Hodgkin, A. L. & Huxley, A. F. Currents carried by sodium and potassium ions through the membrane of the giant axon of *Loligo*. *The Journal of Physiology* **116,** 449–472 (1952).
189. Hodgkin, A. L. & Huxley, A. F. A quantitative description of membrane current and its application to conduction and excitation in nerve. *The Journal of Physiology* **117,** 500–544 (1952).
190. Neher, E. & Sakmann, B. Single-channel currents recorded from membrane of denervated frog muscle fibres. *Nature* **260,** 799–802 (1976).
191. Hamill, O. P., Marty, A., Neher, E., Sakmann, B. & Sigworth, F. J. Improved patch-clamp techniques for high-resolution current recording from cells and cell-free membrane patches. *Pflügers Archiv - European Journal of Physiology* **391,** 85–100 (1981).
192. Sakmann, B. & Neher, E. Patch Clamp Techniques for Studying Ionic Channels in Excitable Membranes. *Annual Review of Physiology,* 21 (1984).
193. Ogden, D. & Stanfield, P. in *Microelectrode Techniques* 53–76 (1994).
194. Hille, B. *Ion Channels of Excitable Membranes* 3rd ed. (Sinaur Associates, 2001).
195. Llinás, R. R. The Intrinsic Electrophysiological Properties of Mammalian Neurons: Insights into Central Nervous System Function. *Science* **242,** 1654–1664 (1988).
196. Connors, B. W. & Gutnick, M. J. Intrinsic firing patterns of diverse neocortical neurons. *Trends in Neurosciences* **13,** 99–104 (1990).

197. Toledo-Rodriguez, M., Blumenfeld, B., Wu, C., Luo, J., Attali, B., Goodman, P. & Markram, H. Correlation maps allow neuronal electrical properties to be predicted from single-cell gene expression profiles in rat neocortex. *Cerebral Cortex* **14,** 1310–1327 (2004).
198. Kawaguchi, Y., Karube, F. & Kubota, Y. Dendritic branch typing and spine expression patterns in cortical nonpyramidal cells. *Cerebral Cortex* **16,** 696–711 (2006).
199. McGarry, L. M., Packer, A. M., Fino, E., Nikolenko, V., Sippy, T. & Yuste, R. Quantitative classification of somatostatin-positive neocortical interneurons identifi es three interneuron subtypes. *Frontiers in Neural Circuits* **4,** 1–19 (2010).
200. Holmgren, C., Harkany, T., Svennenfors, B. & Zilberter, Y. Pyramidal cell communication within local networks in layer 2/3 of rat neocortex. *The Journal of Physiology* **551,** 139–153 (2003).
201. Crick, F. H. C. Thinking about the Brain. *SCIENTIFIC AMERICAN,* 16 (1979).
202. Oesterhelt, D. & Stoeckenius, W. Rhodopsin-like Protein from the Purple Membrane of Halobacterium halobium. *Nature New Biology* **233,** 149–152 (1971).
203. Harz, H. & Hegemann, P. Rhodopsin-regulated calcium currents in Chlamydomonas. *Nature* **351,** 489–491 (1991).
204. Zemelman, B. V., Lee, G. A., Ng, M. & Miesenböck, G. Selective Photostimulation of Genetically ChARGed Neurons. *Neuron* **33,** 15–22 (2002).
205. Nagel, G., Szellas, T., Huhn, W., Kateriya, S., Adeishvili, N., Berthold, P., Ollig, D., Hegemann, P. & Bamberg, E. Channelrhodopsin-2, a directly light-gated cation-selective membrane channel. *Proceedings of the National Academy of Sciences* **100,** 13940–13945 (2003).
206. Lima, S. Q. & Miesenböck, G. Remote Control of Behavior through Genetically Targeted Photostimulation of Neurons. *Cell* **121,** 141–152 (2005).
207. Boyden, E. S. A history of optogenetics: The development of tools for controlling brain circuits with light. *F1000 Biology Reports* **3,** 1–12 (2011).
208. Marshel, J. H. *et al.* Cortical layer-specific critical dynamics triggering perception. *Science* **365,** 1–23 (2019).
209. Adamantidis, A. R., Zhang, F., Aravanis, A. M., Deisseroth, K. & De Lecea, L. Neural substrates of awakening probed with optogenetic control of hypocretin neurons. *Nature* **450,** 420–424 (2007).
210. Arenkiel, B. R., Peca, J., Davison, I. G., Feliciano, C., Deisseroth, K., Augustine, G. J., Ehlers, M. D. & Feng, G. In Vivo Light-Induced Activation of Neural Circuitry in Transgenic Mice Expressing Channelrhodopsin-2. *Neuron* **54,** 205–218 (2007).
211. Wang, Q. & Burkhalter, A. Area map of mouse visual cortex. *The Journal of Comparative Neurology* **502,** 339–357 (2007).
212. Deisseroth, K. Optogenetics. *Nature Methods* **8,** 26–29 (2011).
213. Deisseroth, K. Optogenetics: 10 years of microbial opsins in neuroscience. *Nature Neuroscience* **18,** 1213–1225 (2015).
214. Schneider, F., Grimm, C. & Hegemann, P. Biophysics of Channelrhodopsin. *Annual Review of Biophysics* **44,** 167–186 (2015).
215. Nagel, G., Ollig, D., Fuhrmann, M., Kateriya, S., Musti, A. M., Bamberg, E. & Hegemann, P. Channelrhodopsin-1: A Light-Gated Proton Channel in Green Algae. *Science* **296,** 2395–2398 (2002).

216. Mattis, J. *et al.* Principles for applying optogenetic tools derived from direct comparative analysis of microbial opsins. *Nature Methods* **9,** 159–172 (2012).
217. Mittelmeier, T. M., Boyd, J. S., Lamb, M. R. & Dieckmann, C. L. Asymmetric properties of the Chlamydomonas reinhardtii cytoskeleton direct rhodopsin photoreceptor localization. *Journal of Cell Biology* **193,** 741–753 (2011).
218. Petreanu, L., Huber, D., Sobczyk, A. & Svoboda, K. Channelrhodopsin-2-assisted circuit mapping of long-range callosal projections. *Nature Neuroscience* **10,** 663–668 (2007).
219. Klapoetke, N. C. *et al.* Independent Optical Excitation of Distinct Neural Populations. *Nature Protocols* **9,** 828–841 (2014).
220. Hooks, B. M., Lin, J. Y., Guo, C. & Svoboda, K. Dual-channel circuit mapping reveals sensorimotor convergence in the primary motor cortex. *Journal of Neuroscience* **35,** 4418–4426 (2015).
221. Bauer, J., Weiler, S., Fernholz, M., Laubender, D., Scheuss, V., Hübener, M., Bonhoeffer, T. & Rose, T. Selective connectivity limits functional binocularity in the retinogeniculate pathway of the mouse. *bioRxiv* (2020).
222. Averbeck, B. B., Latham, P. E. & Pouget, A. Neural correlations, population coding and computation. *Nature Reviews Neuroscience* **7,** 358–366 (2006).
223. Panzeri, S., Harvey, C. D., Piasini, E., Latham, P. E. & Fellin, T. Cracking the Neural Code for Sensory Perception by Combining Statistics, Intervention, and Behavior. *Neuron* **93,** 491–507 (2017).
224. Hubel, D. H. Tungsten Microelectrode for Recording from Single Units. *Science* **125,** 549–550 (1957).
225. Buzsáki, G. Large-scale recording of neuronal ensembles. *Nature Neuroscience* **7,** 446–451 (2004).
226. Harris, K. D., Quiroga, R. Q., Freeman, J. & Smith, S. L. Improving data quality in neuronal population recordings. *Nature Neuroscience* **19,** 1165–1174 (2016).
227. Houweling, A. R., Doron, G., Voigt, B. C., Herfst, L. J. & Brecht, M. Nanostimulation: Manipulation of Single Neuron Activity by Juxtacellular Current Injection. *Journal of Neurophysiology* **103,** 1696–1704 (2010).
228. Cardin, J. A., Carlén, M., Meletis, K., Knoblich, U., Zhang, F., Deisseroth, K., Tsai, L.-H. & Moore, C. I. Driving fast-spiking cells induces gamma rhythm and controls sensory responses. *Nature* **459,** 663–667 (2009).
229. Kim, C. K., Adhikari, A. & Deisseroth, K. Integration of optogenetics with complementary methodologies in systems neuroscience. *Nature Reviews Neuroscience* **18,** 222–235 (2017).
230. Grienberger, C. & Konnerth, A. Imaging calcium in neurons. *Neuron* **73,** 862–885 (2012).
231. Berridge, M. J. Neuronal Calcium Signaling. *Neuron* **21,** 13–26 (1998).
232. Nakai, J., Ohkura, M. & Imoto, K. A high signal-to-noise Ca2+ probe composed of a single green fluorescent protein. *Nature Biotechnology* **19,** 137–141 (2001).
233. Chen, T.-W. *et al.* Ultrasensitive fluorescent proteins for imaging neuronal activity. *Nature* **499,** 295–300 (2013).
234. Dana, H. *et al.* High-performance calcium sensors for imaging activity in neuronal populations and microcompartments. *Nature Methods* **16,** 649–657 (2019).
235. Packer, A. M., Russell, L. E., Dalgleish, H. W. & Häusser, M. Simultaneous all-optical manipulation and recording of neural circuit activity with cellular resolution in vivo. *Nature Methods* **12,** 140–146 (2015).

236. Lichtman, J. W. & Conchello, J.-A. Fluorescence microscopy. *Nature Methods* **2,** 910–919 (2005).
237. Helmchen, F. & Denk, W. Deep tissue two-photon microscopy. *Nature Methods* **2,** 932–940 (2005).
238. Druga, R. in *The Claustrum: Structural, Functional, and Clinical Neuroscience* 29–84 (2014).
239. Overstreet-Wadiche, L. & McBain, C. J. Neurogliaform cells in cortical circuits. *Nature Reviews Neuroscience* **16,** 458–468 (2015).
240. Chevée, M. & Brown, S. P. The development of local circuits in the neocortex: recent lessons from the mouse visual cortex. *Current Opinion in Neurobiology* **53,** 103–109 (2018).
241. Qadir, H., Stewart, B. W., Van Ryzin, J., Wu, Q., Chen, S., Seminowicz, D. A. & Mathur, B. N. The mouse claustrum synaptically connects cortical network motifs. *bioRXiv* (2022).
242. Torgerson, C. M., Irimia, A., Goh, S. Y. M. & Van Horn, J. D. The DTI connectivity of the human claustrum: Claustrum Connectivity. *Human Brain Mapping* **36,** 827–838 (2015).
243. Grimstvedt, J. S., Shelton, A. M., Hoerder-Suabedissen, A., Oliver, D. K., Berndtsson, C. H., Blankvoort, S., Nair, R. R., Packer, A. M., Witter, M. P. & Kentros, C. G. A multifaceted architectural framework of the mouse claustrum complex. *bioRXiv* (2022).
244. Kim, E. J., Jacobs, M. W., Ito-Cole, T. & Callaway, E. M. Improved Monosynaptic Neural Circuit Tracing Using Engineered Rabies Virus Glycoproteins. *Cell Reports* **15,** 692–699 (2016).
245. Peng, H. *et al.* Brain-wide single neuron reconstruction reveals morphological diversity in molecularly defined striatal, thalamic, cortical and claustral neuron types. *bioRXiv* (2019).
246. Wang, Y. *et al.* Complete single neuron reconstruction reveals morphological diversity in molecularly defined claustral and cortical neuron types. *bioRxiv* **7,** 31–38 (2019).
247. LeVay, S. Synaptic organization of claustral and geniculate afferents to the visual cortex of the cat. *Journal of Neuroscience* **6,** 3564–3575 (1986).
248. Rudy, B., Fishell, G., Lee, S. H. & Hjerling-Leffler, J. Three groups of interneurons account for nearly 100% of neocortical GABAergic neurons. *Developmental Neurobiology* **71,** 45–61 (2011).
249. Basu, J., Zaremba, J. D., Cheung, S. K., Hitti, F. L., Zemelman, B. V., Losonczy, A. & Siegelbaum, S. A. Gating of hippocampal activity, plasticity, and memory by entorhinal cortex long-range inhibition. *Science* **351,** aaa5694 (2016).
250. Boon, J., Clarke, E., Kessaris, N., Goffinet, A., Molnár, Z. & Hoerder-Suabedissen, A. Long-range projections from sparse populations of GABAergic neurons in murine subplate. *Journal of Comparative Neurology* **527,** 1610–1620 (2019).
251. Jinno, S., Klausberger, T., Marton, L. F., Dalezios, Y., Roberts, J. D. B., Fuentealba, P., Bushong, E. A., Henze, D., Buzsaki, G. & Somogyi, P. Neuronal diversity in GABAergic long-range projections from the hippocampus. *Journal of Neuroscience* **27,** 8790–8804 (2007).
252. Lee, A. T., Vogt, D., Rubenstein, J. L. & Sohal, V. S. A class of GABAergic neurons in the prefrontal cortex sends long-range projections to the nucleus

accumbens and elicits acute avoidance behavior. *Journal of Neuroscience* **34,** 11519–11525 (2014).
253. Melzer, S., Michael, M., Caputi, A., Eliava, M., Fuchs, E. C., Whittington, M. A. & Monyer, H. Long-Range–Projecting GABAergic Neurons Modulate Inhibition in Hippocampus and Entorhinal Cortex. *Science* **335,** 1506–1511 (2012).
254. Melzer, S. & Monyer, H. Diversity and function of corticopetal and corticofugal GABAergic projection neurons. *Nature Reviews Neuroscience,* 17 (2020).
255. Molnár, Z. & Butler, A. B. in *Progress in Brain Research* 21–38 (Elsevier, 2002).
256. Calvert, G. A. Crossmodal Processing in the Human Brain: Insights from Functional Neuroimaging Studies. *Cerebral Cortex* **11,** 1110–1123 (2001).
257. Ettlinger, G. & Wilson, W. Cross-modal performance: behavioural processes, phylogenetic considerations and neural mechanisms. *Behavioural Brain Research* **40,** 169–192 (1990).
258. Yuan, T., Packer, A. M., Pettit, N., Chun, S., Lau, J. Y. N. & Hausser, M. Integration of multisensory inputs by single neurons in the claustrum. *Society for Neuroscience Annual Meeting* (2015).
259. Cortimiglia, R., Crescimanno, G., Salerno, M. & Amato, G. The role of the claustrum in the bilateral control of frontal oculomotor neurons in the cat. *Experimental Brain Research* **84** (1991).
260. Tsumoto, T. & Suda, K. Effects of stimulation of the dorsocaudal claustrum on activities of striate cortex neurons in the cat. *Brain Research,* 5 (1982).
261. Berg, J. Lumping and splitting. *Science* **359,** 1309–1309 (2018).
262. Watson, B. O., Yuste, R. & Packer, A. M. PackIO and EphysViewer: software tools for acquisition and analysis of neuroscience data. *bioRXiv,* 29 (2016).
263. Pachitariu, M., Stringer, C., Dipoppa, M., Schröder, S., Rossi, L. F., Dalgleish, H., Carandini, M. & Harris, K. D. *Suite2p: beyond 10,000 neurons with standard two-photon microscopy* preprint (Neuroscience, 2016).
264. Morel, P. Gramm: grammar of graphics plotting in Matlab. *The Journal of Open Source Software* **3,** 568 (2018).
265. Caselles, V., Kimmel, R. & Sapiro, G. Geodesic active contours. *Proceedings of IEEE International Conference on Computer Vision,* 694–699 (1995).
266. Kass, M., Witkin, A. & Terzopoulos, D. Snakes: Active contour models. *International Journal of Computer Vision* **1,** 321–331 (1988).
267. Otsu, N. A Threshold Selection Method from Gray-Level Histograms. *IEEE Transactions on Systems, Man, and Cybernetics* **C,** 62–66 (1979).
268. Gonzalez, R. C., Woods, R. E. & Masters, B. R. Digital Image Processing, Third Edition. *Journal of Biomedical Optics* **14** (2009).